



DEPARTAMENTO DE FÍSICA

Universidade de Coimbra



Dissertação de Mestrado em Engenharia Biomédica

*Methodologies for Hemodynamic  
Parameters Assessment*



Tânia Maria Pereira Lopes

Setembro 2009

## *Supervisors*

<p>Prof. Dr. Carlos Correia</p> <p>Prof. Dr. Luís Requicha Ferreira</p> <p>Dr. João Cardoso</p>	  <p>Centro de Electrónica e Instrumentação Departamento de Física FCTUC</p>
---	---

## *In collaboration with*

 <p>Intelligent Sensing Anywhere</p>	 <p>Instituto Investigação &amp; Formação Cardiovascular, S.A.</p>
---	---

This report is made in fulfilment of the requirements of Project, a discipline of the 5th year of the Biomedical Engineering graduation.



## *Abstract*

---

Nowadays, there is a huge concern to develop and explore methods able to detect physiological parameters that indicate hazards or health problems. In the case of cardiovascular disease, leading cause of death in developed countries, the arterial stiffness is the main risk factor. The pulse-wave velocity (PWV), i.e. the velocity with which the pressure wave spreads over an artery, is considered the standard method to assess arterial stiffness. However, the equipment that is available on the market is very expensive, difficult to operate and with limitations.

This research project is focused on the development of new piezoelectric based probes, allowing simple and non-invasive access to different hemodynamic parameters. In particular the double probe, whose great potential is the determination of PWV. In this project it was built two benches test that reproduce the properties of the cardiovascular system, which allowed the characterization of sensors and validation of the developed algorithms.

The probes allow to obtain the original pressure waveform by the Deconvolution algorithm. For the double probe, it was show that it has temporal resolution for studies of PWV.

This report, aims to describe aspects of architecture of the probes, the different versions explored, developed the algorithms and results obtained.

### *Keywords*

Cardiovascular Diseases, Arterial Stiffness, Pulse Wave Velocity, Test Bench, Piezoelectric Sensor, Impulse Response, Deconvolution.

## *Resumo*

---

No mundo actual, há uma enorme preocupação em desenvolver e explorar métodos capazes de detectar parâmetros fisiológicos que indiquem riscos ou problemas de saúde. No caso das doenças cardiovasculares, principal causa de morte nos países desenvolvidos, a rigidez arterial é o principal factor de risco. A velocidade de onda de pulso (VOP), ou seja, a velocidade com que a onda de pressão se propaga ao longo de uma artéria, é considerada o método padrão para avaliar a rigidez arterial. Os equipamentos que se encontram disponíveis no mercado são muito dispendiosos, difíceis de operar e com limitações.

Este projecto de investigação centrou-se no desenvolvimento de novas sondas, baseadas em sensores piezoeléctricos, capazes de permitir o acesso a diferentes parâmetros hemodinâmicos de forma simples e não-invasiva, em especial a sonda dupla, cujo grande potencial seria o cálculo da VOP. Foram construídas duas bancadas de teste que reproduzem as propriedades do sistema cardiovascular, e que permitiram a caracterização dos sensores e validação dos algoritmos desenvolvidos.

As sondas criadas permitem obter a onda de pressão original através do algoritmo de Desconvolução. Para a sonda dupla, demonstrou-se que esta tem resolução temporal para os estudos da VOP.

O presente trabalho pretende descrever aspectos ligados à arquitectura das sondas, as diferentes versões exploradas, os algoritmos criados e os resultados obtidos.

### *Palavras-chave*

Doenças Cardiovasculares, Rigidez Arterial, Velocidade de Onda de Pulso, Bancada de Teste, Sensor Piezoeléctrico, Resposta a Impulso, Desconvolução.



## *Acknowledgments*

---

This research project was to me an academic experience of high growth and would like to thank everyone who has been by my side during this journey.

Foremost, I would like to thank my supervisors, Prof. Dr. Carlos Correia and Prof. Dr. Luís Requicha, for their support and aid along all this work. A special thanks to Prof. Dr. Carlos Correia, for the great ideas of his “powerful mind”, throughout the patience and clarity in explanation. Prof. Dr. Requicha Ferreira with his creative mind to solve the practical problems it is essential to carry out this project.

A huge thanks to Dr. João its major entropy questions, my partner Vânia for its friendship and companionship in this walk, and Eng. Elisabeth by all councils.

I want to show especial gratitude to Eng. Catarina for their guidance, patience and companionship that has at all times.

I want to thanks Edu for reminding me that I must hear the voice of conscience and that I should "work more and seriously"; to Miguel for all discussions and for teaching me to fish, without ever giving me the fish; to Xico for said me "Mim ajuda".

I thank my parents and sisters for all the support and courage that always gave me and sustain my entire world of fantasy, thanks to Doroti for being with me always, never leave me alone.

To my mother who brings me the light at all times I dedicate this work.





# Contents

---

Abstract.....	iv
Resumo.....	v
Acknowledgments.....	vii
List of Figures.....	xi
List of Tables.....	xiv
<b><u>1. Introduction</u></b> .....	<b>1</b>
Motivation .....	1
Purposes.....	2
Hemodynamic project team.....	2
Overview of the Dissertation.....	3
<b><u>2. Theoretical Background</u></b> .....	<b>4</b>
2.1 – Cardiovascular physiology Concepts.....	4
2.2 – Cardiovascular diseases.....	7
2.3 – Pressure waveform.....	9
2.4 – Hemodynamic Parameters.....	12
2.5 – State of the art.....	15
2.6 – Piezoelectric Sensors.....	18
<b><u>3. Process Methodology</u></b> .....	<b>20</b>
3.1 – Introduction.....	20
3.2 – Acquisition System.....	20
3.2.1 – Probes.....	21
3.2.2 – Acquisition Unit.....	22
3.2.2.1 – Circuit signal conditioning.....	22
3.2.2.2 – DAQ Module.....	22
3.3 – Clinical Trials.....	23
3.3.1 – Data Acquisition.....	23
3.3.2 – Data Processing.....	23
3.3.2.1 – General Algorithm.....	23
3.3.2.2 – PWV Algorithm in test bench.....	24
3.3.2.3 – Double Probe Algorithms.....	26
3.4 – Discussion.....	27
<b><u>4. Test Bench</u></b> .....	<b>28</b>
4.1 – Introduction.....	28
4.2 – Test Bench System I.....	28
4.2.1 – Instrumentation.....	28
4.2.2 – Study of waves propagation.....	30
4.2.3 – Conclusions.....	31
4.3 – Test Bench System II.....	32
4.3.1 – Instrumentation.....	32

4.3.2– Study of waves propagation.....	34
4.3.4– PWV determination in the tube.....	35
4.4– Conclusions.....	47
<b><u>5. Characterization of probes.....</u></b>	<b>48</b>
5.1– Developed Sensors.....	48
5.2– Methods.....	48
5.2.1– Deconvolution.....	48
5.2.2– IR Determination.....	49
5.3– Differential Simple probe.....	53
5.3.1– Characterization of sensor probe.....	53
5.3.2– Results.....	54
5.4– Integrative Simple probe.....	55
5.4.1– The new probe.....	55
5.4.2– Characterization of sensor.....	56
5.4.3– Signals of sensor.....	57
5.5– Double probe.....	59
5.5.1– Characterization of sensor.....	59
5.5.2– Signals of sensor.....	60
5.6– Convolution.....	61
5.7– Conclusions.....	65
<b><u>6. Double Probe</u></b>	
6.1–Pulse Wave Velocity Determination – The Double Probe.....	66
6.2– Study of the sensors.....	68
6.2.1– Study of Reproducibility.....	68
6.2.2– Study of the crosstalk.....	69
6.2.3– Study of the mass of inertia.....	72
6.3– Signals Deconvolution and Reflections Time Determination.....	73
6.4– Temporal Resolution.....	77
<b><u>7. Conclusions and Future Work.....</u></b>	<b>83</b>
7.1– Conclusions.....	83
7.2– Future Work.....	84
<b>References.....</b>	<b>85</b>
<b>Appendices.....</b>	<b>89</b>



## List of Figures

---

<b>Figure 1</b> Anatomy of heart, interior view.....	4
<b>Figure 2</b> Electrical system of heart.....	5
<b>Figure 3</b> Physiology of veins and arteries.....	6
<b>Figure 4</b> The gradual process of arteriosclerosis.....	8
<b>Figure 5</b> Pressure Waveform.....	9
<b>Figure 6</b> Changes of pressure waveform.....	10
<b>Figure 7</b> Changes in the pressure wave shape due to different diseases.....	11
<b>Figure 8</b> Measurement of PWV with the foot-to-foot method.....	13
<b>Figure 9</b> PWV values for different points of arterial tree.....	13
<b>Figure 10</b> Representation of $AI(\%)$ in pressure waveform.....	14
<b>Figure 11</b> Applanation tonometry, and radial artery pressure waveform recordings.....	15
<b>Figure 12</b> The acquisition unit of Complior®.....	16
<b>Figure 13</b> Methods used for calculating the pulse propagation time.....	16
<b>Figure 14</b> Structure of crystal piezoelectric.....	18
<b>Figure 15</b> Basic equivalent circuits of a PZ sensor.....	19
<b>Figure 16</b> General measurement system architecture.....	20
<b>Figure 17</b> Simple probe.....	21
<b>Figure 18</b> Double Probe.....	21
<b>Figure 19</b> Acquisition Unit of the system.....	22
<b>Figure 20</b> Type of signal processing for general PZ probes – block diagram.....	23
<b>Figure 21</b> Type of signal processing to determination the PTT, through the signal generated by the actuator and the pressure sensor - block diagram.....	24
<b>Figure 22</b> Type of signal processing to determination the PTT, through the signals of pressure sensors - block diagram.....	25
<b>Figure 23</b> Type of signal processing to calculate the PTT.....	26
<b>Figure 24</b> Test bench System I.....	29
<b>Figure 25</b> Scheme of the test bench System I.....	29
<b>Figure 26</b> Raw and deconvolved are represented in the a) and b), respectively.....	30
<b>Figure 27</b> Propagation of wave in the tube and reflection.....	30
<b>Figure 28</b> Test bench System II.....	32
<b>Figure 29</b> Scheme of the test bench System II.....	33
<b>Figure 30</b> Raw data of scanning of tube with PZ sensor, for triangular wave with 100ms of width.....	34
<b>Figure 31</b> Study points of reflection of waves in the tube, marking lines on the most visible components of the wave.....	34
<b>Figure 32</b> Identification the first component of the wave to reach the end of the tube.....	35
<b>Figure 33</b> The maximum detection of the two waves of pressure sensors.....	36
<b>Figure 34</b> Detection of the value of the abscissa to the threshold set.....	36
<b>Figure 35</b> Detection of the value of the abscissa to the threshold set.....	37
<b>Figure 36</b> The maximum detection of the two waves of pressure sensor and actuator.....	37
<b>Figure 37</b> Signals of two pressure sensors, for a Gaussian wave of 50ms, without filtering.....	38

<b>Figure 38</b>	Result of cross correlation between the signals of two pressure sensors.....	38
<b>Figure 39</b>	Signals of two pressure sensors, for a Gaussian wave of 50ms, with filter...	39
<b>Figure 40</b>	Signal of the pressure sensor of the end of the tube and the differential signal of the actuator, without filtering.....	39
<b>Figure 41</b>	Signals of two pressure sensors, for a Gaussian wave of 800ms.....	42
<b>Figure 42</b>	Study of changes in the PWV values calculated by different algorithms.....	43
<b>Figure 43</b>	Study of changes in the PWV values calculated by the algorithm using cross-correlation.....	44
<b>Figure 44</b>	Changes in the PWV for different values of pressure.....	45
<b>Figure 45</b>	Theoretical curve of compliance versus pulse wave velocity (PWV) at 95 mm Hg pressure.....	46
<b>Figure 46</b>	Schematic of the deconvolution process.....	49
<b>Figure 47</b>	Linear sweep generated by the actuator.....	49
<b>Figure 48</b>	The process of obtaining the IR of each sensor - diagram block.....	50
<b>Figure 49</b>	Scheme of the experimental assembly for the IR acquisition.....	51
<b>Figure 50</b>	Methodology to obtain the impulse response of sensor, and IR obtained.....	53
<b>Figure 51</b>	Programmed pressure wave fed to the actuator. Probe output, and the its deconvolution.....	54
<b>Figure 52</b>	Wave of pressure in carotid human.....	54
<b>Figure 53</b>	Impulse response for the integrative simple probe.....	56
<b>Figure 54</b>	Triangular wave with 1s width, acquired by integrative simple probe.....	57
<b>Figure 55</b>	Triangular wave with 1s width, acquired by integrative simple probe placed in 16cm of tube.....	57
<b>Figure 56</b>	Impulse response for the new simple probe.....	58
<b>Figure 57</b>	Programmed pressure wave fed to the actuator. Probe output, and the its deconvolution.....	58
<b>Figure 58</b>	IR for piezoelectric 1 sensor for one sweep 10mHz until 1kHz.....	59
<b>Figure 59</b>	IR for piezoelectric 2 sensor for one sweep 10mHz until 1kHz.....	59
<b>Figure 60</b>	Wave of pressure in carotid human.....	60
<b>Figure 61</b>	Schematic of the convolution process.....	61
<b>Figure 62</b>	The triangular wave, and signal obtained by convolution with IR.....	62
<b>Figure 63</b>	The triangular wave with inflexions, and signal obtained by convolution...	63
<b>Figure 64</b>	The triangular wave with different types of inflexions, and signal obtained by convolution.....	63
<b>Figure 65</b>	The triangular wave, and signal obtained by convolution.....	64
<b>Figure 66</b>	Probe output, and the its deconvolution. Triangular wave of 250ms width..	64
<b>Figure 67</b>	Methodology of calculation of the PWV.....	67
<b>Figure 68</b>	IR for piezoelectric sensor 1 for different testes.....	68
<b>Figure 69</b>	IR for piezoelectric sensor 2 for different testes.....	68
<b>Figure 70</b>	IR for two sensors, actuating only on one piezoelectric.....	69
<b>Figure 71</b>	Acquisition signals in the tube, only one sensor of double probe.....	70
<b>Figure 72</b>	Waveform result of deconvolution for the sensor 1 and sensor 2.....	71
<b>Figure 73</b>	IR for sensor 2, with normal mass and extra mass.....	72
<b>Figure 74</b>	Schematic of release the double probe in the silicone tube.....	73
<b>Figure 75</b>	Schematic representative of the tube and the positions where the signals were acquired.....	73
<b>Figure 76</b>	Deconvolved signal and reflections timings for position 10 cm.....	74
<b>Figure 77</b>	Deconvolved signal and reflections timings for position 100cm.....	75
<b>Figure 78</b>	Deconvolved signal and reflections timings for position 194cm.....	76
<b>Figure 79</b>	Different algorithms used to identify specific part of the pulse signal.....	77

<b>Figure 80</b>	Signal of actuator. Burst of 15 gaussian pulse for 600ms width.....	78
<b>Figure 81</b>	Actuator signal. Local of first point to exceed the threshold. Maximum of signal.....	79
<b>Figure 82</b>	Signal of actuator with the points that mark the limits of analysis of pulses.....	79
<b>Figure 83</b>	The actuator signal convolved and the response of PZ sensors.....	80
<b>Figure 84</b>	Signals for the 13 pulses that are analyzed.....	80
<b>Figure 85</b>	Overlap of results for each segment for cross-correlation for PZ signal1 and the signal from the PZ actuator deconvolved.....	81
<b>Figure 86</b>	Overlap of results for each segment for cross-correlation for PZ signal2 and the signal from the PZ actuator deconvolved.....	81
<b>Figure 87</b>	Signal conditioning box: Electronic Circuit Schematic 1.....	89
<b>Figure 88</b>	Signal conditioning box: Electronic Circuit Schematic 2.....	90
<b>Figure 89</b>	Simple Probe: Electronic Circuit Schematic.....	91
<b>Figure 90</b>	Double Probe: Electronic Circuit Schematic.....	92

## *List of tables*

---

<b>Table I</b> Team members of the Hemodynamic Parameters.....	2
<b>Table II</b> Comparison of commercial devices that measure PWV.....	17
<b>Table III</b> Study of PWV for different algorithms.....	40
<b>Table IV</b> Study of PWV for different algorithms with cross correlation.....	41
<b>Table V</b> Study of PWV for large pulse widths.....	42
<b>Table VI</b> Study of PWV for different algorithms with cross correlation for large pulse widths.....	43
<b>Table VII</b> Study of PWV for different DC pressure levels.....	45
<b>Table VIII</b> Sweep main characteristics.....	52
<b>Table IX</b> Determination of time constant.....	55
<b>Table X</b> Results of PWV obtained by cross correlation for signals of PZ double for different pulse widths.....	82





*Chapter 1***Introduction**

---

***1.1 - Motivation***

In a context where cardiovascular diseases are the leading cause of death in the developed world is urgent to find new methods for determination of risk parameters. As arterial stiffness the most important for this type of pathologies, and in a market where devices that detect this factor are very expensive and difficult to operate, there is a need to develop new sensors and algorithms to access the hemodynamic parameters, non-invasive and low cost.

Arterial stiffness can be assessed by the measurement of the pulse wave velocity, i.e., the velocity at which the pressure wave propagates along an artery. PWV measurement is universally accepted as the most simple, non-invasive, robust and reproducible method to determine arterial stiffness. In fact, the aortic PWV measurement is considered as the ‘gold-standard’ since aorta and its first branches are responsible for most of the pathophysiological effects of arterial stiffness.<sup>[19]</sup>

At present, several commercial devices are available, that provide automated measurement of aortic PWV. The two systems in common use are the Complior® (Colson) and the Sphygmocor® (AtCor), based in piezoelectric (PZ) sensors and arterial tonometry, respectively. Although these devices are based in different sensor technologies, they are both extremely expensive.

This work tries to bring a new concept of probes for the determination of PWV, based on piezoelectric sensors, low cost, easy to operate, high precision and accurate. The probes together with the adequate software analysis tool, information carried in the shape of PZ sensors, with their excellent signal-to-noise ratio and large bandwidth, allow the determination of various hemodynamic parameters.

## 1.2 - Purposes

The main objective of this project is to develop new methods for the assessment of hemodynamic parameters, i.e. it pretends to create low cost, accurate and easy to operate sensors, and the algorithms for the signal-processing. For validation and characterization of sensors it was built test bench which simulate the conditions of an artery. Among the sensors that were developed, have special emphasis on studies of the double probe, which aimed to determine their temporal resolution.

## 1.3 – Hemodynamic project team

This work was developed at *Grupo de Electrónica e Instrumentação* (CEI), one of the research groups of *Centro de Instrumentação* of the University of Coimbra, in the framework of a partnership with *Intelligent Sensing Anywhere*. It is inserted on a project research named *Hemodynamic Parameters*. The following table provides a brief description about the people that make this group work and contribution of each element.

**Table I – Team members of the Hemodynamic Parameters**

Team Members	Main Contribution	Institution
Prof. Dr. Carlos Correia	Scientific and Technical Supervisors	CEI
Prof. Dr. Requicha Ferreira		
Dr. João Cardoso		
Eng. Helena Catarina	PhD student	Assessment of Pulse Wave Velocity CEI/ISA
Eng. Edite Figueiras	PhD student	Assessment of Blood Perfusion in Microcirculation CEI
Eng. Elisabeth Borges	Researcher	Assessment of Hemodynamic Parameters CEI
Tânia Pereira	MSc Students	Assessment of Hemodynamic Parameters Department of Physics - University of Coimbra
Vânia Almeida	MSc Students	Department of Physics - University of Coimbra

### ***1.4 – Overview of the Dissertation***

In order to guide the reading throughout the dissertation a brief summary of the contents of each chapter is presented:

Chapter 2- *Theoretical Background*: approach to the theory that underpins the work, emphasis on the part of physiology, hemodynamic parameters and properties of piezoelectric sensors;

Chapter 3 – *Process Methodology*: a description of the developed hardware and of the procedures for signal acquisition and analysis;

Chapter 4 – *Test Bench*: description of the benches test created for the characterization of sensors, validation of algorithms, and studies to understand the phenomena of wave propagation;

Chapter 5 – *Characterization of probes*: characterization of sensors for each probe and application the algorithm Deconvolution of the signals obtained in the benches test.

Chapter 6 – *Double Probe*: studies with a double probe for the characterization of this type of probe and analysis of algorithms developed to prove the temporal resolution.

Chapter 7 – *Future Work*: ideas and suggestions that may be implemented to improve results.

## Chapter 2

**Theoretical Background**

The basic fundamentals of this work are very different sciences: medicine and exact hard sciences such as physics and maths. All of these are essential to the progress of the studies.

This chapter begins with an approach to the circulatory system, its anatomy, physiology and diseases. Afterwards, a discussion on the relationships between pressure pulse and other hemodynamic parameters is pursued. The last section is devoted to the basic principles of piezoelectric sensors, a key element on the development of this work.

***2.1 - Cardiovascular physiology Concepts***

The circulatory system performs many vital functions. It plays an important role on respiration, nutrition, removal of wastes and poisons, and several other body processes. This system is made up of vessels and muscles that help and control the blood flow around the body. This process is called circulation. The main parts of the system are the heart, arteries, capillaries and veins.

***Cardiac cycle***

The cardiac cycle can be subdivided into two major phases, the systolic phase and the diastolic phase. Systole occurs when the heart's ventricles contract. Therefore, systole results in the highest pressure within the systemic and pulmonary circulatory system. Diastole is the period between ventricular contractions, when the right and left ventricles relax and fill with blood.

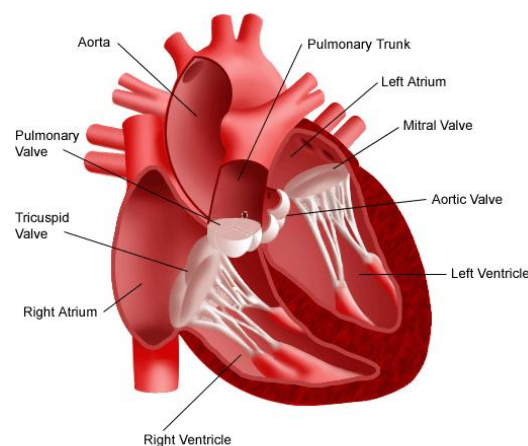


**Figure 1** - Anatomy of heart, interior view.

Adapted from [20]

### The path of blood in the heart

The venous blood returns to the right side of the heart through the caval vein. The blood enters in the right auricle, passes through the tricuspid valve into the right ventricle. It then goes to the lungs, through the pulmonary artery to receive oxygen and blood, flowing back to the left side of the heart to be pumped to the rest of the body. This segment, which involves the lungs, is named the *pulmonary circuit*.

The oxygenated blood returns to the left side of the heart driven by the pulmonary (driving) pressure available for the left auricle and passes into the left ventricle through the mitral valve (bicuspid). The oxygenated blood then leaves the left ventricle to the body through the aorta. The circuit that provides the blood throughout the body is named of *systemic circuit*.<sup>[1]</sup>

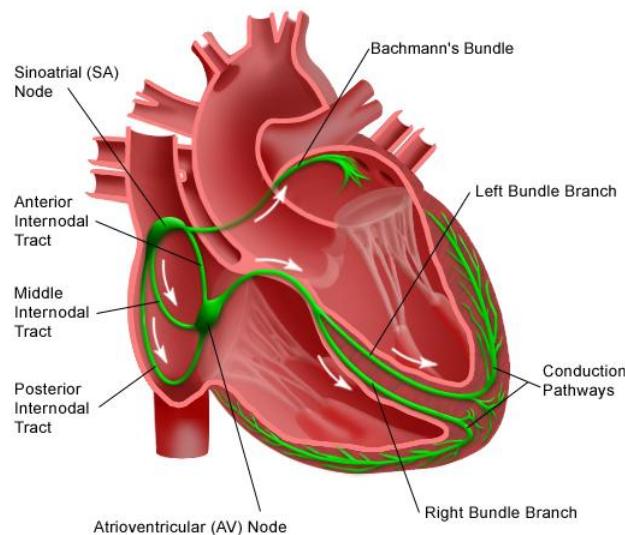


**Figure 2** – Electrical system of heart.  
Adapted from [21]

The heart is, in the simplest term, a pump made up of muscle tissue. Like all pumps, the heart requires a source of energy in order to function. The heart's pumping action comes from an intrinsic electrical conduction system (figure 2). An electrical stimulus is generated by the sinus node, which is a small mass of specialized tissue located in the right atrium of the heart. The sinus node generates an electrical stimulus regularly (60-100 times per minute under normal conditions). This electrical stimulus travels down through the conduction pathways and causes the heart's lower chambers to contract and pump out blood.

### *Circulatory system*

On the systole (period of contraction), blood leaves the heart from the left ventricle and goes into the aorta. The aorta is the largest artery in the body, the blood leaving is full of oxygen, allowing body and brain cells to operate correctly. This blood circulates throughout the body in its system of arteries into the smallest arterioles.

On its way back to the heart, the blood circulates through a system of veins. As it reaches the lungs, the carbon dioxide (a waste product) is removed from the blood and replaced with fresh oxygen, inhaled through the lungs. Each component of this system has specific characteristics to perform its functions (figure 3).

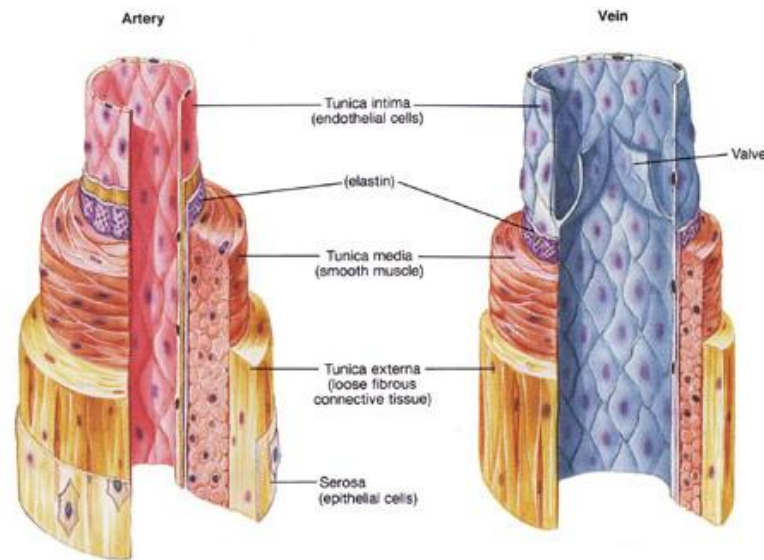


**Figure 3** – Physiology of veins and arteries.  
Adapted from [22]

Arteries carry blood from the heart to all organs. With the exception of the pulmonary arteries, which carry deoxygenated blood to the lungs, all arteries carry oxygenated blood. Arteries receive blood under high pressure from the ventricles. Therefore, they must be able to stretch each time the heart beats, without collapsing under the increased pressure. The walls of arteries consist of three layers, namely, an outer layer, a thick middle layer and an inner layer. The outer layer consists of white fibrous connective tissue which merges to the outside with the loose connective tissue in which artery is found. This helps to anchor the arteries because the heart pumps the blood through the arteries at great pressure. The thick middle layer consists of elastic connective tissue and involuntary muscle tissue. This layer is supplied with two sets of nerves: one stimulating the muscles to relax, so that the artery is allowed to widen, and the other one causing the circular muscles to contract, making the artery become narrower. The inner layer of endothelium consists of flat epithelial cells which are packed closely together and which are continuous with the endocardium (layer of tissue that lines the chambers of the heart). The flat cells smooth the inside lining of the arteries to limit friction between the blood and the lining to a minimum.

Veins carry deoxygenated blood from the organs and tissues back to the heart. The pulmonary veins carry oxygenated blood from the lungs to the left atrium, veins also carry waste products away from the organs and tissues, while the veins associated with the small intestine carry digested food via the liver to the inferior caval vein.

Since veins conduct blood back to the heart, the pressure exerted by the heartbeat on them is much less than in the arteries. Therefore, the middle muscular wall

of a vein is thinner than such of an artery. Veins differ from arteries also in semi-lunar valves, which prevent the blood from flowing backwards.

Large artery stiffness represents the dynamic force opposing ejection (also called impedance), if low, it helps in ejection. The higher the stiffness, the less efficient the diastolic facilitation of ejection. Arterial stiffness is an alteration of the arterial wall properties with multiple causes, some of which are ageing, diabetes, hypertension and medial calcification.

Windkessel theory treats the circulation as a central elastic reservoir (the large arteries), into which the heart pumps, and from which blood travels to the tissues through relatively nonelastic conduits (peripheral arteries). The elasticity of the proximal large arteries is the result of the high elastin to collagen ratio in their walls, which progressively declines toward the periphery.

## ***2.2 - Cardiovascular disease***

Cardiovascular disease (CVD), and the resulting complications, is the main cause of death in developed countries and one of the top five causes in lesser-developed countries. Diseases of the cardiovascular system include those that compromise the pumping ability of the heart, cause failure of its valves, or result in narrowing or hardening its arteries. In addition, toxins and infectious agents may damage the heart and blood vessels. Injury or failure of the cardiovascular system, especially the heart, will also affect the peripheral tissues that depend on the delivery of nutrients and the removal of wastes through the blood vascular system. CVD is a family of diseases that includes hypertension, atherosclerosis, coronary heart disease, and stroke. <sup>[4]</sup>

### **Hypertension (High Blood Pressure)**

Blood pressure is a measure of the force of blood against the walls of arteries. It is recorded as two figures: the systolic pressure over the diastolic pressure. Systolic pressure is the pressure as the heart beats, while diastolic pressure measures the pressure when the heart relaxes between beats.

Blood pressure is normally measured at the brachial artery with a sphygmomanometer (pressure cuff) in millimetres of mercury (mm Hg) and given as systolic over diastolic pressure. Normal blood pressure is less than 140 mm Hg systolic and less than 90 mm Hg diastolic—usually expressed as "140 over 90." [5] However, the normal for an individual varies according to the height, weight, fitness level, age, and health of a person. Blood pressure is normally maintained within narrow limits, but it can drop during sleep or increase during exercise. Hypertension, or high blood pressure, occurs when the force of blood passing through blood vessels is above normal. The increase in pressure forces the blood to hit the blood vessel walls. Hypertension is often known as "the silent killer" because many people do not know they have the condition, and affects 30-40% of the world's population.

## Artherosclerosis

Arteriosclerosis is a general term for a number of diseases in which the arterial walls become thickened and loses elasticity. Some hardening of arteries normally occurs when people grow older. Any vessel in the body may be affected by atherosclerosis; however, the aorta and the coronary, carotid and iliac arteries are the most frequently affected. Atherosclerosis is a type of arteriosclerosis. It comes from the Greek words athero (meaning gruel or paste) and sclerosis (hardness). This is a systemic disease which involves a tunica intima of bigger arteries. It involves deposits of fat substances, cholesterol, macrophage cells, cellular waste products, calcium and fibrin (a clotting material in the blood) in the inner lining of an artery (figure 4). The build-up that results is called plaque. <sup>[2][3]</sup>

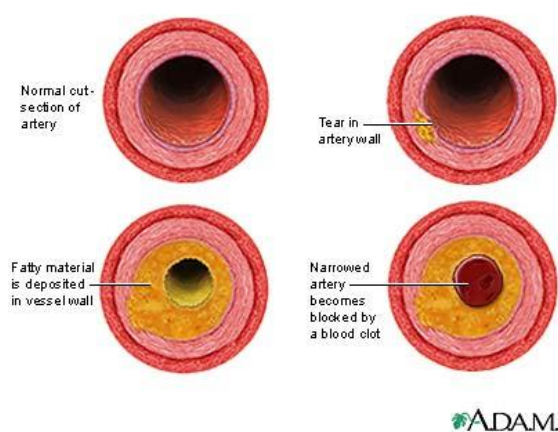


**Figure 4** – The gradual process of arteriosclerosis. <sup>[24]</sup>

## Coronary Artery Disease

Coronary artery disease (CAD) refers to any of the conditions that affect the coronary arteries and reduces blood flow and nutrients to the heart. Atherosclerosis is the primary cause of CAD. Controlled risk factors associated with CAD include hypertension, cigarette smoking, elevated blood lipids (e.g., cholesterol, triglyceride) and low levels of HDL, a high-fat diet (especially saturated fats and trans-fatty acids), physical inactivity, obesity, diabetes, and stress. Lifestyle changes can assist in prevention of CAD. Uncontrolled risk factors include a family history of CAD, gender (higher in males), and increasing age.

## Stroke

Stroke, or a cerebrovascular accident (CVA), occurs when the brain does not receive sufficient oxygen-rich blood through blood vessels or when a blood vessel bursts. A stroke may result from blockage of the blood vessels due to a blood clot (ischemic) or from ruptures of the blood vessels (hemorrhagic bursts). Uncontrolled hypertension is a major risk factor for strokes.



### 2.3 - Pressure waveform

The contraction of left ventricle generates a wave pressure which propagates along of circular system. The wave detected in carotid has one systolic peak (A) and some interference of the different factors (figure 5a). One of them is originated by bifurcation of vessel, in the femoral,(figure 5b) part of component suffer reflections and originated the backward wave that is going to add and increase the forward wave (B). The downward deflection observed on the downstroke of an arterial pressure waveform is a *dicrotic wave* (D). It represents the closure of the aortic valve at the onset of ventricular diastole.

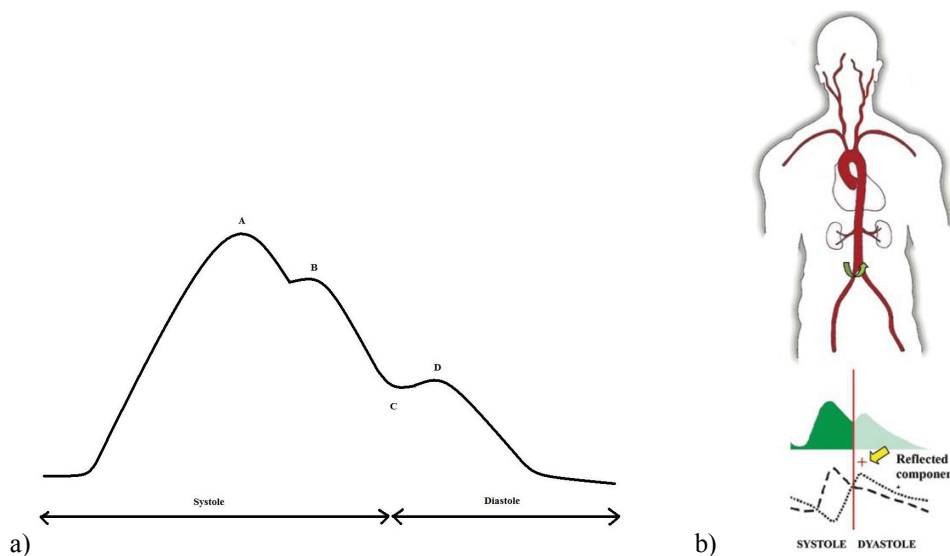


**Figure 5** –a) Pressure Waveform.  
 A- Systolic peak; B- Reflected wave;  
 C- Dicrotic incisura; D- Dicrotic wave.  
 b) Origin of reflected component.  
 Adapted from [23]

The arterial pressure waveform is the result of an interaction between the heart and the arterial system. Therefore, the magnitude and shape of the pressure pulse are affected by changes in aortic (or other vessels) or alterations in cardiac function. Thus, the measured carotid pressure consists of incident and reflected waves, and their magnitude and timing determine the aortic wave contour. At young ages, the reflected waves arrive in the aorta, in the late systole. With ageing and/or hypertension, the magnitude and speed of the reflected waves increase, and they add to the forward wave in the early systole. [7]

The arterial wall stiffness creates an early aortic pulse-wave reflection that causes a systolic blood pressure increase and a diastolic blood pressure decrease.

The pressure waveform changes from person to person, varies along the arterial tree (figure 6a), and it is age-dependent (figure 6b). An influence of vascular aging on the contour of the peripheral pressure and volume pulse in the upper limb is also well recognized. In part, this change in pulse contour may be due to an increased large-artery stiffness, with an increase in pulse wave velocity decreasing the time taken for pressure waves reflected from the periphery of the circulation (mainly from the lower body) to return to the aorta and then to the upper limb. Consequently, reflected waves arrive earlier in the cardiac cycle. [12]

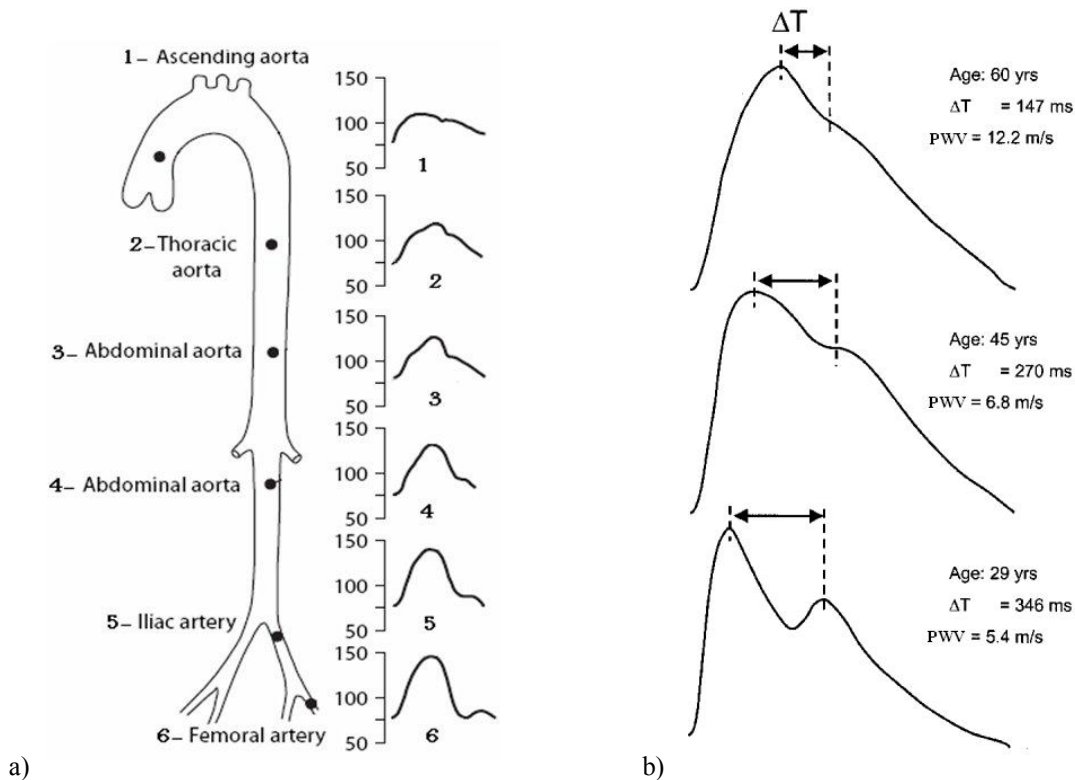


**Figure 6** – Changes of pressure waveform.

- a) The pressure waveform changes thorough descending arteries. [28]
- b) Typical waveforms showing that the characteristics change with age. Adapted from [29]

Amendments to the carotid pulse may represent specific cardiovascular changes. Therefore, cardiac pulse shape analysis can provide information on the patient's clinical condition, allowing the recognition of a particular pathology of the cardiovascular system (figure 7).<sup>[13]</sup>

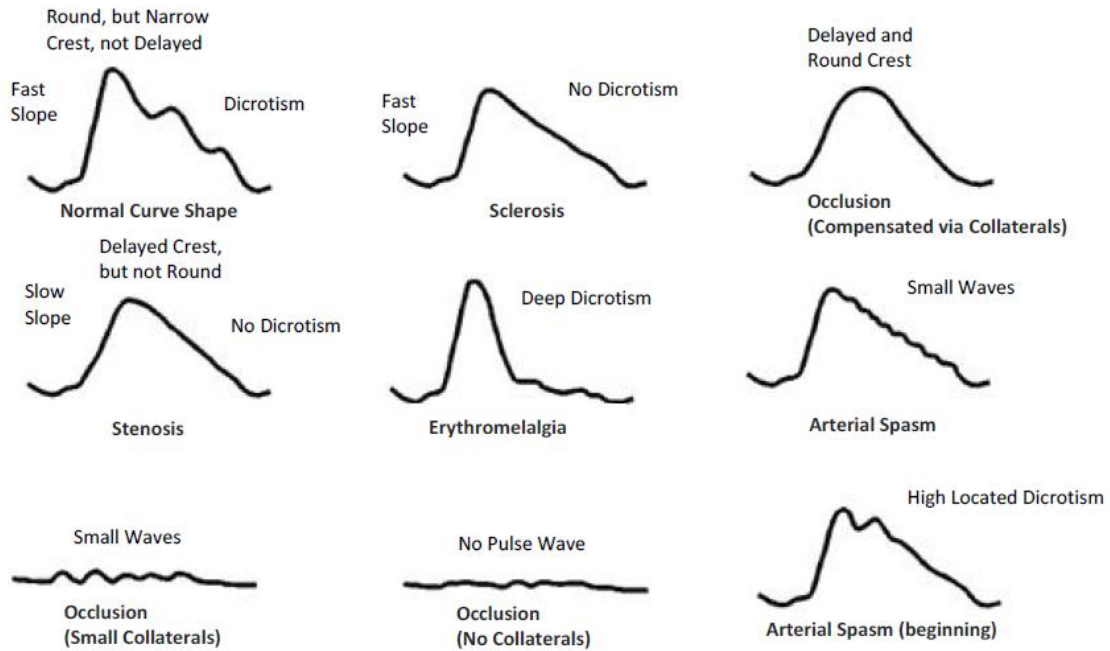


**Figure 7** – Changes in the pressure wave shape due to different diseases. Adapted from [13].

## 2.4 - Hemodynamic parameters

Wave propagation through the arterial system changes with age and disease state. There has been developed a number of techniques to measure blood velocity and vessel wall motion from which we can calculate aortic PWV, augmentation index (AI), and forward and backward waves. With age or atherosclerotic PWV and AI are increased, peripheral resistance and arterial compliance are decreased, and wave reflections are enhanced. We found that the initial decreased of carotid velocity is caused by peripheral reflections, and that increased of velocity in the aortic arch in patients is caused by enhanced carotid reflections returning to the heart and travelling forward in the aorta.

### 2.4.1 - Pulse Wave Velocity

Pulse wave velocity is the velocity at which pressure waves propagate along the vessels. It is also a marker for arterial stiffness. The loss of elasticity of the arterial wall increases the velocity of the blood flow through the arterial system.

PWV is a measure of regional arterial stiffness of the arterial territory between the two measurement sites. This parameter is related to the elastic modulus ( $E$ ) of the arterial wall (which represents the intrinsic wall stiffness), and the arterial geometry (thickness:  $h$  and radius:  $R$ ) and blood density ( $\rho$ ). The first relationship was formulated by Moens and Korteweg and expresses:

$$PWV = \sqrt{(Eh/2R\rho)} \quad (1)$$

Later on, Bramwell and Hill described the association in terms of relative change in volume ( $DV/V$ ) and pressure ( $DP$ ) during ex vivo experiments:

$$PWV = \sqrt{(\Delta P \cdot P / \Delta V \cdot \rho)} \quad (2)$$

It is to be noticed that PWV is a direct measurement of arterial stiffness since it is the square value of inverse of distensibility. In this aspect, it differentiates itself from indirect methods based on the models of circulation. The assessment of PWV involves measurement of two quantities: transit time ( $\Delta T$ ) of the arterial pulse along the analyzed arterial segment and distance ( $D$ ) between both recording sites (figure8).<sup>[6]</sup>

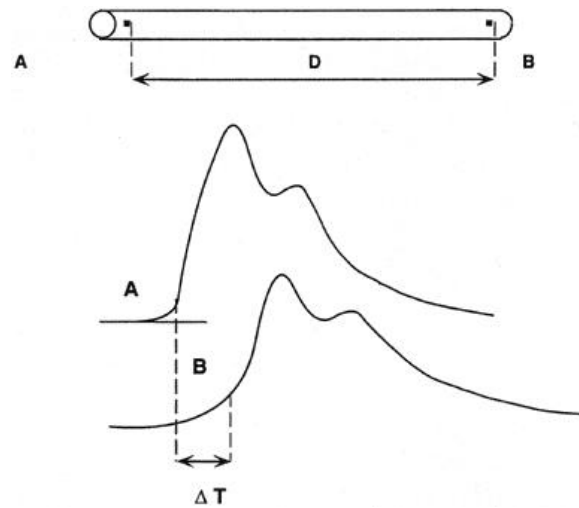


**Figure 8** - Measurement of PWV with the foot-to-foot method. Adapted from [25].

The changes of pulse wave velocity depending on the vessel to consider. With the increase of the distance from the heart there is a progressive increase in the wavefront velocity of the pulse wave. For this reason, the peripheral vessels have PWV of around 10m/s, and the PWV of the ascending aorta is 5.2m/s (figure 9).

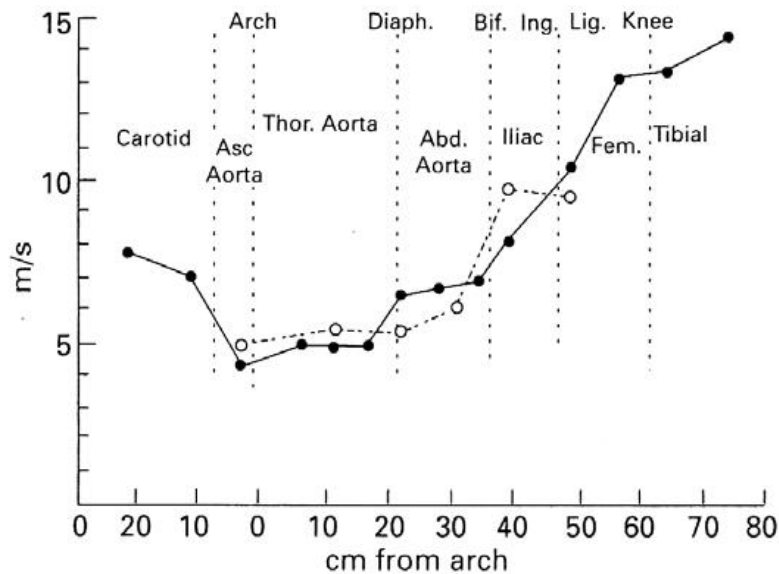


**Figure 9** – PWV values for different points of arterial tree. Measured indicated by broken line are in humans, in dog are indicated by continuous line. [30]

### 2.4.2 - Augmentation Index

One of the most useful parameters of pressure wave analysis is the augmentation index, which measures the interaction of the forward pressure wave with reflected waves from the distal circulation. Analysis of AI and associated wave functions show differences related to cardiac risk, presence of diseases, effects of drug administration, and overall mechanical properties of the vasculature.

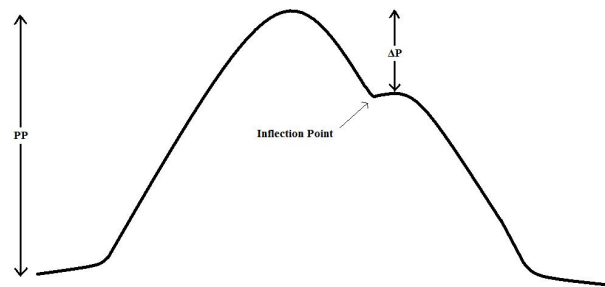


**Figure 10** - Representation of AI (%) in pressure waveform.

The timing of the reflected wave can be determined by measuring the time interval between the basis of the pressure wave and the inflection point. This point occurs at the beginning of the secondary pressure rise (the reflected wave) and represents the time of travel of the pressure wave from the heart to the periphery and back. The  $PP$  is the central pressure pulse and  $\Delta P$  is the difference between the early and late pressure peaks, i.e. the systolic wave and the reflected wave (at the inflection point). The augmentation index, defined as the ratio of  $\Delta P/PP$ . With ageing, arterial stiffness and, hence,  $PWV$  are greater, causing the reflected wave to arrive earlier, increasing pressure amplitude and originating  $AI$  higher values. <sup>[9]</sup>

## 2.5 – State of the art

The ‘gold Standards’ for PWV clinical evaluating are the Complior® and the Shpymocor® systems, both based on pressure sensors. Understanding that the offer is on the market and what is the method of operation is a key step towards the creation of new devices, capable of detecting different hemodynamic parameters.

The SphygmoCor® system is a non-invasive diagnostic technology that enables pulse-wave analysis of the central ascending aortic pressure wave. The SphygmoCor® system allows a peripheral arterial pressure waveform to be obtained by applying an arterial applanation tonometer to the wrist. The tonometer partially compresses the radial artery and records a pressure wave over several cardiac cycles. This pressure wave is calibrated to brachial cuff blood pressure measurements. The averaged peripheral waveform is then converted to an ascending aortic waveform using a generalised mathematical transfer function. The data collection screen allows the operator to see the peripheral signal and displays the last 10 seconds of data.



**Figure 11** –Applanation tonometry, and radial artery pressure waveform recordings. <sup>[26]</sup>

There are three registered SphygmoCor® systems on the market; all are listed with the Therapeutic Goods Administration (TGA) on the Australian Registry of Therapeutic Goods under the listing number L64615. These systems are approved for marketing in Australia, the United States of America, the European Union, Korea, China and Japan. The *SphygmoCor Px* system is a non-invasive method of measuring peripheral arterial pressure waveforms that, through the use of a validated transfer function, allows calculation of the ascending aortic pressure waveform. The *SphygmoCor Mx* system measures radial waveforms and provides a real-time method of deriving aortic pressure waveforms. The *SphygmoCor Vx* system uses an electrocardiogram (ECG) in combination with a tonometer to measure the pressure waveform sequentially at two peripheral artery sites. <sup>[10]</sup>

The Complior® is produced by Artech Medical (Pantin, France). This device measures pulse wave velocity by placing two small recording transducers on top of the skin (figure 12). For this it uses four piezoelectric pressure sensors (carotid, radial, femoral, and distal) for simultaneous arterial waveform measurement. The sensors allow for measurement of PWV at various arterial segments: one transducer is positioned at

the carotid artery and the other on the upper thigh at the femoral artery, for obtaining the aortic stiffness. There are three more possible conformations, which provide different clinical information. Those are carotid-radial (upper extremity arterial stiffness), brachial-radial (forearm arterial stiffness), and femorotibial (lower extremity arterial stiffness). The Complior® calculates the time it takes for the pulse wave to travel the distance between those two recording sites. In addition, estimated central aortic pulse pressure and an arterial stiffness index are measured. The device connects to a computer and uses a USB port for its power source. <sup>[11]</sup>



**Figure 12** –The acquisition unit of Complior ®. <sup>[27]</sup>

The 2 systems in common use, the SphygmoCor (AtCor) and Complior (Artech) differ with respect to their sensor technology and the algorithm used for calculating the pulse propagation time. The SphygmoCor device uses an arterial tonometer for recording pressure waveforms. Propagation time is measured from the foot of the carotid waveform to that of the femoral waveform using sequential recordings referenced to the ECG (Figure 13 a). In the Complior system, carotid and femoral waveforms are recorded simultaneously using mechanotransducers, and timing is referenced to the point of maximum systolic upstroke (Figure 13 b). <sup>[16]</sup>

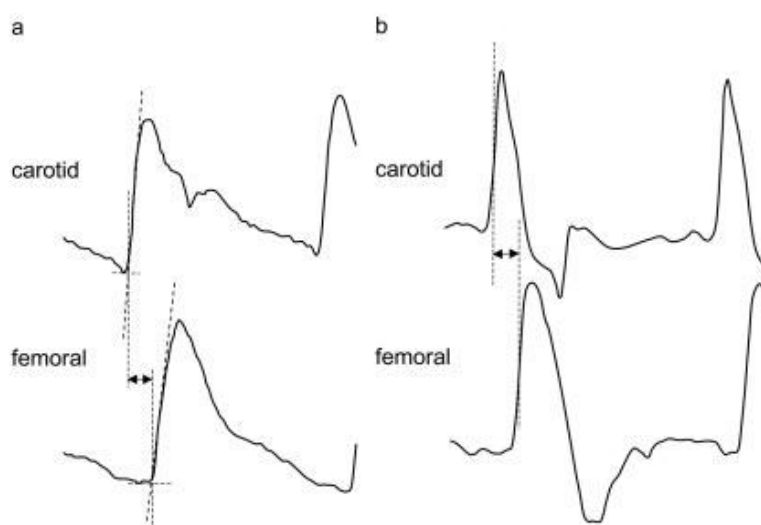


**Figure 13** – Methods used for calculating the pulse propagation time.

- a) Measurement of carotid to femoral propagation time using the intersecting tangent foot-to-foot algorithm as used in the *SphygmoCor* system.
- b) Measurement of propagation time from the point of maximum upstroke of the signal as used in the *Complior* system. <sup>[16]</sup>



Complior and SphygmoCor do not differ significantly in calculating transit time, differences in pulse wave velocity obtained using the two devices are attributable to differences in calculating traveled distance.<sup>[17]</sup> The main differences for these two devices are summarized in the next table.

**Table II – Comparison of commercial devices that measure PWV<sup>[18]</sup>**

Device	Manufacturer	Measure	Pros	Cons
SphygmoCor	AtCor Medical (www.atcormedical.com)	PWV <i>via</i> applanation tonometry	Measures central PWV and AI	Limited by technical difficulty in obtaining measurements
Complior	Artech Medical (www.artechmedical.com)	PWV two mechanotransducers	Obtains central PWV, taking simultaneous measures at carotid and femoral sites	Digitized waveforms create difficulty in discerning foot of the wave

## 2.6 - Piezoelectric sensor

The word piezo comes from the Greek word piezein, meaning to press or squeeze. Piezoelectricity refers to the generation of electricity or of electric polarity in dielectric crystals when subjected to mechanical stress and conversely, the generation of stress in such crystals in response to an applied voltage. In 1880, the Curie brothers found that quartz changed its dimensions when subjected to an electrical field and generated electrical charge when pressure was applied. <sup>[15]</sup>



**Figure 14-** Structure of crystal piezoelectric. <sup>[31]</sup>

Each crystal cell has an electric dipole, and the cells are oriented such that the electric dipoles are aligned (figure 14). Again, this results in excess surface charge which attracts free charges from the surrounding atmosphere making the crystal electrically neutral. If a sufficient force is applied to the piezoelectric crystal, a deformation will take place. This deformation disrupts the orientation of the electrical dipoles and creates a situation in which the charge is not completely cancelled. This results in a temporary excess of surface charge, which subsequently is manifested as a voltage which is developed across the crystal.

In order to utilize this physical principle to make a sensor to measure force, we must be able to measure the surface charge on the crystal. Two metal plates are used to sandwich the crystal, making a capacitor. As mentioned previously, an external force causing a deformation on the crystal results in a charge which is a function of the applied force. In its operating region, a greater force will result in more surface charge. This charge results in a voltage

$$V = Q_f / C \quad (3)$$

Where  $Q_f$  is the charge resulting from a force  $f$ , and  $C$  is the device's capacitance.

A piezoelectric sensor is modelled as a charge source with a shunt capacitor and resistor, or as a voltage source with a series capacitor and resistor. The charge produced depends on the device's piezoelectric constant. The capacitance is determined by the area, the width, and the dielectric constant of the material, the resistance accounts for the dissipation of static charge.

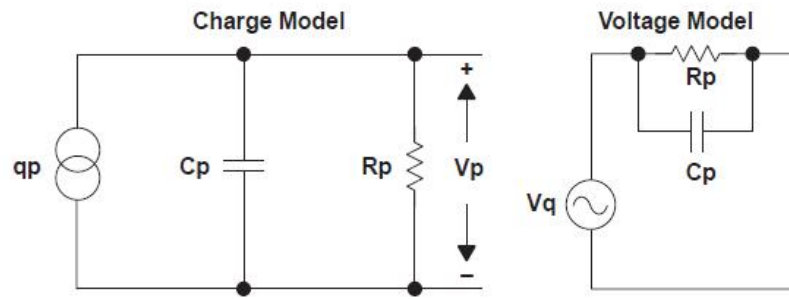


Figure 15– Basic equivalent circuits of a PZ sensor. <sup>[32]</sup>

The external electrodes and the charge arrangement within the piezo material give the piezo element a capacitance,  $C_p$ . As a result the equivalent circuit for a piezo element is the capacitance,  $C_p$ , and internal voltage,  $V_p$  arranged in series as shown in figure 15.

## Chapter 3

Process Methodology

This chapter starts by addressing the work that was done previously, in the instrumentation area. It also introduces the developed main tool for signal processing, the PZ PulScope.

### 3.1 - Introduction

The piezo sensors have been widely exploited, however, in the form of little functional probes. At the beginning of this project, had been thoughtful new settings for both the single probe and for the double probe.

With the probes based on piezoelectric sensors it could be easily captured the pressure wave in a human carotid artery. By means of the impulse response of each sensor, the deconvolution based algorithms allowed to find a pressure wave through the signal from the sensor PZ. The Deconvolution was the method that showed better results to get the signal into the sensor. <sup>[14]</sup>

### 3.2 - Acquisition System

The new probes developed are of two types, simple probe and double probe. In addition to the sensors, it was developed an acquisition box composed of a circuit for signal conditioning and a module NI that acquires and sends the data to the PC via USB. Data are recorded using NI software and then processed in Matlab.

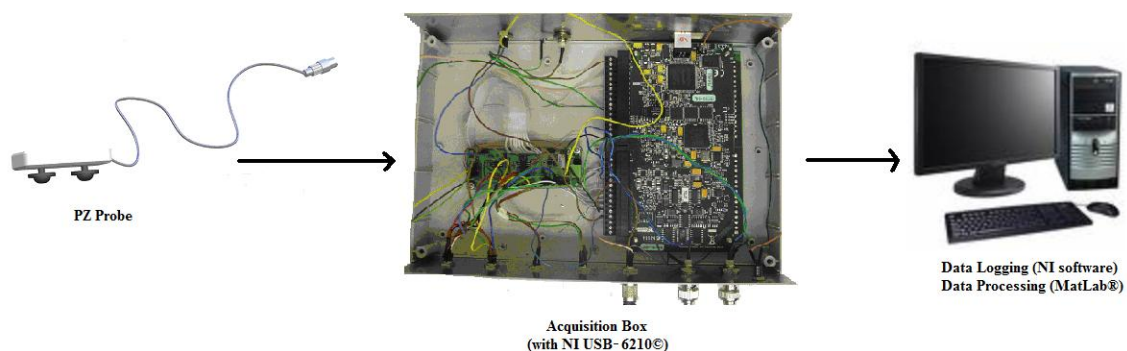


Figure 16 - General measurement system architecture.

### 3.2.1 – Probes

The probe uses a typical circularly shaped sensor (MuRata®), based on a simple layer printed circuit board (*PCB*) the sensor signal PZ is amplified. On the piezoelectric disc pasted a screw that allows us to hold a “mushroom-shaped” piece made of Polychloroethanediyl (PVC) which is the interface of the sensor. This whole structure is in a box, which has a hole leaving the “mushroom”.



**Figure 17**– Simple probe.

The Double probe consists of two dual piezoelectric sensors that distance between them of two centimeters, and are placed in the same PCB. All the electronic structure of the probe is protected by a plastic box in which we made two holes where two mushrooms out, that are responsible for interfacing the sensors.



**Figure 18**– Double Probe.

### 3.2.2 - Acquisition Unit

The acquisition box supports all types of sensors mentioned above and others that may be used in the future. There is an entry for the double probe, which is common with the entry the simple probe, an entry for accelerometric sensors, one for sensing the respiratory signal, two entries for pressure sensors, one for the synchronism of Agilent, two outputs for the oscilloscope manipulation and a USB connection.

The box consists of a signal conditioning circuit and a data acquisition system. Initially it was powered by the PC through the USB cable-15V / +15 V, however it was found that this was a source of noise to the signals, so it had to be replaced by a voltage source that greatly minimized this drawback.

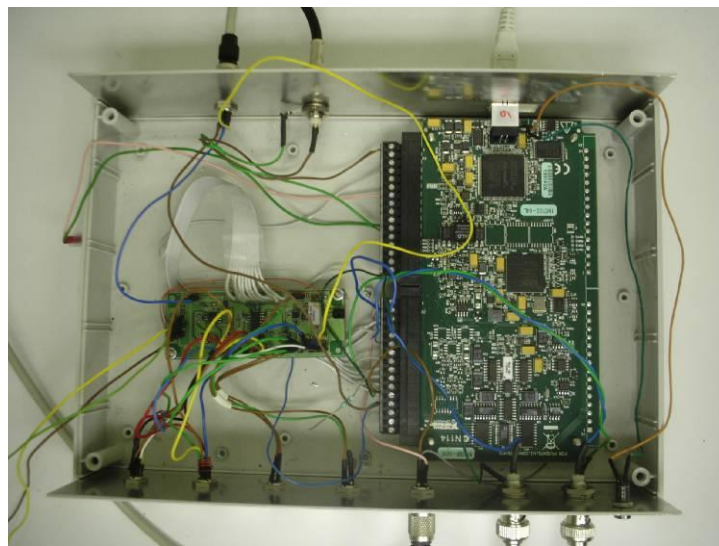


Figure 19 – Acquisition Unit of the system.

#### 3.2.2.1 - Circuit signal conditioning

The circuit is designed to amplify the signals originated by the hemodynamic probes and to convey them to a data acquisition module.

The main functions of this circuit are: piezo probe amplifier, 3 axis accelerometer amplifiers, respiration detector and power supply. The circuit also supports an external switch intended to start the acquisition or the logging of signals. <sup>[33]</sup>

#### 3.2.2.2 - DAQ Module

The DAQ module used in the acquisition unit is the NI USB-6210©. It has 16 analog inputs and can sample up to 250KSps.

This device comes with a driver software, the NI-DAQmx©, running on Windows Operative System®, for interactive configuration and programming interfaces (ex. DAQ Assistant). Besides, a copy of NI LabVIEW SignalExpress LE data-logging software, a configuration software package, is also provided and used for data logging. The logged data can be saved in a .txt format for further processing in *Matlab*.

### 3.3 - Clinical Trials

#### 3.3.1 - Data Acquisition

The experimental data obtained were mainly of two types: from test bench and from human carotid. The experimental procedure is quite different in these two cases, which will be described separately.

Data was acquired under the following protocol for human carotids: start up the process, defining the attributes of the task for the data to be acquired, the patient sits in a comfortable position, waiting a few minutes so that all his pace pulsatory stabilize, then the sensor is placed in the area of the carotid artery, after having found the signal to start acquiring, it is then exported in the .txt to be processed.

In the case of data collected in the test bench, the procedure will begin by defining the attributes of the task in this situation are purchased the channels of the sensor in question, the two pressure sensors, and the signal generated at Agilent, the pressure is put the desired level DC for the test, sets up the waveform generated at Agilent, and the sensor is placed in the tube. The data is saved and exported to files .txt to be processed.

#### 3.3.2 - Data Processing

The acquired data are then processed and analyzed in Matlab. The most important algorithms developed are explained below in a brief outline by block diagrams.

##### 3.3.2.1 – General Algorithm

The algorithm used for signals collected in the test bench or in human carotid was deconvolution. In order to achieve the original pressure wave signal, it is essential to know the impulse response of the sensor, so that it can be deconvolved with the output of piezoelectric sensor.

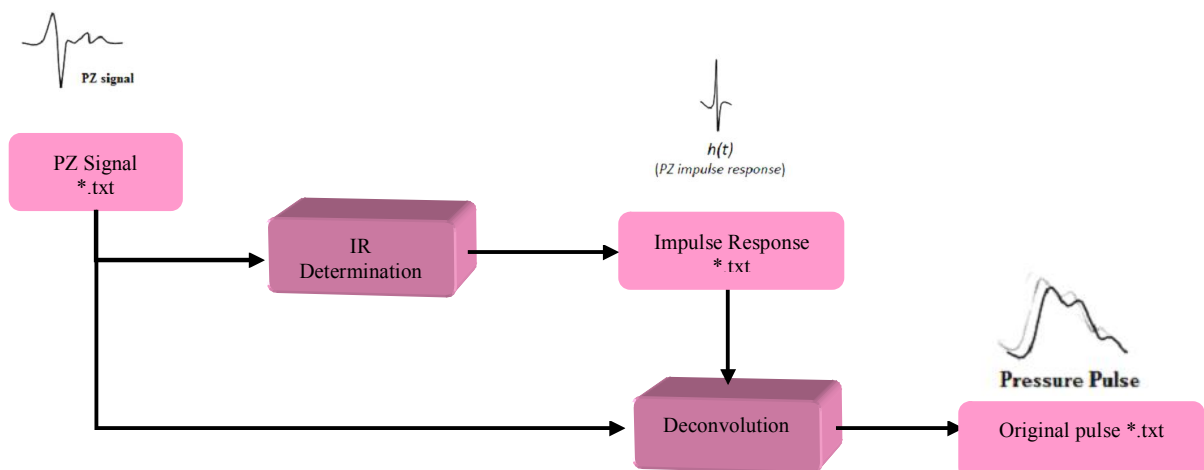
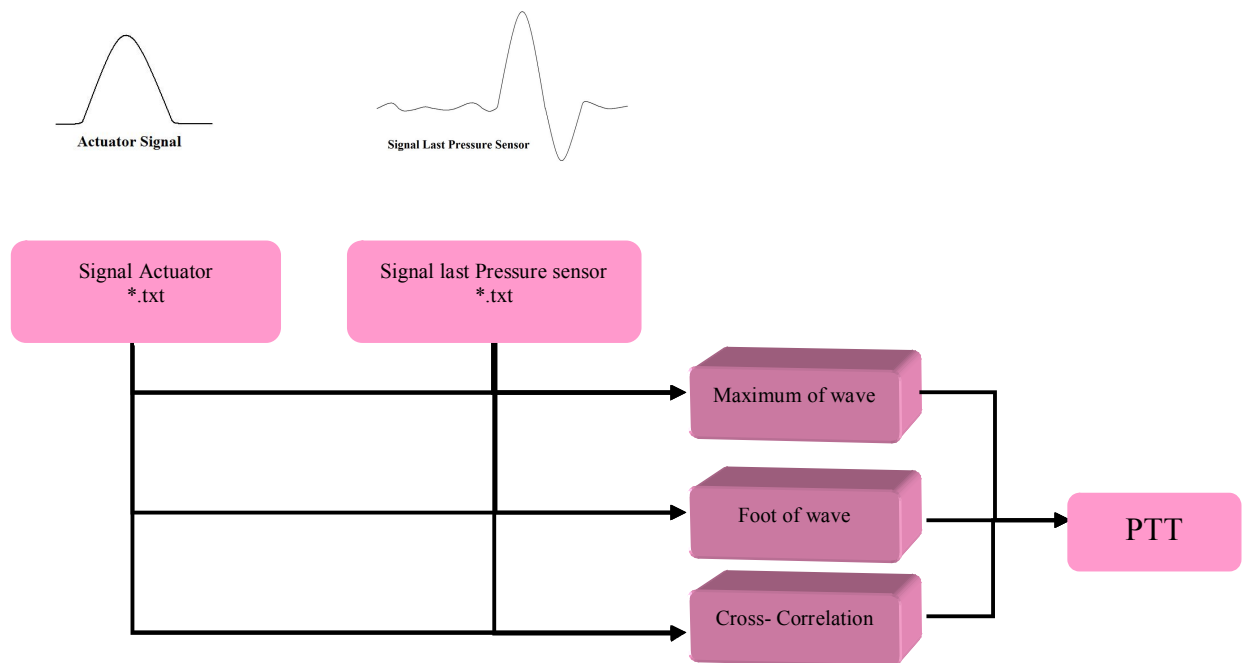


Figure 20– Type of signal processing for general PZ probes – block diagram.

### 3.3.2.2 – PWV Algorithm in test bench

In order to calculate the velocity inside the test bench tube algorithms based on the actuator waveform and piezo signal output were developed. The time difference between the two waves, correspond to the pulse transit time (PTT). The ratio value of the distance between the two sensors, allows us to obtain the PWV. This algorithm uses the wave generated by the actuator and the shape of the signal received by the pressure sensor.



**Figure 21**–Type of signal processing to determination the PTT, through the signal generated by the actuator and the sensor of pressure - block diagram.



The same based algorithms were also applied to another types of signals, for two sensor of pressure, for determination the pulse wave velocity.

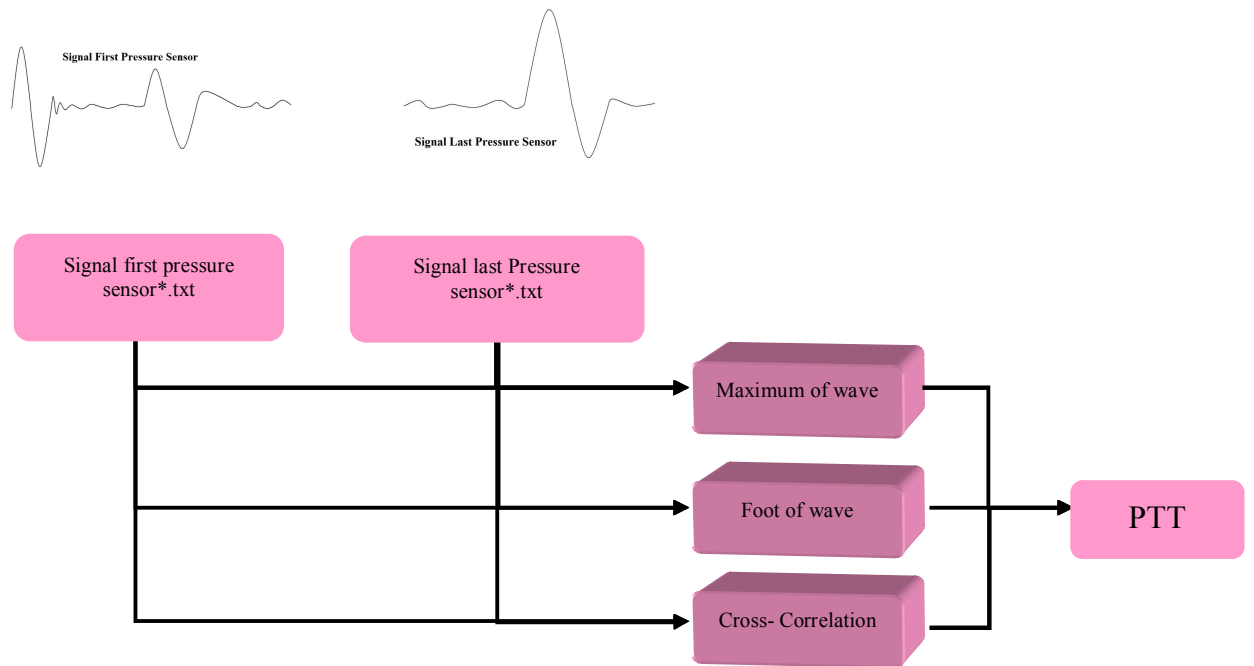


**Figure 22**– Type of signal processing to determination the PTT, through the signals of pressure sensors - block diagram.

### 3.3.2.3 – Double Probe Algorithms

For the double probe were developed algorithms for transit time resolution determination. The algorithms based on the signal received by each of the piezoelectric sensor probe, were intended to calculate the time difference between these two signals, i.e. the PTT.

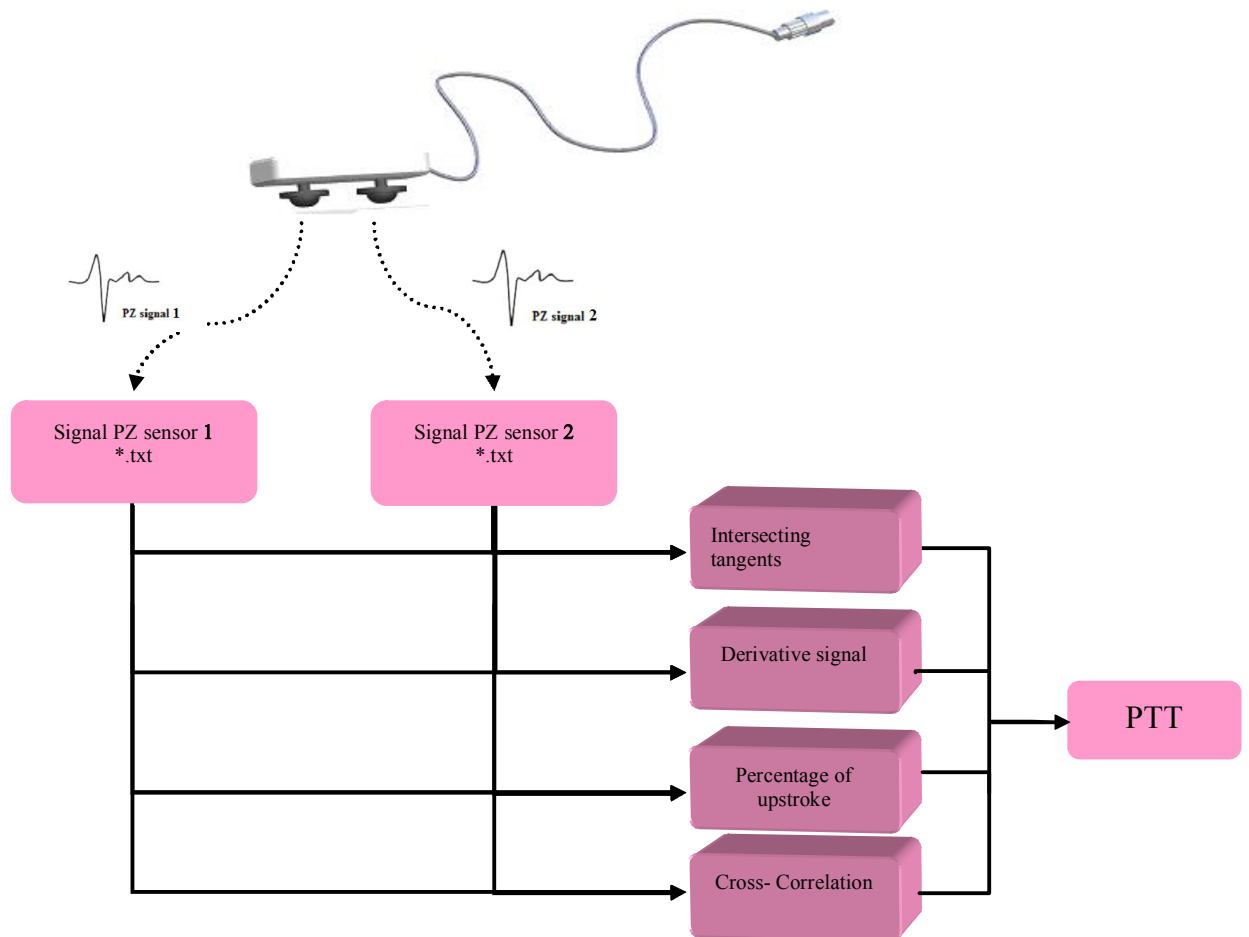


**Figure 23**– Type of signal processing to determination the PTT through signals received by two of the piezoelectric probe double - block diagram.

### ***3.4 – Discussion***

The Deconvolution has proven the best method for obtaining the input signal of the sensor <sup>[14]</sup>, but it requires sensor characterization. That is to say their impulse response determination.

The various algorithms developed for the calculation of the PTT and the study done for the results obtained by each, allowed us to choose the most reliable, that is to say the one that could be taken as the "gold standard".

For the algorithms of the double probe tried to explore what exists in the literature for calculating the time delay but most of them do not produce good results, since the signal received by the sensors is complex because of overlapping of reflections.

*Chapter 4***Test Bench**

---

This chapter discuss two models of bench developed for the characterization of the sensor, which allowed us to study phenomena of propagation of the incident wave and reflected wave.

***4.1 - Introduction***

A test system capable of replicating some of the basic properties of the cardiovascular system, especially the ones related with the propagation of the arterial pressure wave (APW), is a powerful tool in the development of those probes and in the validation of the various algorithms that extract clinically relevant information from the data that they collect.

This work describes a new test bench system, based on the combination of a programmable pressure wave generator with a flexible tube, capable of emulating some of these properties.

Two versions of the system have been set up: one that generates a short duration pulse-like pressure wave from an actuator operated in a switched mode, appropriate to characterizing the system itself. A second one using a long stroke actuator, operated under program control, capable of generating complex cardiac-like pressure waveforms. This configuration finds its main use in algorithm test and validation.

***4.2 - Test Bench System I******4.2.1 - Instrumentation***

In the first assembly an 80 cm long silicone rubber tube (Lindemann, 8 mm inner wall thickness) is kept under a constant DC pressure level of 50 mm Hg by piston at one of its extremity, monitored by manometer (Honeywell S&C - 40PC015G1A ) as can be seen in figure 24.

The dynamic pressure wave is generated at the other extremity of the tube, by the combination of an actuator and a high voltage power driver. A rubber membrane interface terminates the tube at this end.

The stroke of actuator is a 70  $\mu\text{m}$  (Piezomechanik, PSt-HD200/10/45 VS 15) driven by a power switcher (Piezomechanik, HVP200/50) controlled by an Agilent 33220A arbitrary waveform generator that also delivers the synchronizing signal that triggers the data acquisition system, the module used in the acquisition unit is the NI USB.6210©, can accommodate up to 16 single ended or 8 differential 16 bit resolution data channels with a combined sampling rate up to 250KSps. <sup>[34]</sup>

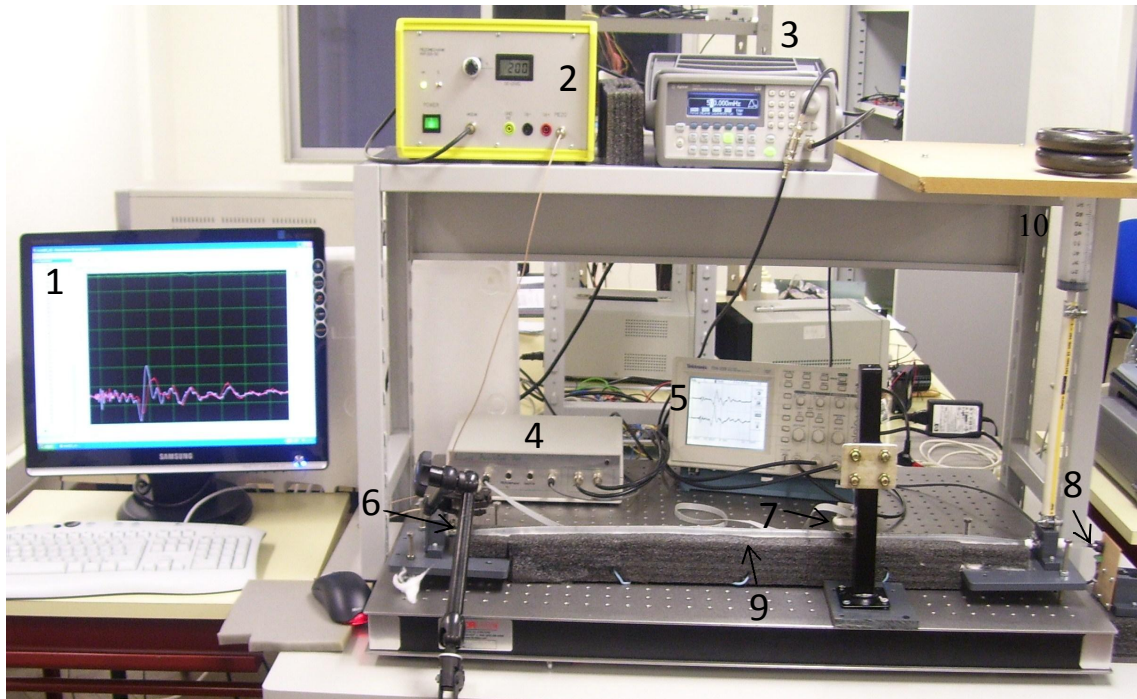


**Figure 24 – Test bench System I.**

- 1- Personal Computer; 2- Switcher HVP; 3- Pulse Generator (Agilent);
- 4- Acquisition Box; 5-Oscilloscope; 6- Pz Actuator; 7- PZ Probe;
- 8- Pressure Sensor; 9- Silicone Tube; 10- Piston DC level pressure.

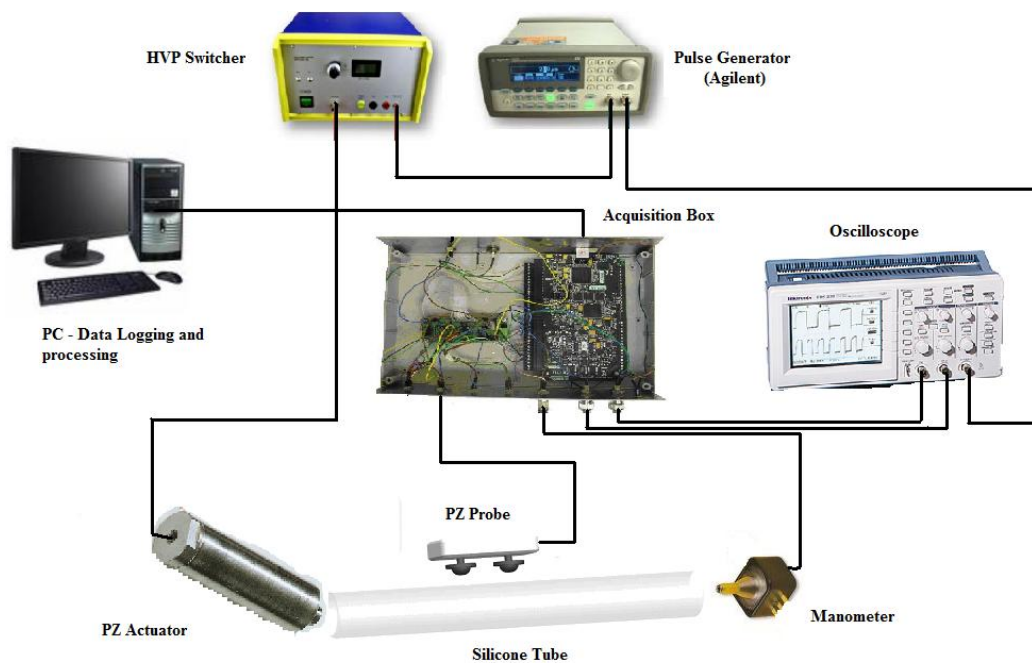


**Figure 25 – Scheme of the test bench System I.**

The oscilloscope placed in the assembly, shows the signals from the sensor, synchronized with the trigger of the actuator, through the link pulse generator. (figure 25)

### 4.2.2 - Study of waves propagation

With this assembly it can be study the propagation of pressure wave, the incident and the different reflections that originate at the ends of the tube. The pressure waves were generated by the actuator, in position -4 cm, and the simple *PZ* sensor placed on the tube was a acquired of 2 in 2cm of distance. The signals detected by piezoelectric sensors allow us to reconstruct the wave phenomena.

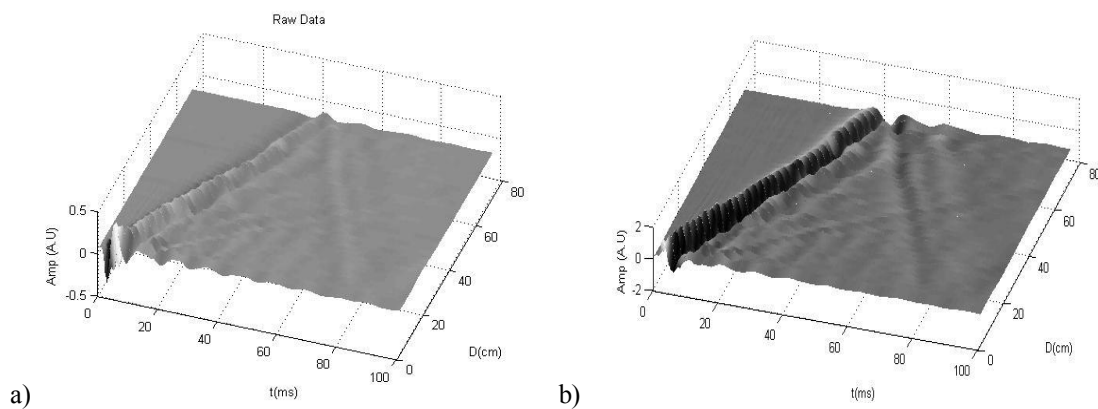


**Figure 26**– Raw and deconvolved data are represented in the a) and b), respectively.

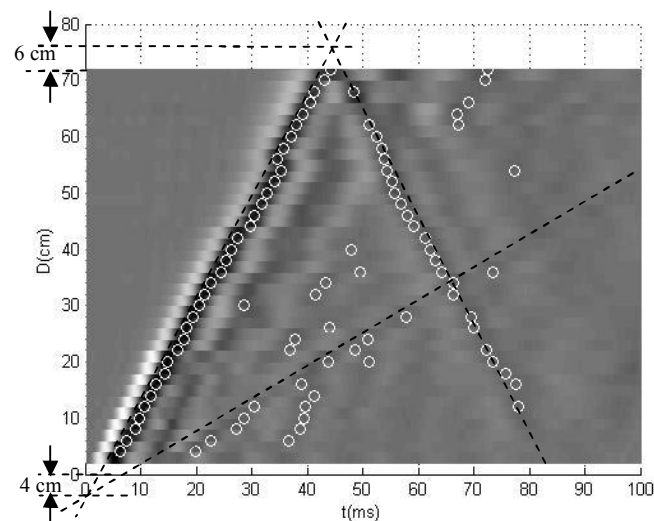


**Figure 27** – Propagation of wave in the tube and its reflection. Peak detection and dashed lines support discussion developed (see text).

The mesh of the data acquired by the *PZ* sensor enabled to see that there are reflected in the end of tube. Furthermore, the scanning of the signal along the tube allowed to determination the velocities within the tube, as the figure can know for sure that the distances to points of reflection and timings of these. The lines converge precisely in the physical reflection site located at 6 cm of the end of the flexible tube. Likewise, the longitudinal and transversal components cross together in the point where they originate, -4 cm. These lengths exactly match the ones of the structures that hold the two tops of the tube (figure 24). The incident wave takes about 45ms to go the 84cm tube so it can be concluded that its speed is of the order of 19m / s.

### 4.2.3 – Conclusions

This assembly allowed the comprehension of wave phenomena that is to say the several reflections to mitigate, to develop methodologies for the study of these phenomena, the calculation of velocities, characterized the PZ sensors and conclude on the capability of our sensors capturing the wave of pressure generated within the tube.

However, due to the dimensions of the tube and the reflections that occur at the ends of this, there are limitations on the width of the pulses to study, since the reflected waves will add to the received signal, preventing the acquisition of waves free of reflections. In parallel, the actuator used in this assembly was not linear, and only allowed the generation of *Dirac* pulses necessary for the characterization of sensors, which as shall see further ahead, it is experimentally difficult to find the impulse response by this method.

Consequently and in order to explore other pulse widths it was required for an assembly with a larger tube, and a linear actuator. This actuator could be capable of generating waves of different shapes and different pulse widths, and that could execute sweeps in frequency, allowing a characterization more efficient use of our sensors. In this context, a new assembly was developed to overcome the limitations that were identified in the previous.

### 4.3 - Test Bench System II

#### 4.3.1 – Instrumentation

The new assembly has two meters of silicone tubing, and a pressure sensor with a voltmeter at each end (Honeywell S & C - 40PC015G1A) (Digital Panel Meter 3-1/2D LCD), in order to know that the value of the pressure and thereby control the DC value for each test (figure 28).

The test bench has an actuator with 700  $\mu\text{m}$  of stroke (Physik Instrumente GmbH, P-287) connected to the high-voltage linear amplifier (Physik Instrumente GmbH, E-508). This configuration is controlled by an Agilent 33220A arbitrary waveform generator that also delivers the synchronizing signal that triggers the data acquisition system.



**Figure 28**– Test bench System II.

1- PZ Actuator; 2- Silicon tube; 3- PZ Probe; 4- Manometer;  
5- Piston DC level pressure; 6- Agilent; 7- Power Switcher;  
8- Oscilloscope; 9- Acquisition Unit; 10- Voltage Source.



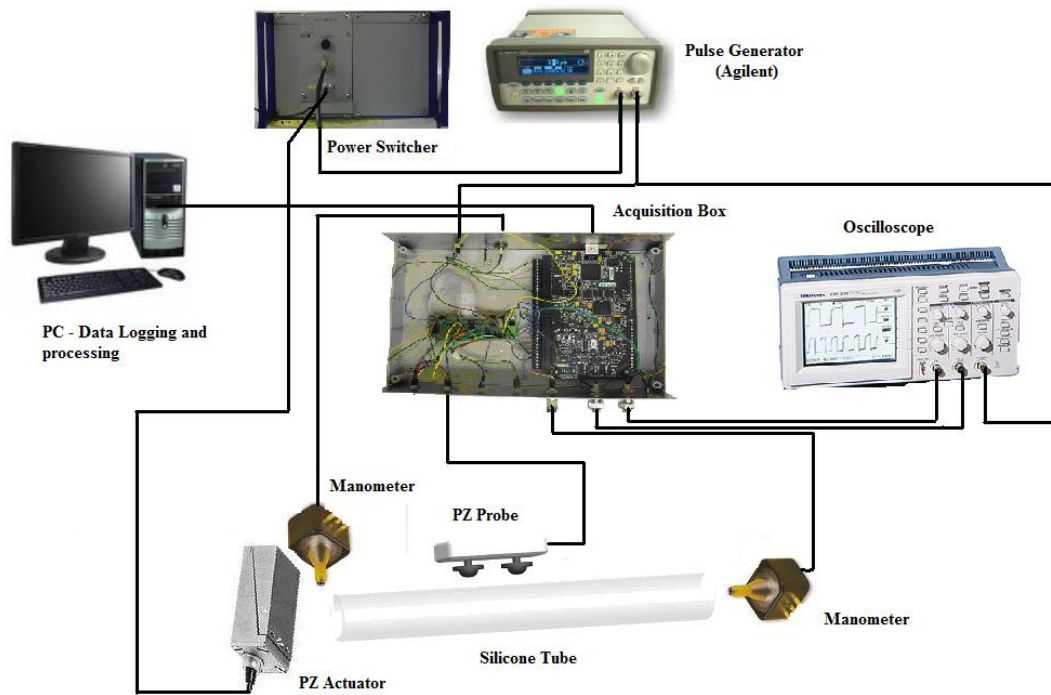
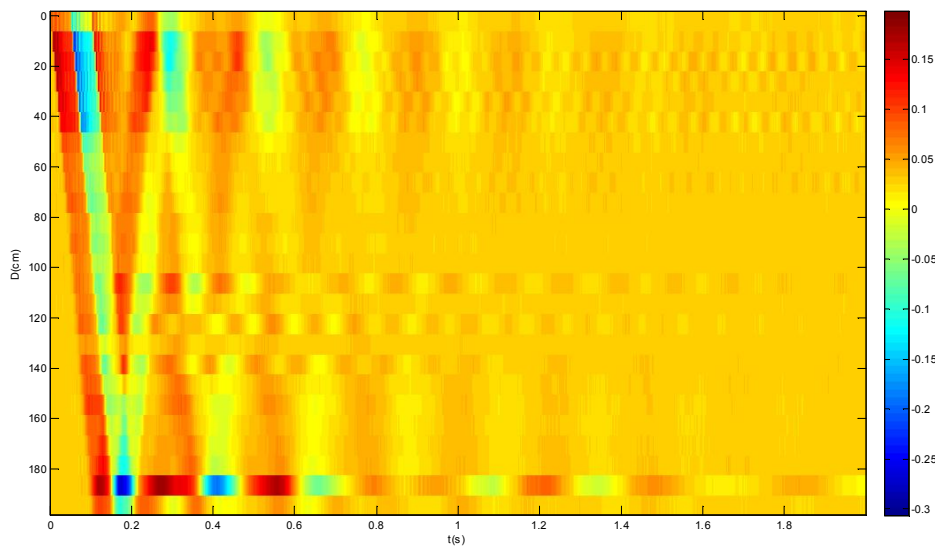


Figure 29 – Scheme of the test bench System II.

### 4.3.2 - Study of waves propagation

In order to see the wave phenomena in this new assembly it was made a scan of the tube. Triangular waves were generated by the actuator and the sensor PZ simple acquired the sent signals from 2 cm to 2 cm. With the acquired data it was possible to do the image in function of time scale data, with the function *imagesc* of *Matlab* to the full range of the *colormap* and display the propagation of wave inside the tube.

In these studies it was used triangular waves by the actuator, since they are the waves that produce that produce better results in terms of detection of the signal, and therefore more easily it allow to identify the phenomena of wave propagation and reflection.



**Figure 30** – Raw data of scanning of tube with PZ sensor, for triangular wave with 100ms of width.

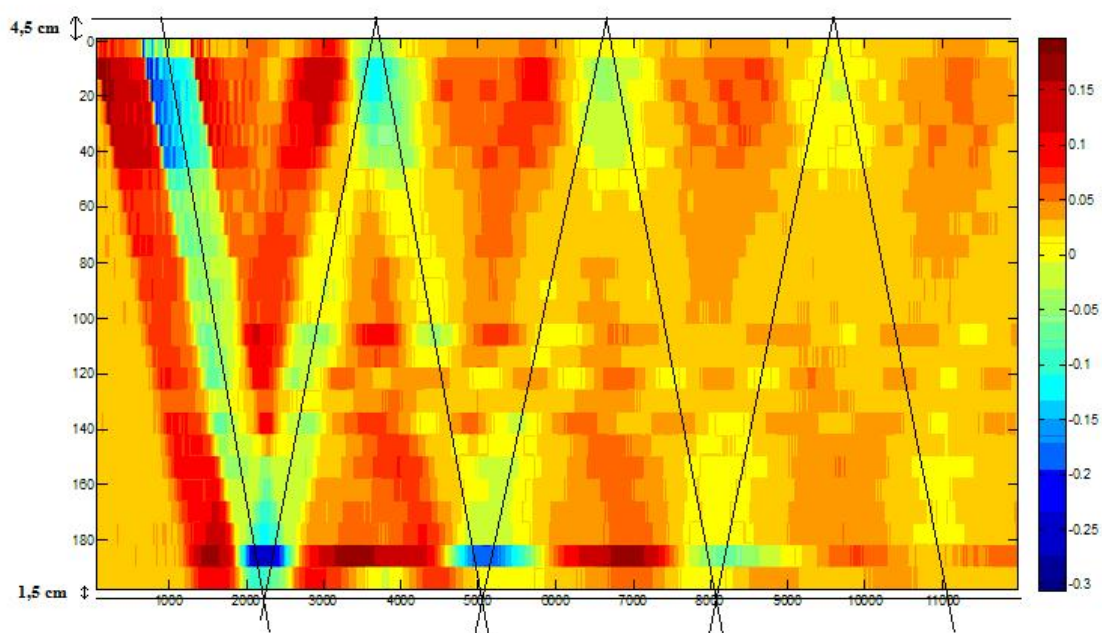


**Figure 31**- Study points of reflection of waves in the tube, marking lines on the most visible components of the wave.

The image 30 shows that there are multiple reflections, before the pressure wave suffer attenuation. By the data collected can determine the locations of reflection of waves, the ends of the tube and the velocity of propagation of pressure wave, by the time of arrival of the first component of the wave at the end of the tube.

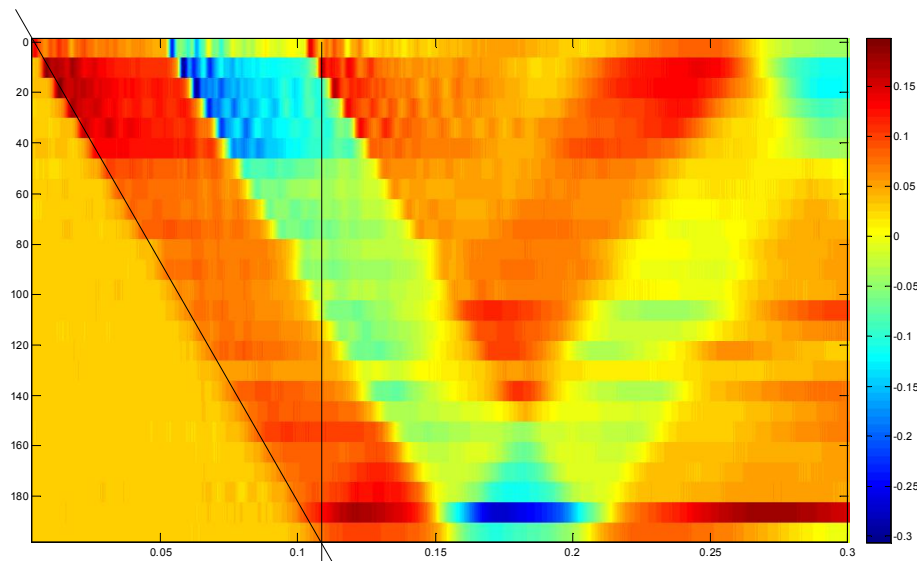


**Figure 32** – Identification of the first component of the wave to reach the end of the tube for calculation of transit time and determination of velocity of propagation the pressure wave.

The first component of the wave through the 2m tube in 110ms, i.e. the velocity of the wave of pressure is approximately 18.2 m/s.

#### 4.3.4 – PWV determination in the tube

To prove the value of velocity found, and it was essential that the velocity of the pressure wave in the tube was known for different values of pressure DC, algorithms were developed based on the values acquired by pressure sensors.

Generate Gaussian waves, this wave was chosen for not present the discontinuities. Generated pressure waves with different widths and acquired the signals from two sensors of pressure and the signal generated by *Agilent*. All the algorithms developed were intended to calculate the time delay between the generated signal or the signal of the first pressure sensor, and signal detected by the pressure sensor at the end of the tube. The distance considered in all cases is 2.06 meters. For this study, we maintained the pressure DC, so we could see that the pulse widths for which our algorithms would be valid, since for very large pulse width, the signal detected by the pressure sensor at the end of the tube loses definition so as no longer possible to use your information to any calculation.

### Algorithms

#### 1. *Maximum of two waves - the pressure sensor*

The time difference, or transit time between the two sensors of pressure, is calculated by the difference between the maximum of the two waves.

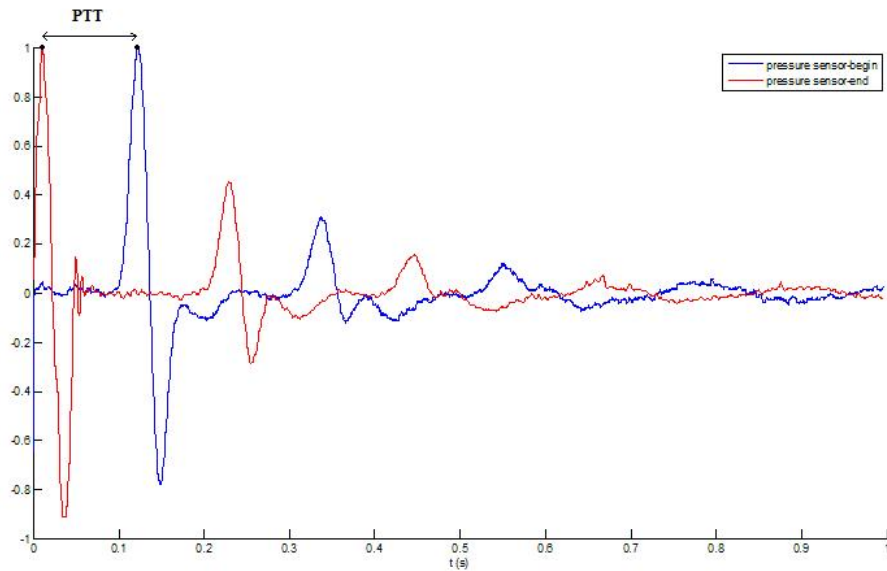


**Figure 33** –The maximum detection of the two waves of pressure sensors for the calculation of PTT, for a Gaussian wave generated of 50ms.

#### 2. *Foot of two waves - the pressure sensors*

The foot of the wave is determined by setting a threshold very close to zero, in this case of 0.05. The transit time between the two waves is calculated by the difference between the first value of the abscissa waves intersect the value of the threshold.

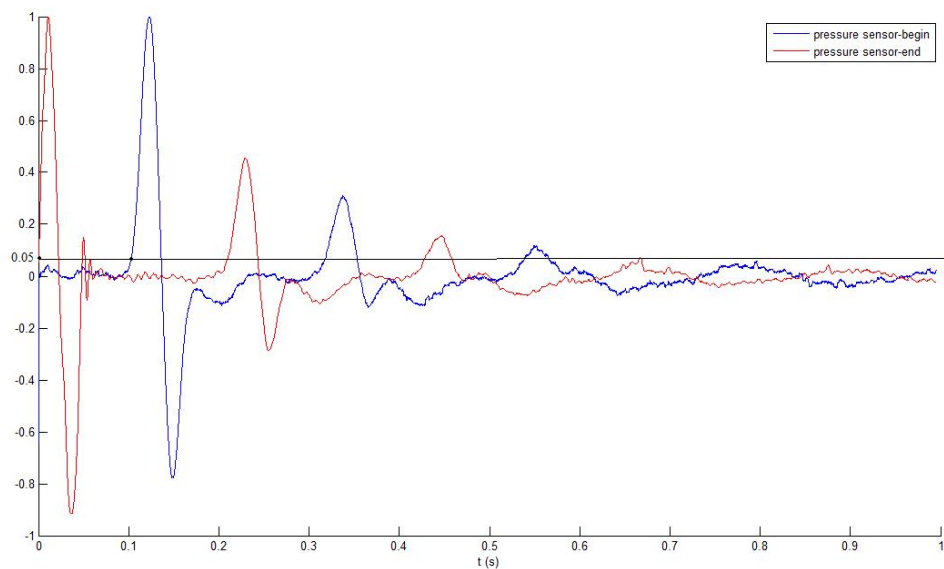


**Figure 34** - Detection of the value of the abscissa to the threshold set. Signals of two pressure sensors, for a Gaussian wave of 50ms.

### 3. *Foot of the wave - actuator and last pressure sensor*

The procedure is exactly the same as before, but the signals used to calculate the transit time are the actuator and the pressure sensor at the end of the tube.

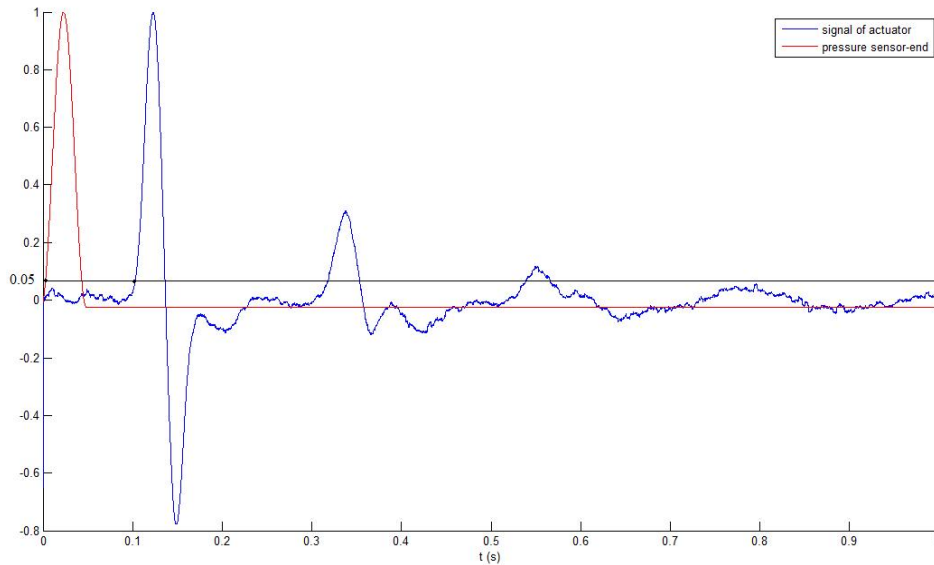


**Figure 35** – Detection of the value of the abscissa to the threshold set. Signal of the actuator and the pressure sensor, for a Gaussian wave of 50ms.

### 4. *Maximum of wave - actuator and last pressure sensor*

The PTT is calculated by the difference between the maximum signal of the actuator and the maximum of the signal of the pressure sensor at the end of the tube.

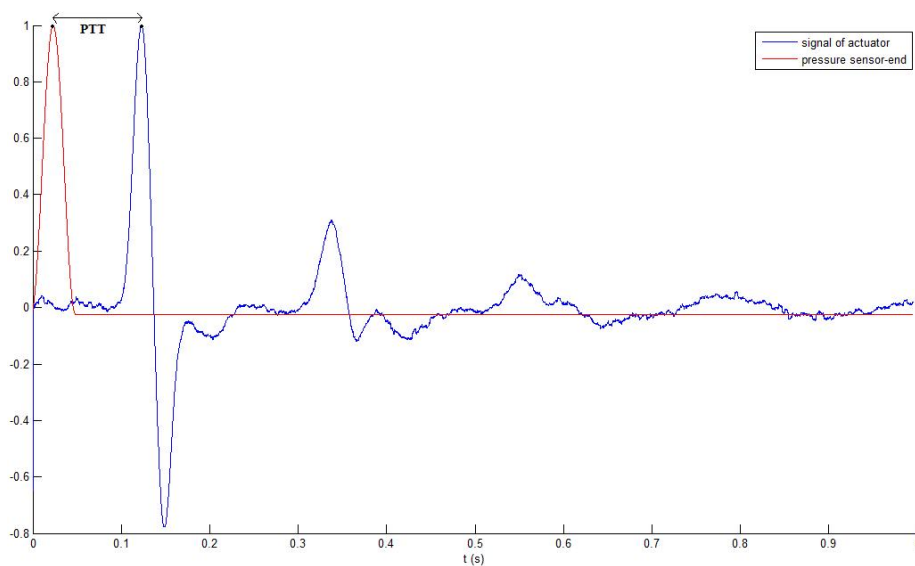


**Figure 36** – The maximum detection of the two waves of pressure sensor and actuator, for the calculation of PTT, for a Gaussian wave generated of 50ms

### Methods using cross-correlation

In signal processing, cross-correlation is a measure of similarity of two waveforms as a function of a time-lag applied to one of them. The cross-correlation is similar in nature to the convolution of two functions. Whereas convolution involves reversing a signal, then shifting it and multiplying by another signal, correlation only involves shifting it and multiplying (no reversing).

#### 5. Cross correlation - two pressure sensors on unfiltered

To signals from sensors, pressure is applied the algorithm of cross correlation, without any filtering.

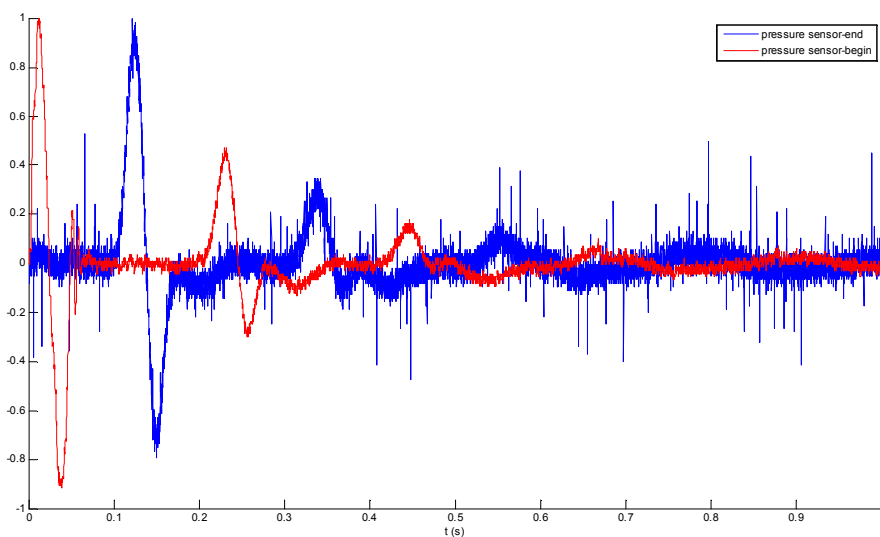


Figure 37 – Signals of two pressure sensors, for a Gaussian wave of 50ms, without filtering.

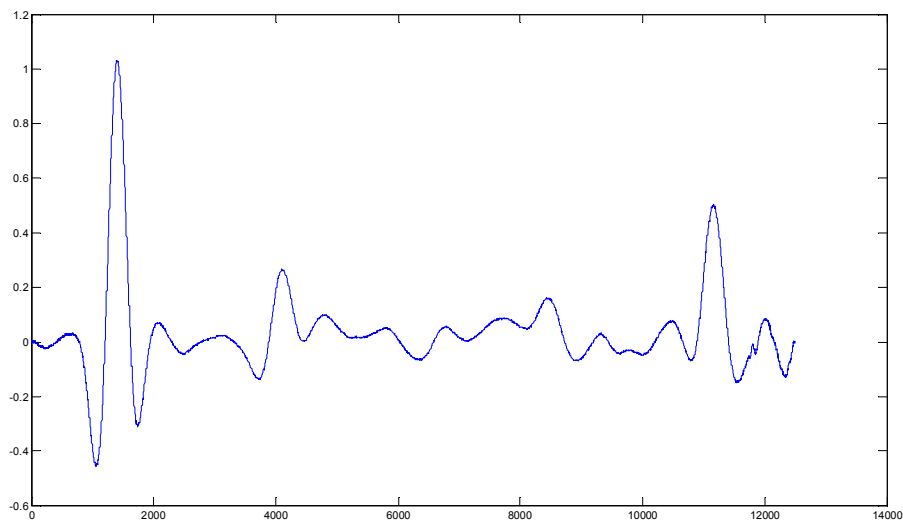


Figure 38 – Result of cross correlation between the signals of two pressure sensors.

### 6. Cross correlation - two pressure sensors, with filtering

The transit time of the wave of pressure is calculated from the signals of pressure sensors, which are filtered by the moving average of 50 points.

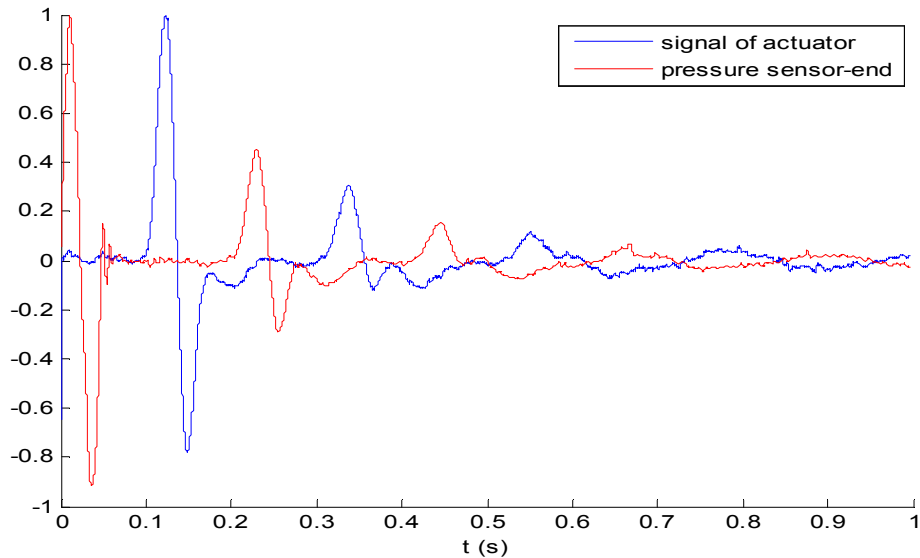


Figure 39 – Signals of two pressure sensors, for a Gaussian wave of 50ms, with filter.

### 7. Cross correlation - signal from the actuator and sensor of pressure

For the calculation of PTT, using the signal from the actuator and the differentiation of signal pressure sensor of the end of the tube. In this case the signals do not suffer any filtering.

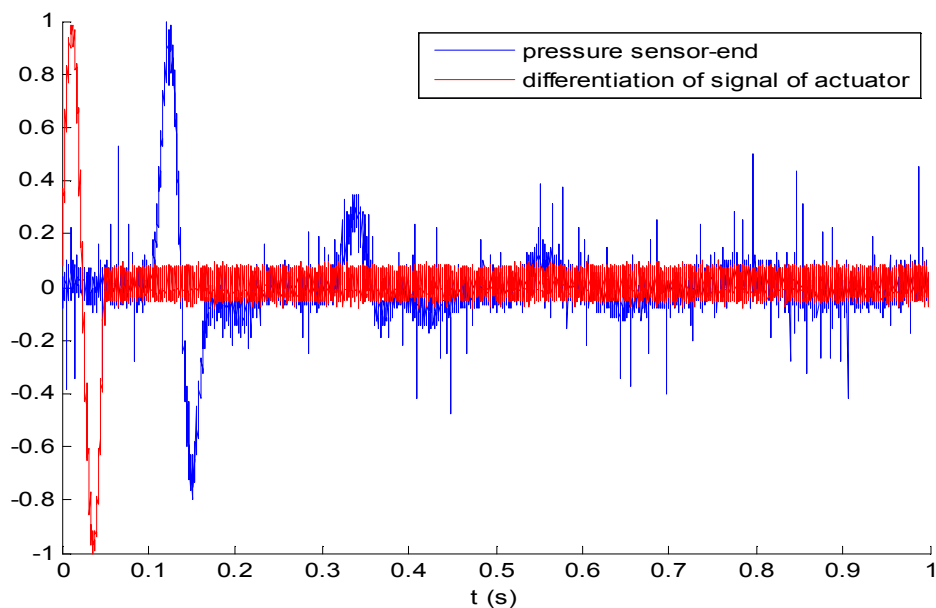


Figure 40 – Signal of the pressure sensor of the end of the tube and the differential signal of the actuator, for a Gaussian wave of 50ms, without filtering.

With the algorithms were developed to calculate the transit times and their velocities for different pulse widths, keeping the pressure constant DC. It always wave Gaussian pulse width of very small because the algorithms developed, based on the wave form of the signal work better for these cases. The results are in the following tables.

**Table III – Study of PWV for different algorithms**

Pulse Gauss (ms)	Foot of waves- two pressure sensors		Maximum of waves - two pressure sensors		Foot of waves - signal of actuator and last pressure sensor		Maximum of waves - signal of actuator and last pressure sensor	
	PTT (s)	Pulse wave velocity (m/s)	PTT (s)	Pulse wave velocity (m/s)	PTT (s)	Pulse wave velocity (m/s)	PTT (s)	Pulse wave velocity (m/s)
10	0.1009	20,4203	0.1092	18,8645	0.1009	20,4203	0.1086	18,9617
20	0.0999	20,6165	0.1092	18,8645	0.0999	20,6165	0.1059	19,4486
30	0.1017	20,2596	0.1106	18,6189	0.1017	20,2596	0.1035	19,8995
40	0.1038	19,8535	0.1106	18,6189	0.1038	19,8535	0.1017	20,2596
50	0.1047	19,6715	0.1118	18,4192	0.1042	19,7773	0.0997	20,6661
60	0.1066	19,3173	0.1122	18,3666	0.1052	19,5817	0.0976	21,1066
70	0.1073	19,2021	0.1134	18,1594	0.1049	19,6415	0.0965	21,3516
80	0.1084	19,0037	0.1143	18,0196	0.1050	19,6116	0.0934	22,0462
90	0.1096	18,7956	0.1130	18,2236	0.1052	19,5817	0.0916	22,4891
100	0.1112	18,5252	0.1107	18,6055	0.1072	19,2164	0.0883	23,3243
125	0.1173	18,5252	0.1135	18,1466	0.1089	18,9199	0.0848	24,2925
150	0.1186	17,3752	0.1147	17,9568	0.1103	18,6730	0.0794	25,9577
200	0.1206	17,0869	0.1148	-	0.1004	20,5179	0.0701	29,3950
Average Pulse Wave Velocity		19,1271		18,4053		19,7439		22,2460



The results of the PTT and pulse wave velocity, obtained by algorithms based on the cross correlation of the signals are represented in the following table.

**Table IV – Study of PWV for different algorithms with cross correlation**

Pulse Gauss (ms)	Signal of two sensors - unfiltered		Signal of two sensors - with filter (MA 50npts)		Differential signal of the actuator and last pressure sensor - unfiltered	
	PTT (s)	Pulse wave velocity (m/s)	PTT (s)	Pulse wave velocity (m/s)	PTT (s)	Pulse wave velocity (m/s)
10	0.1098	18,7682	0.1095	18,8093	0.1154	17,8571
20	0.1110	18,5519	0.1113	18,5119	0.1138	18,1083
30	0.1115	18,4720	0.1114	18,4986	0.1130	18,2236
40	0.1122	18,3535	0.1120	18,3929	0.1125	18,3144
50	0.1120	18,3929	0.1121	18,3797	0.1130	18,2365
60	0.1126	18,3014	0.1127	18,2754	0.1136	18,1338
70	0.1130	18,2236	0.1129	18,2495	0.1141	18,0575
80	0.1137	18,1210	0.1132	18,1979	0.1148	17,9443
90	0.1146	17,9818	0.1136	18,1338	0.1148	17,9443
100	0.1153	17,8695	0.1143	18,0196	0.1161	17,7464
125	0.1149	17,9318	0.1158	17,7831	0.1172	17,5768
150	0.1169	17,6249	0.1168	17,6370	0.1196	17,2241
200	0.1173	17,5648	0.1170	17,6008	0.1209	17,0417
<b>Average Pulse Wave Velocity</b>		18,1659		18,1915		17,8776

For values recorded in the tables can conclude that the algorithms that have more consistent results are those of the cross correlation. The value of the velocity determinate is approximately 18.2 m / s, equal to what had previously been determined for conditions of equal pressure, but by other method.

Although it is apparent that the larger the width of the Gaussian pulse less accurate, the velocity is calculated, did acquisition of signals with pulse widths greater, to determine whether in fact this is confirmed, can conclude that it is impossible for the calculation of PTT signal through large pulse width.

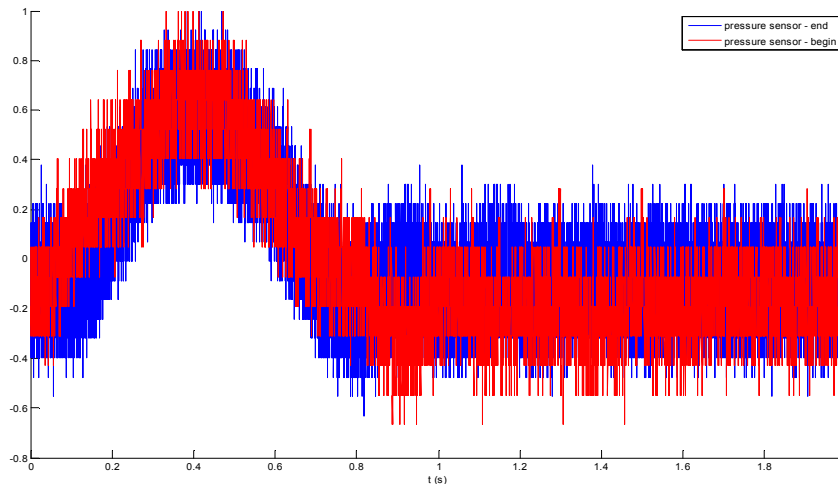


**Figure 41** - Signals of two pressure sensors, for a Gaussian wave of 800ms.

For very large pulse width of the signal received by the sensors of pressure not a resolution that imposes a limit to the algorithms developed based on all forms of wave recorded by pressure sensors.

For very large pulse width of the signal received by the sensors of pressure, lose the resolution which imposes a limit to the algorithms developed based on all forms of wave recorded by pressure sensors (figure 41).

**Table V – Study the velocity of pressure for large pulse widths**

Pulse Gauss (ms)	Foot of waves- two pressure sensors		Maximum of waves - two pressure sensors		Foot of waves - signal of actuator and last pressure sensor		Maximum of waves - signal of actuator and last pressure sensor	
	PTT (s)	Pulse wave velocity (m/s)	PTT (s)	Pulse wave velocity (m/s)	PTT (s)	Pulse wave velocity (m/s)	PTT (s)	Pulse wave velocity (m/s)
300	0.1370	15,0321	-	-	0.1032	19,9612	0.0581	35,4683
400	0.1654	12,4516	0.1344	15,3274	0.1085	18,9897	0.0337	61,1639
500	0.1632	12,6225	0.1053	19,5669	0.1062	19,4047	-	-
300	0.1370	15,0321	-	-	0.1032	19,9612	0.0581	35,4683
400	0.1654	12,4516	0.1344	15,3274	0.1085	18,9897	0.0337	61,1639

This study, there were situations where due to distortions in the form of a wave was not possible using the algorithm. Phenomenon explained in figure 41.

**Table VI – Study of PWV for different algorithms with cross correlation for large pulse widths**

Pulse Gauss (ms)	Signal of two sensors - unfiltered		Signal of two sensors - with filter (MA 50npts)		Differential signal of the actuator and last pressure sensor - unfiltered	
	PTT (s)	Pulse wave velocity (m/s)	PTT (s)	Pulse wave velocity (m/s)	PTT (s)	Pulse wave velocity (m/s)
300	0.1191	17,2935	0.1198	17,2011	0.1153	17,8695
400	0.1270	16,2154	0.1252	16,4537	0.1104	18,6594
500	0.1082	19,0459	0.1118	18,4192	0.1396	14,7564
600	0.0948	21,7300	0.0948	21,7300	0.1538	13,3975
700	0.0486	42,4217	0.0486	42,4217	0.2158	9,5441

Analyzing the results obtained in the last two tables it is obvious that the algorithms developed can not be applied to large pulse widths, for the reasons set out above.

The following graphs show the changes in the value of PWV calculated by different methods for different pulse widths.

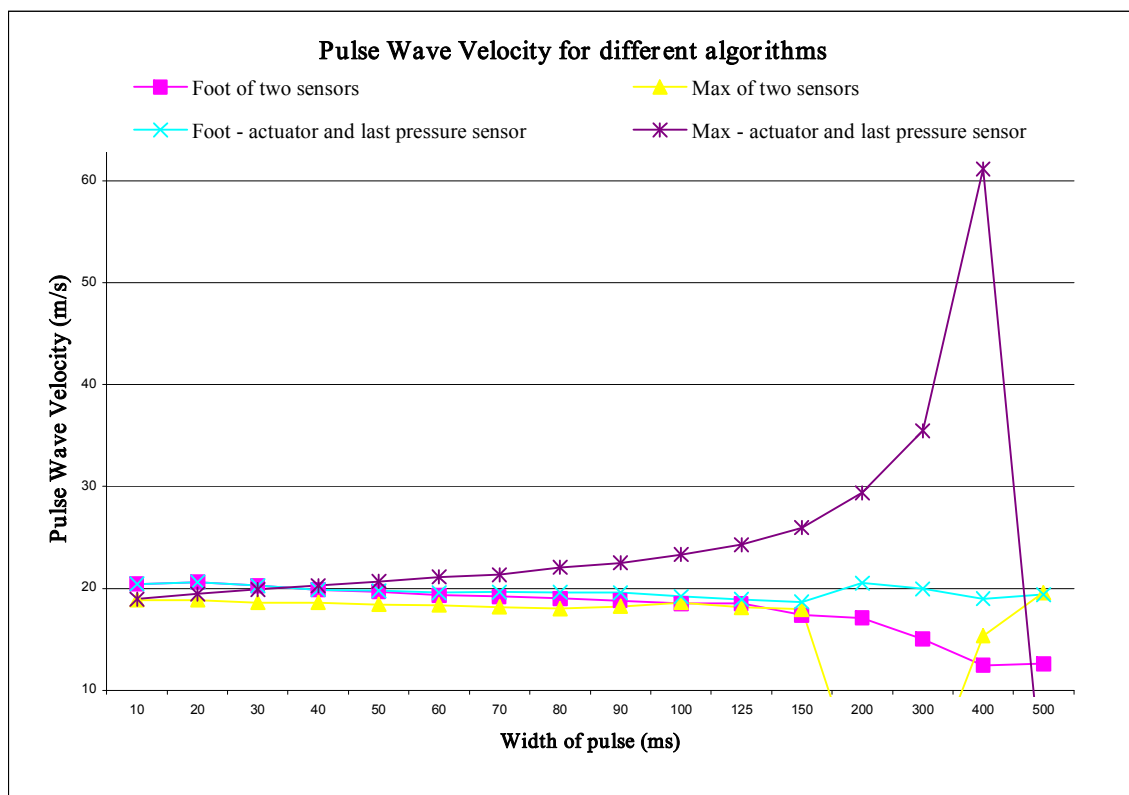
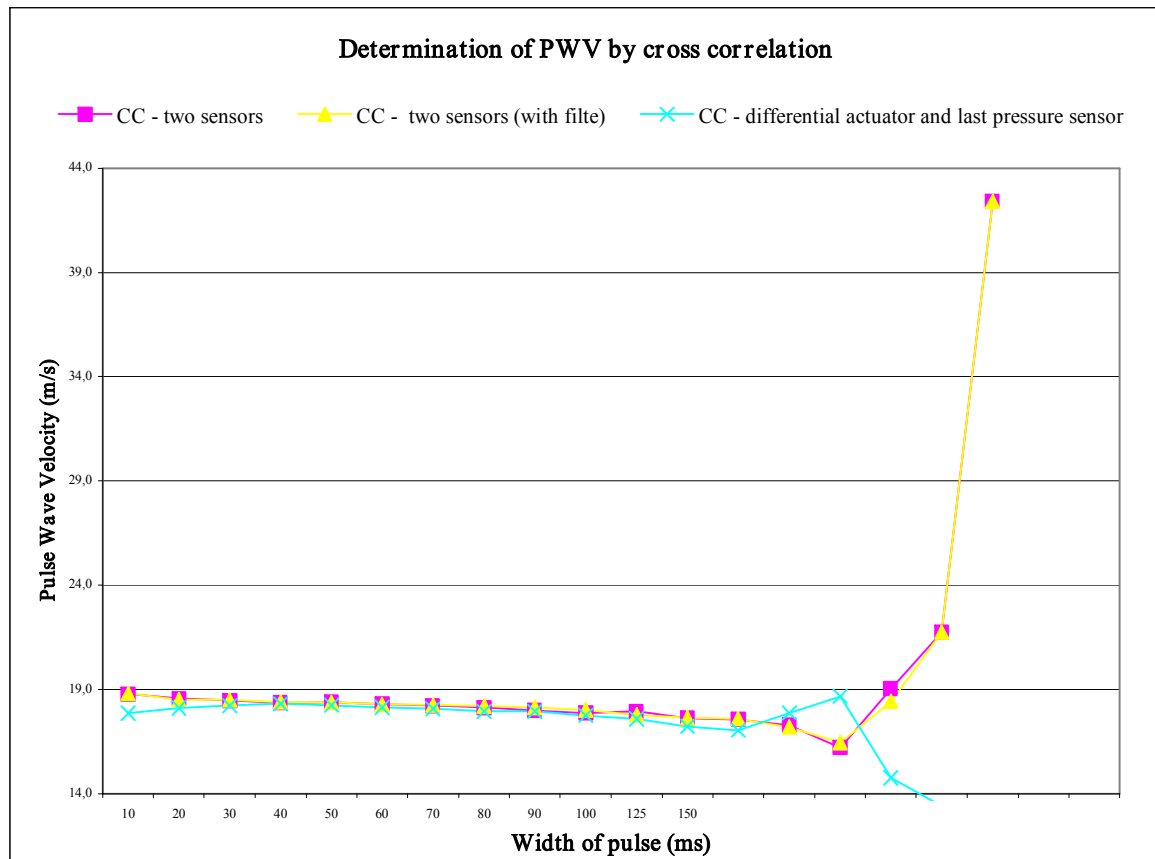


**Figure 42 – Study of changes in the PWV values calculated by different algorithms.**



For this experiment tests were made with Gaussian waves of 150ms, in different the value of DC pressure, and each acquisition was determined to velocity in the tube, the algorithm of cross correlation for pressure sensors. Collected two sets of data, so there was no doubt about the shape of the curve obtained. The DC value of pressure is read by the pressure sensor at the end of the tube. The results are in the following table.

**Table VII – Study of PWV for different DC pressure levels**

Pressure DC level (V)	Test 1		Test 2	
	PTT (s)	Pulse wave velocity (m/s)	PTT (s)	Pulse wave velocity (m/s)
0,57	0.1296	15,8951	0.1378	14,9449
0,63	0.1161	17,7464	0.1168	17,6370
0,68	0.1123	18,3405	0.1122	18,3535
0,72	0.1110	18,5652	0.1114	18,4853
0,77	0.1110	18,5652	0.1103	18,6730
0,83	0.1114	18,4986	0.1110	18,5519
0,89	0.1122	18,3535	0.1116	18,4588
0,95	0.1130	18,2365	0.1130	18,2236
1,00	0.1139	18,0829	0.1154	17,8571
1,06	0.1153	17,8695	0.1158	17,7831
1,10	0.1166	17,6612	0.1167	17,6491

The behaviour of the velocity depending on the pressure changes in the system is represented in following graph.

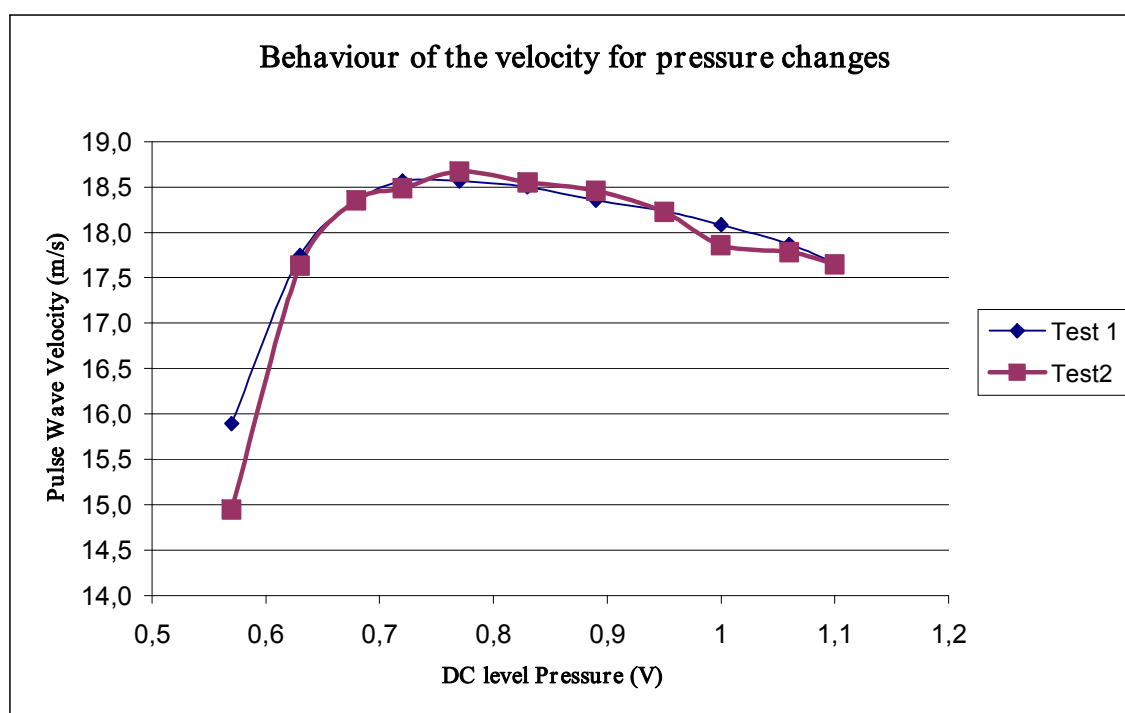


**Figure 44 – Changes in the PWV for different values of pressure.**

Compliance ( $C$ ) is an expression of the elastic nature of materials, the compliance of a blood vessel describes the volume of blood vessel ( $V$ ) that can contain a certain pressure ( $P$ ), and can be expressed as follows:

$$C = V/P \quad (4)$$

It is clear that compliance, is indirectly related to and PWV. However, once vessel geometry is changed by vasodilation, the relationships among these variables change, because the arterial wall is essentially incompressible. <sup>[35]</sup> The compliance can be calculated from PWV and blood density ( $\rho$ ) for the expression: <sup>[36]</sup>

$$C = (\rho \cdot PWV)^{-1/2} \quad (5)$$

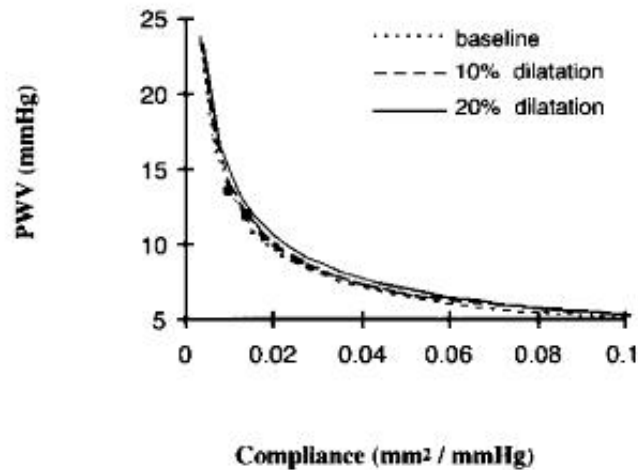


**Figure 45** - Theoretical curve of compliance versus pulse wave velocity (PWV) at 95 mm Hg pressure. <sup>[35]</sup>

For the above graph (figure 45) can see that for very large values of PWV have very small values of compliance, which explains the behaviour observed for the study of PWV.

The compliance of the silicone tube used in test bench can be responsible for the behaviour the PWV with changes of pressure.

#### **4.4 - Conclusions**

Depending on the algorithm and on the sensor under test, two different configurations have been implemented and tested: a fast, short stroke one driven by an electronic switcher, for determining impulse responses, by the impulse of *Dirac*; the second is a long stroke configuration, driven by a high-voltage linear amplifier dedicated to generating arbitrary pressure waveforms. <sup>[34]</sup>

The second test bench was allowed to explore other types of signals, better understand the phenomena of propagation of pressure waves, develop algorithms to calculate the PWV and study the change of velocity according to the changes of pressure DC.

## Chapter 5

**Characterization of the probes**

The sensors developed for the assessment of hemodynamic parameters are all piezoelectric. With different characteristics which confer in practical terms different potential. In this chapter, it is discussed the methods used to characterize the sensors and the contribution of each probe for the evaluation of hemodynamic parameters.

**5.1 - Sensors developed**

Three types of sensors were developed, differential simple probe, integrative simple probe and double probe. The differential simple probe consists of a single piezoelectric sensor which captures the signal differentiates it (the piezo effect) and amplification it. This type of probe can, through methods that will be discussed to reproduce the original wave of pressure and assess to hemodynamic parameters as the index of augmentation.

In the study of literature tried integrating a probe allowed us to see directly the pressure wave. This probe was integrated electronically, which eliminates the effect that the differentiation piezoelectric sensor.

The double probe is composed of two electrically independent piezoelectric sensors, and with local amplification and separated by a constant distance. The great aim of this probe is the determination of pulse wave velocity.

**5.2 – Methods****5.2.1 – Deconvolution**

The piezoelectric sensors can be modelled by a simple RC circuit, which differentiates the signal. Consequently, it is possible to get the original signal, though the integration of the signal or through the Deconvolution. For the sensors described before the method of Deconvolution is more precise.<sup>[14]</sup>

The Deconvolution allows knowing the signal input the sensor from the output signal and the impulse response of the sensor. The theorem of convolution can be represented by the following expression:

$$y(t) = x(t) * h(t) \quad (6)$$

Where  $y(t)$  is the output of the sensor which is the result of convolution of the input signal  $x(t)$  with the impulse response of the sensor  $h(t)$  (figure 46). The theorem says that the Fourier transform of the convolution of two functions is equal to the product of their individual Fourier transforms.



$$Y(j\omega) = X(j\omega) \times H(j\omega) \Leftrightarrow Y(j\omega) = \frac{X(j\omega)}{H(j\omega)} \quad (7)$$

where  $H(j\omega)$  is the system's transfer function, the Fourier transform of IR.

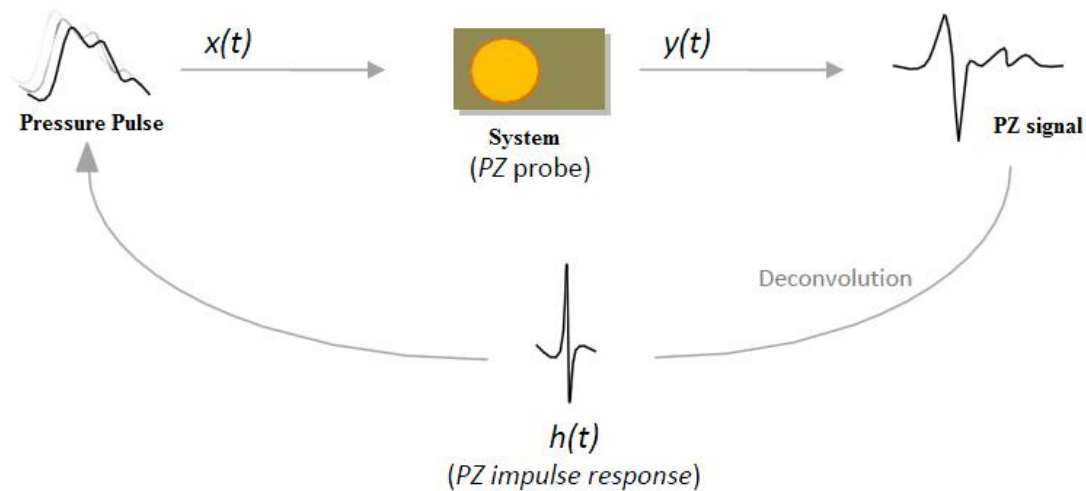


**Figure 46** - Schematic of the deconvolution process.  
Adapted from [14]

### 5.2.2 –IR Determination

The application of deconvolution method involves the determination of impulse response of the sensors. An impulse response refers to the reaction of any dynamic system in response to some external change, as a *Dirac* like impulse generated by the actuator. In the digital domain, the use of a simple *Dirac*  $\delta$  is the best way to extract the transfer function of a system. Problems begin when try to pass from the digital to the analogue domain: it's very difficult (in reality) to generate a *Dirac*  $\delta$  from any kind of sensor. For this reason, various techniques for the extraction of the characteristic of an analogue system have been developed. The most effective and efficient technique for the IR extraction is the one that uses a signal made by a sinusoidal function which goes from the low frequencies to the high ones; a pure tone that increases its frequency with time (figure 47).<sup>[37]</sup>

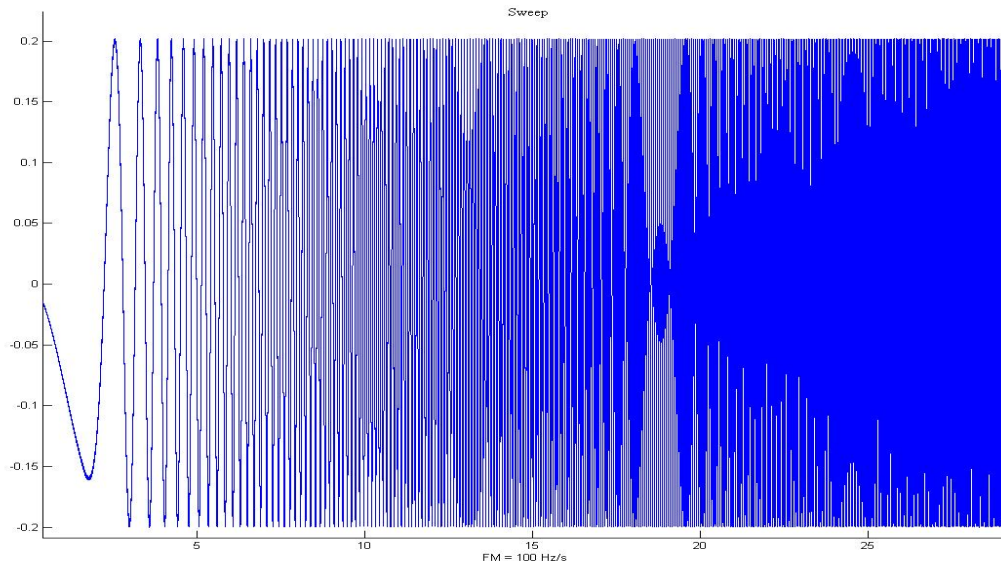


**Figure 47** – Linear sweep generated by the actuator.

The impulse response of sensor is obtained by playing linear sine sweeps, the actuator reproduces it in the sensor piezoelectric and the response is recorded. From the linear sweeps an impulse response is calculated (figure 48).

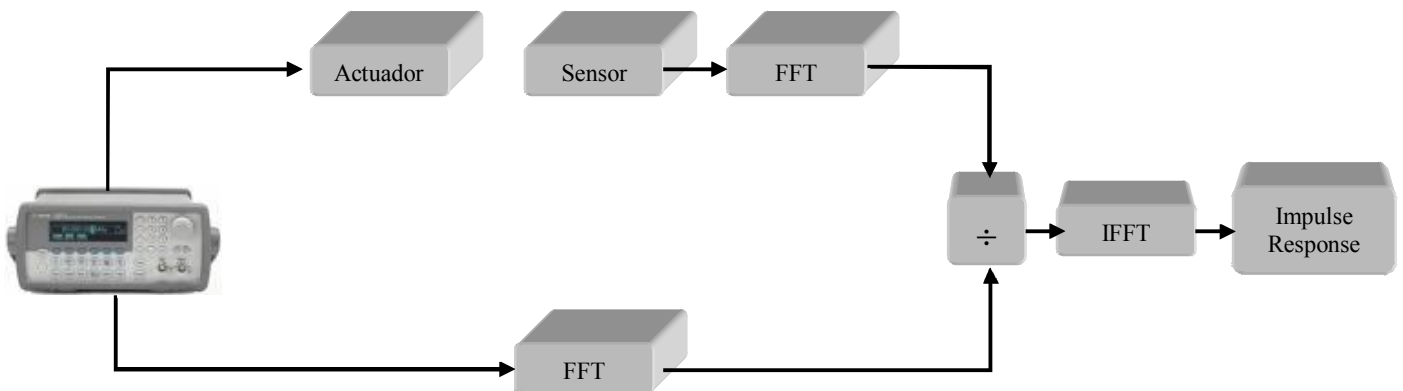


**Figure 48** – The process of obtaining the IR of each sensor - diagram block.

The spectrum (fast Fourier transform (FFT)) of the signal of piezoelectric sensor is compared to a reference spectrum of the sweep. The relation between the sensor signal and the reference signal reveals the frequency response of the sensor. This frequency response is transformed back to the time domain by the inverse fast Fourier transform (IFFT), resulting in the impulse response of the piezoelectric sensor. <sup>[38]</sup>

### Experimental settings to obtain IR

To obtain IR experimentally use the equipment of the test bench II, only this has actuator capable of exciting the system with sweep.

A programmable pulse generator (Agilent©) was used to generated the sweep and trigger the power switcher action. The Agilent had a connection with acquisition box, for the synchronism and other for the acquisition the sweep signal. To acquire IR data, the PZ actuator was hold against the centre of the PZ sensor, both standing on a table, and the experimental assembly schematized figure 49 was set up.

The PZ probe signal follows the normal procedures: it is logged with the software tool provided by the NI USB.6210© and processed using MatLab® routines.

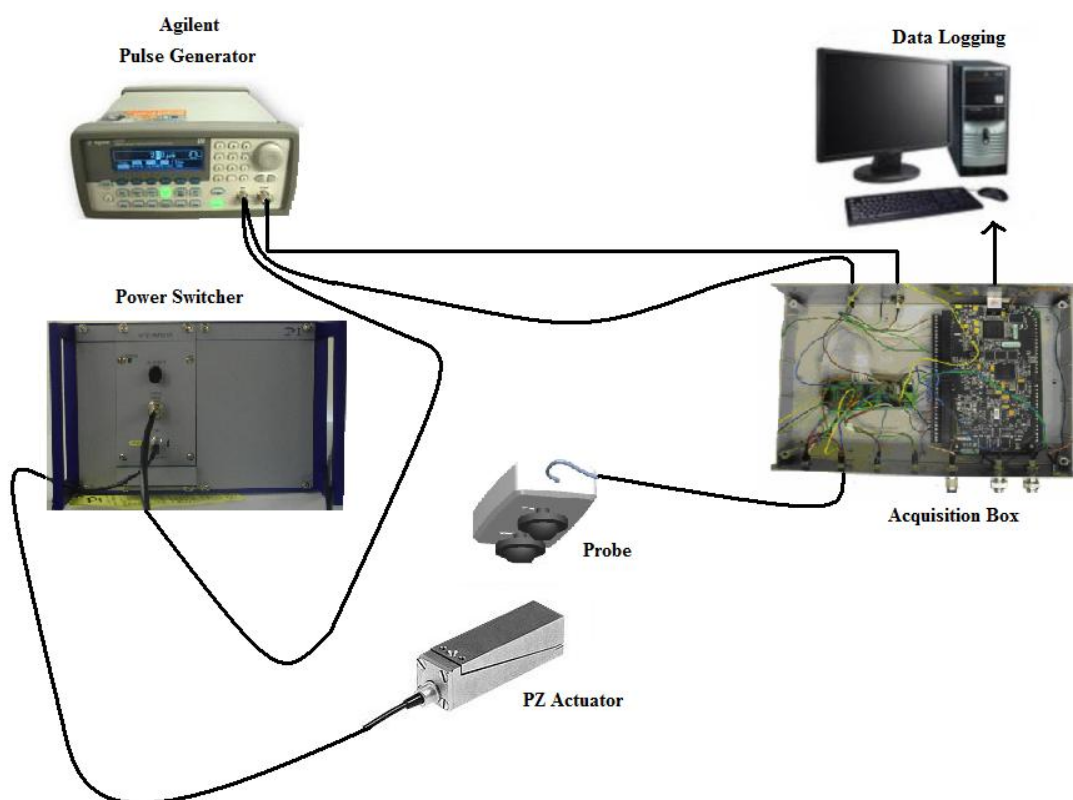


**Figure 49** – Scheme of the experimental assembly for the IR acquisition.

The definitions and parameters for the different instruments of test bench, is in the following table:

**Table VIII – Sweep main characteristics**

Characteristic	Equipment	Value
Sine amplitude	Agilent©	4 V <sub>PP</sub>
Sine offset	Agilent©	2 V <sub>DC</sub>
Frequency Start	Agilent©	10mHz
Frequency Stop	Agilent©	500mHz or 1kHz
Sweep time	Agilent©	100s, 300s,500s
Sample Rate	NI USB – 6210 ©	2.5KSpss, 5KSpss, 12.5 KSpss

In IR sensors determination weren't applied the digital filters or removed the DC component of the signal.

For each piezoelectric sensor of the double probe it was necessary to calculate the IR, since there were small variations in crystal piezoelectric that could originate differences in impulse responses.

### 5.3 – Differential Simple Probe

#### 5.3.1 – Characterization of sensor probe

As mentioned above, and in order to get the IR of each PZ sensor it was made linear sweeps. For each sensor, were made linear sweeps as shown in figure 50, and following the method of processing the signal mentioned above so that it could get the IR of each sensor PZ.

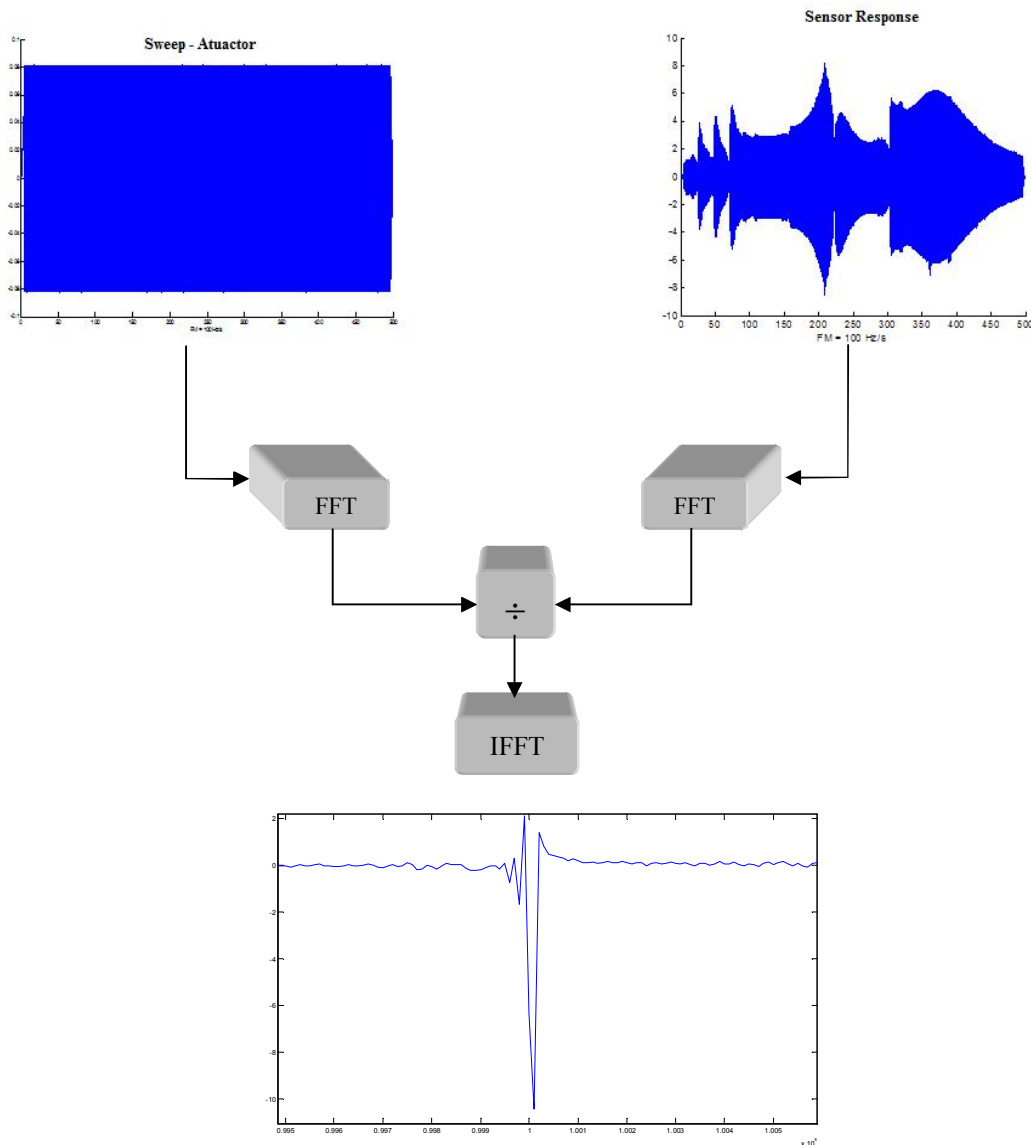
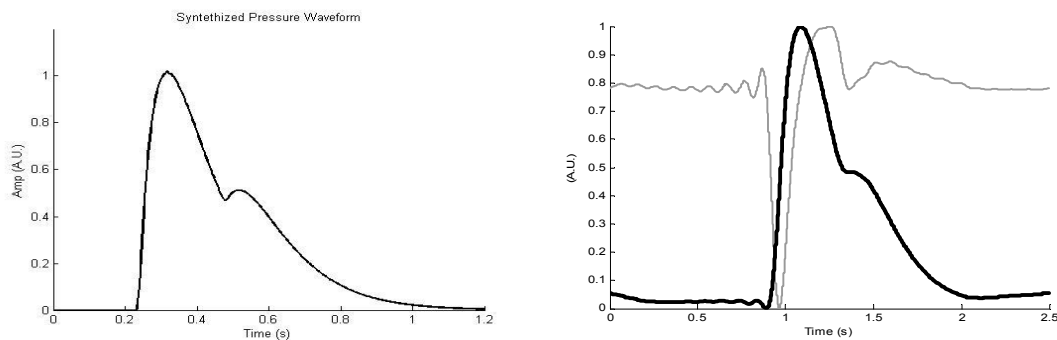


Figure 50 – Methodology to obtain the impulse response of sensor, and IR obtained.

### 5.3.2 – Results

With the IR obtained for the PZ sensor it is possible to apply the deconvolution algorithm, and thus find the pressure wave that the sensor captures. The DC component of the IR and the signal is digitally removed.

Thus, in our test bench II, were generated by the actuator different forms of pressure wave that our sensor detects and verify that they correspond to the wave of pressure generated in the tube.



**Figure 51** – a) Programmed pressure wave fed to the actuator.  
b) Probe output (gray), and the its deconvolution (black). [34]

The main issue is to demonstrate the capability of precisely recovering the true pressure waveform from the signal provided by the probe. To fulfill this endeavor, a cardiac-like signal, shown in figure 51.a, was synthesized and delivered to the system. Deconvolution was used to recover this waveform from the sensor placed at the middle of the tube, using the above referred IR. [34]

Can use the same method to obtain the wave of pressure in carotid human, signals obtained from the sensor and PZ are deconvolved with the IR of sensor and find the original waveform of pressure (figure 52).

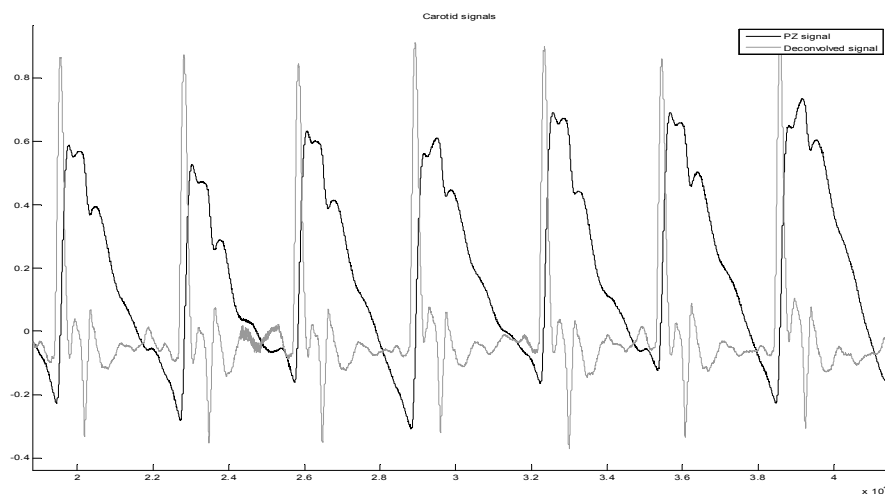


**Figure 52** - Wave of pressure in carotid human.  
Probe output (gray), and the its deconvolution (black).

## 5.4 – Integrative Single Probe

### 5.4.1 – The new probe

As have seen, the piezo is differentiating by nature, hence requiring that the signal has to be submitted to pre-processing, i.e., must be deconvolved. However, in the literature, applications of piezoelectric to obtain the pressure wave, whose electronic configuration, being inclusive allowed the signal to the sensor output signal is the original pressure. In signal conditioning electronics for pulse sensor, the signals are initially passed through CA3140 operational amplifiers whose high input resistance in conjunction with a parasitic capacitance of 200 pF causes the circuit to integrate the signal. Since the piezoelectric sensor provides a current proportional to the derivative of the applied pressure, the integrator circuit is needed to obtain the pressure waveform. <sup>[39]</sup>

Thus, adapting the electrical circuit of one of our probes by putting a capacitor in the negative feedback loop, turns the probe into an integrating one.

In a RC circuit, like that, the value of the time constant (in seconds) is equal to the product of the circuit resistance (in ohms) and the circuit capacitance (in farads), i.e.

$$\tau = R \times C \quad (8)$$

**Table IX – Determination of time constant**

Diferencial constant:	Integration constant:
$R_{124} = 10^6 \Omega$ $C_{\text{piezoelectric}} = 8 \times 10^{-9} \text{F}$ $\tau = 8 \times 10^{-3} \text{ms}$	$R_{122} = 50 \times 10^3 \Omega$ $C = 10^{-5} \text{F}$ $\tau = 5 \times 10^{-1} \text{m}$

The constant of integration is greater than the constant of differentiation, so that the predominant effect in this probe will be the integration of the signal. These values of the components were chosen for this probe to allow the acquisition of the original signal without having had to resort to algorithms for data processing.

### 5.4.2 – Characterization of sensor

For integrative simple probe, sweeps were made to obtain the impulse response for sensor, the same way. Following the full procedure described above, determined that the IR sensor so that can characterize its nature.

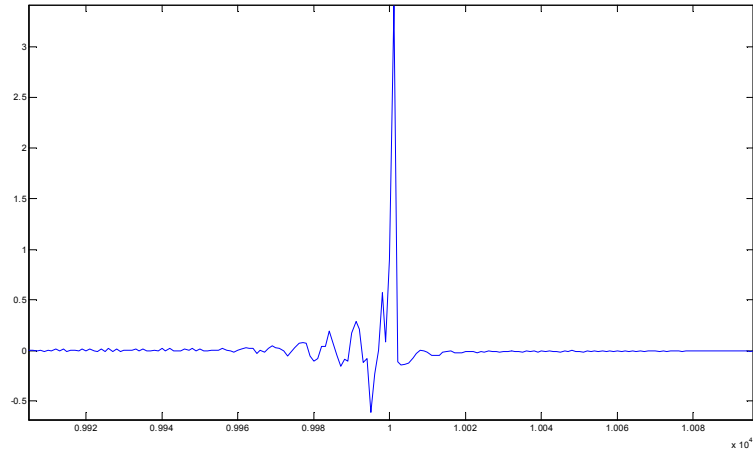


**Figure 53** - Impulse response for the integrative simple probe.

The IR obtained shows the cancellation of the differential effect of PZ sensor by electronic integration. The IR is almost identical to an impulse *Dirac*  $\delta$ .



### 5.4.3 – Signals of sensor

In test bench II generating triangular waves, placing the sensor in different positions and verified that by their integrated nature, get the signal propagates in the tube overlapping of reflections, which are adding to the original wave. The signal that the sensor captures doesn't need processing since the electronic integration cancels the effect of piezoelectric differentiator.

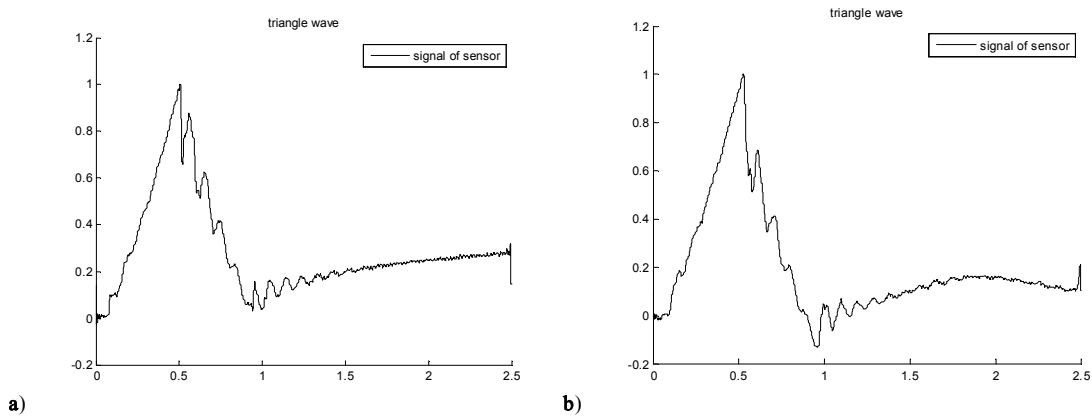


**Figure 54** – Triangular wave with 1s width, acquired by integrative simple probe.

- a) Sensor in position 16cm of tube.
- b) Sensor in position 60cm of tube.

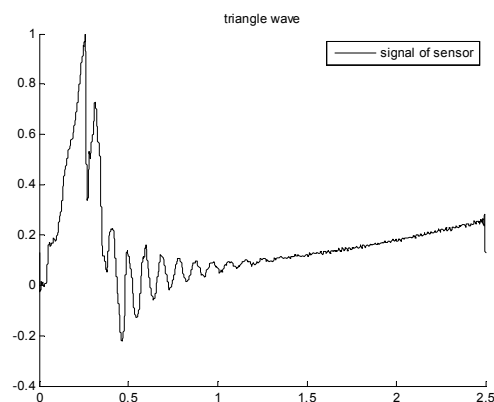


**Figure 55** - Triangular wave with 1s width, acquired by integrative simple probe placed in 16cm of tube.

The figures demonstrated that the signals directly from the probe don't need to be deconvolved. However this only happens for certain pulse width. For how can we check to 500ms from the wave shows a distorted way. This limitation is inherent in the time constant of the probe, and the values of the components that were placed were then changed to that given in electronic integration constant was equal to the constant of differential for the piezoelectric sensor. For that, we replaced the capacitor in the negative feedback of the amplifier, by a 150nF, which made the constant of integration and differentiation equal.

For this new probe was calculated the IR, exactly the same trial. And the tube signals were acquired with this sensor and implemented the deconvolution for different types of wave.

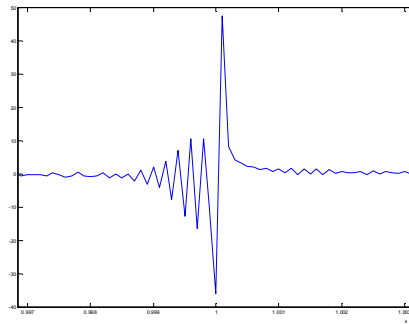


Figure 56 - Impulse response for the new simple probe.

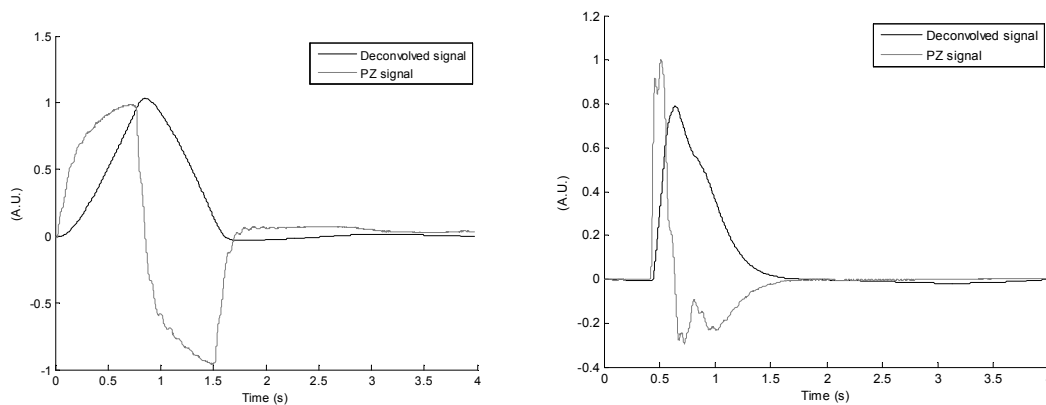


Figure 57 – Programmed pressure wave fed to the actuator.  
 Probe output (gray), and the its deconvolution (black) to position 30cm.  
 a) Triangular wave of 1.5 s width. b) Cardiac-like wave of 1.5 s width.

The main issue is to demonstrate the capability of precisely recovering the true pressure waveform from the signal provided by the probe. It gives results very clean of noise and convolution works well for the IR calculated, allowing us to find the sign that was the input to the sensor, pressure waveform.

## 5.5 – Double Probe

### 5.5.1 – Characterization of sensor

The probe consists of two electrically independent piezoelectric sensors, and with amplification. For each of the piezoelectric sensor of the double probe was calculated the IR, since there are small variations in crystal piezoelectric that could originate differences in impulse responses.

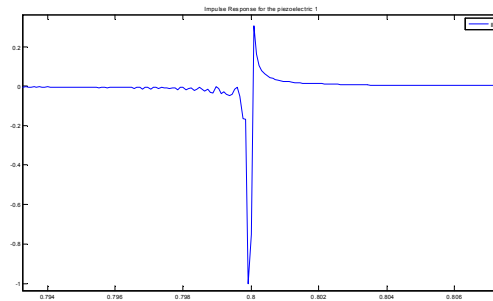


Figure 58 – IR for piezoelectric 1 sensor for one sweep 10mHz until 1kHz.

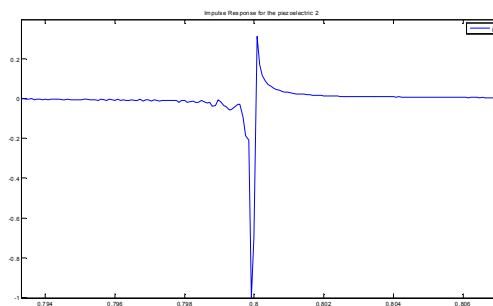
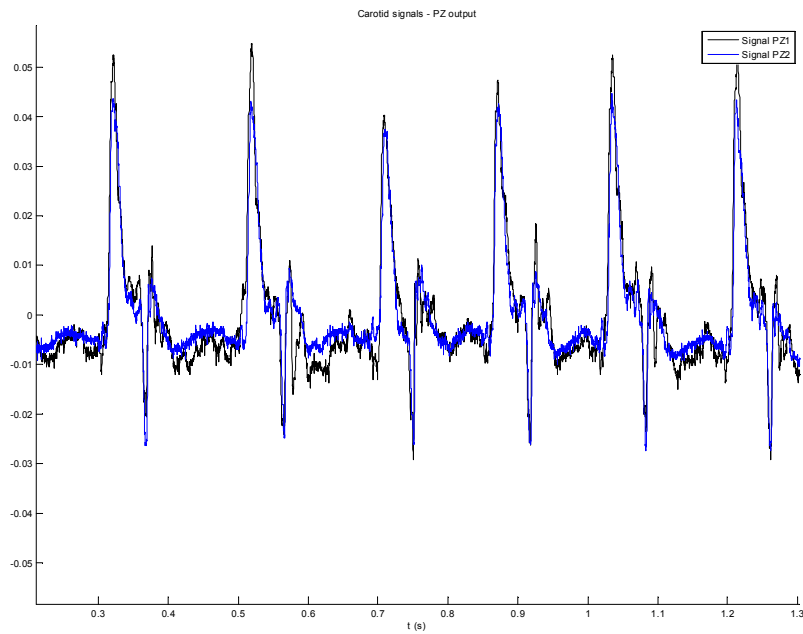


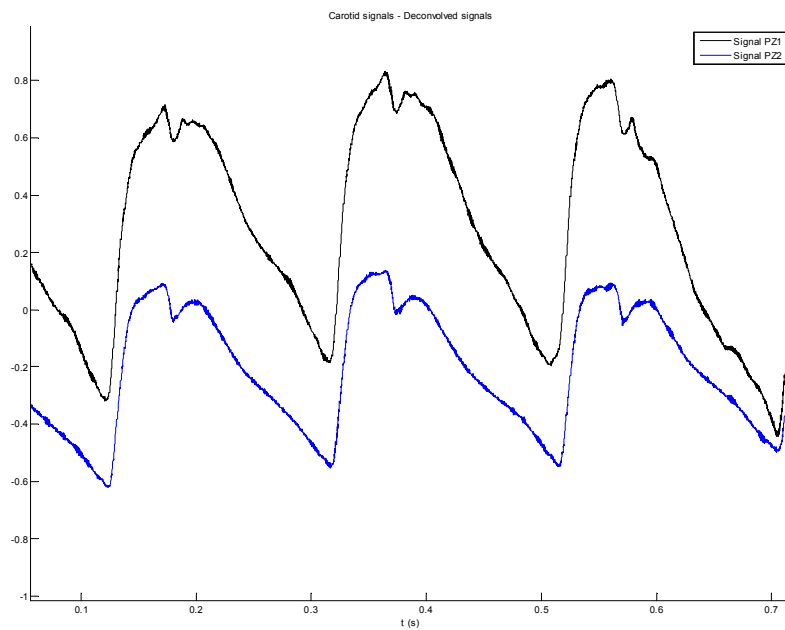
Figure 59 – IR for piezoelectric 2 sensor for one sweep 10mHz until 1kHz.

5.5.2 – Signals of sensor

We can use the deconvolution method for to obtain the wave of pressure in carotid human, signals obtained from the sensor and PZ double are deconvolved with the IR of each sensor and find the original waveform of pressure.



a)



b)

**Figure 60** - Wave of pressure in carotid human.

a) Probe output for two PZ sensors.

b) Deconvolved signals for two PZ sensors.

The graphs show how you can obtain the waveform of pressure in the human carotid however; we have a problem with the base line which is due to small movements caused by the patient as the breath.

The great potential of the double probe will be addressed further in a following chapter.

## 5.6 - Convolution

To verify that the Deconvolution algorithm really works, and certain terms that the interpretation of the shape of the signals is not wrong, do the reverse process, i.e. the convolution (figure 61). From a triangular wave, for example, with several changes in the upward phase and downward phase, we made a convolution with the experimentally obtained IR sensor for the differential simple probe. All this was done in Matlab. Different triangular waves were generated, which it stored in the files .txt were convolved with the impulse response.

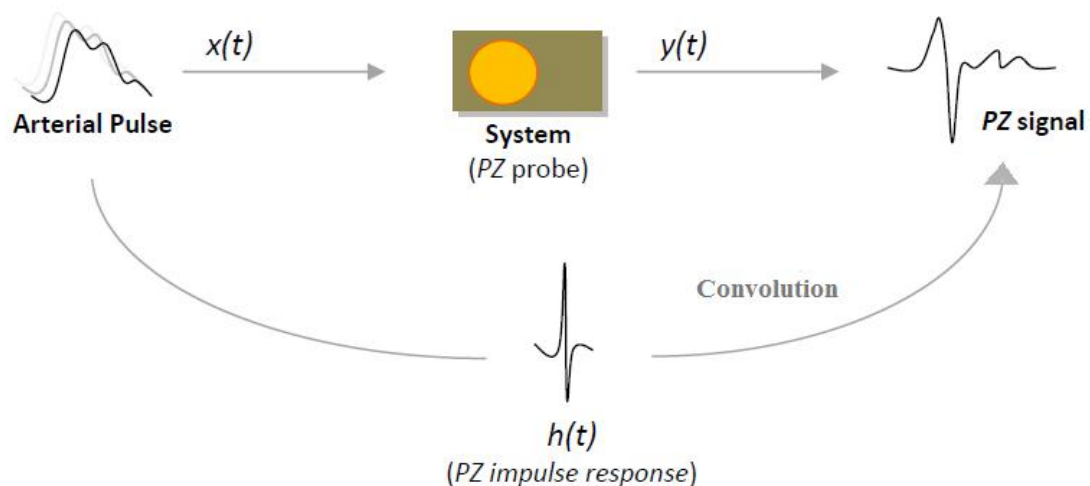


**Figure 61** - Schematic of the convolution process.  
Adapted from [14]

Convolution of a triangular wave with the IR obtained for the differential simple probe (figure 50) would be expected that the result was a signal identical to that of piezoelectric sensors.

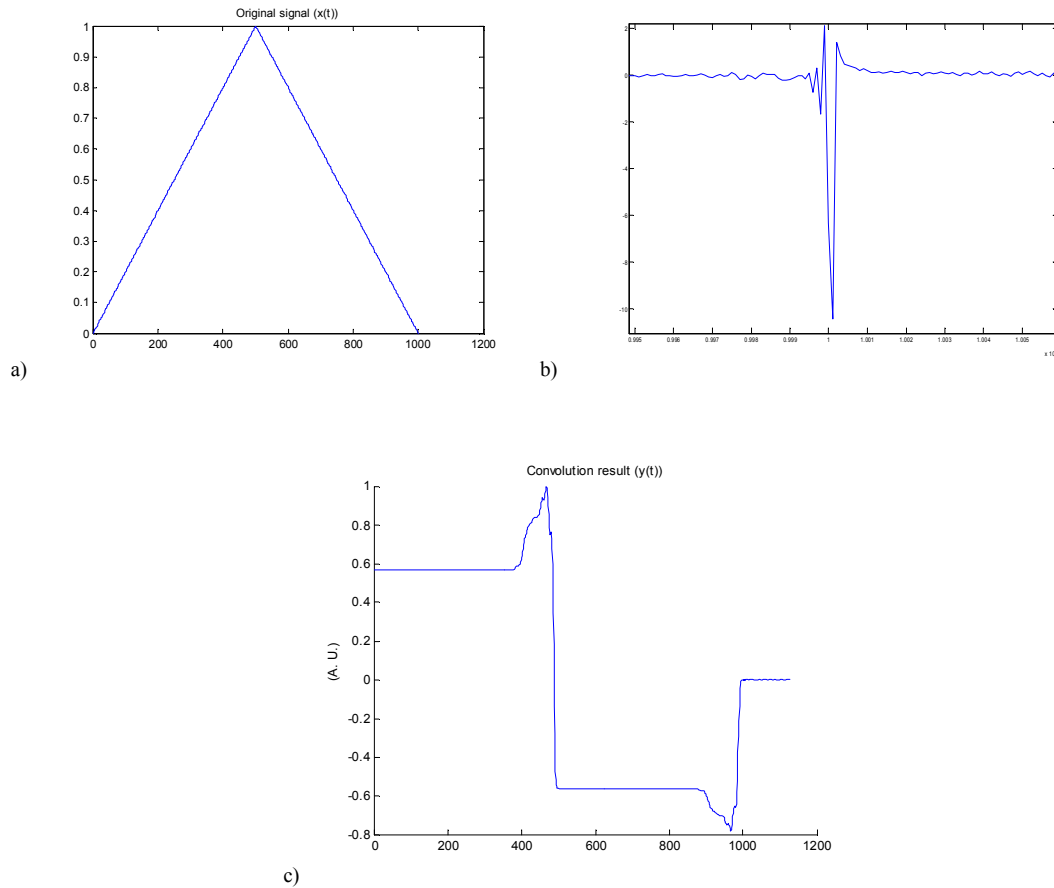


**Figure 62** – The triangular wave, and signal obtained by convolution with IR.

- a) Triangular wave,  $x(t)$ .
- b) IR for differential simple probe.
- c) Signal result of convolution,  $y(t)$ .

The result shows that there is a change from baseline of the signal, an abrupt change. However, our triangular waves are not simple, but with a series of changes caused by the superposition of reflected waves, so generate such a wave and see what the result of convolution (figure 63).

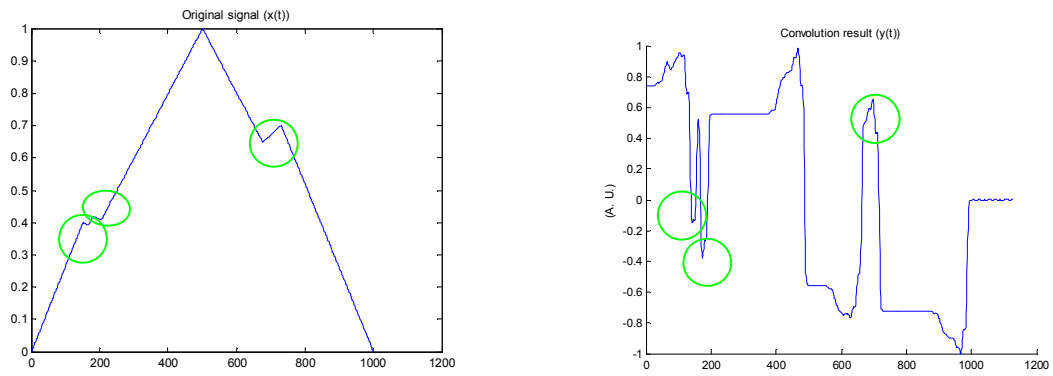


**Figure 63** - The triangular wave with inflexions, and signal obtained by convolution.

The two inflexions in the rising phase, generate two valleys in the initial phase of the resulting signal, the change in the downward phase generates a peak in the final signal, points marked with green circles in both signals. For real signals, captured in the tube, found that the changes are different from the ascending phase of the downward phase we generate a triangular wave with this kind of characteristics, such as that shown in Figure 64.

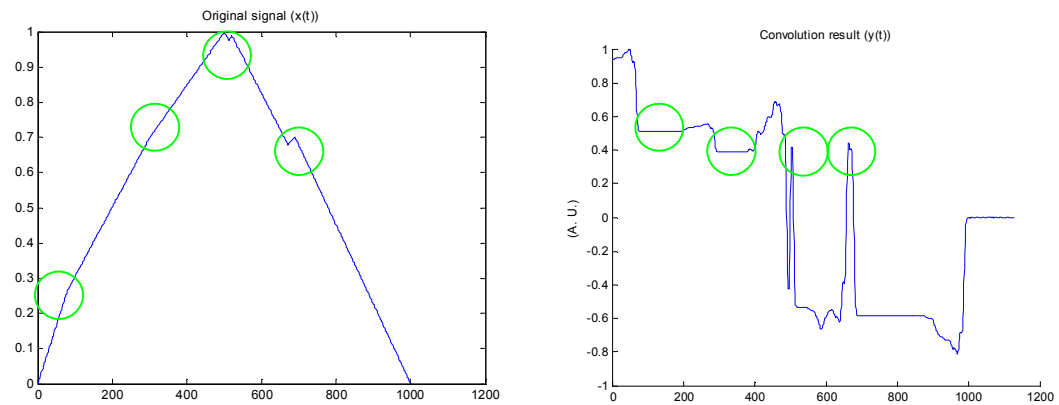


**Figure 64** - The triangular wave with different kinds of inflexions, and signal obtained by convolution.

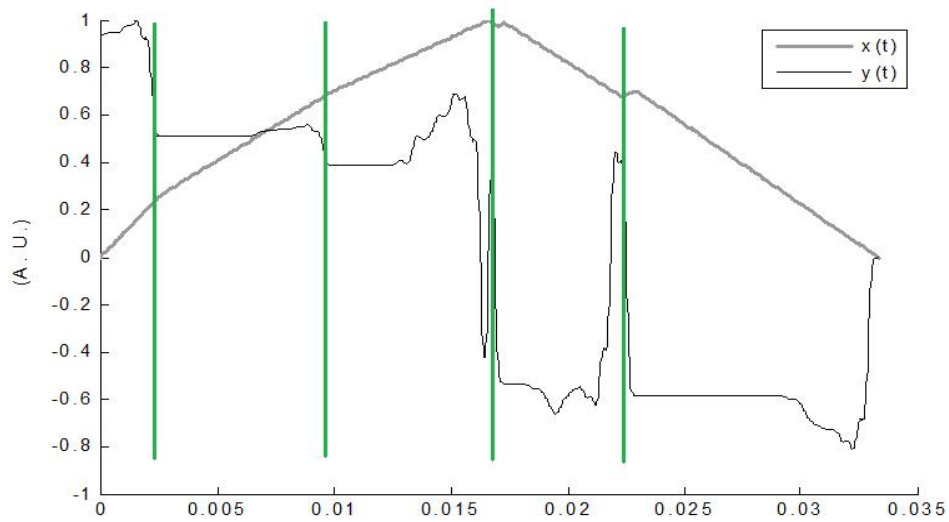


**Figure 65** – The triangular wave, and signal obtained by convolution. Marking of the temporal correlation between the changes of the original signal and the triangular signal from the convolution.

In Figure 65, this emphasizes the coincidence of the changes of wave triangular, with the result in the convolved signal. The changes generated in the initial wave triangular cause different changes in the signal resulting from the convolution. Comparing these results obtained by Deconvolution can return again to see the signs of the piezoelectric sensors and deconvolved signals.

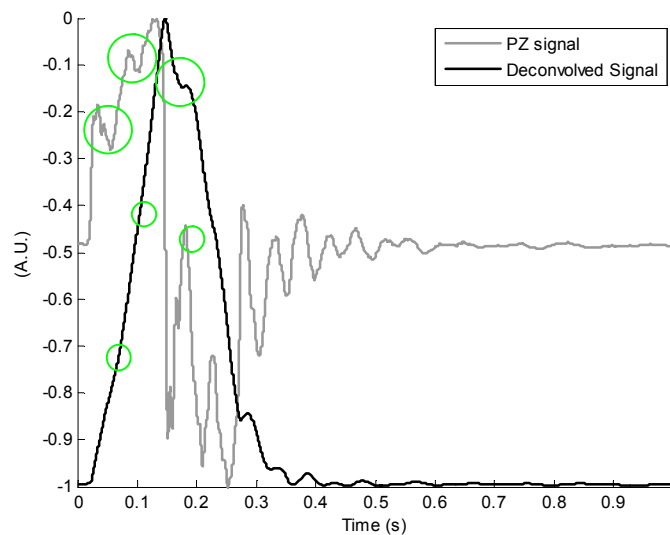


**Figure 66** – Probe output (gray), and the its deconvolution (black) to position 36cm. Triangular wave of 250ms width.

In Figure 66 the circles in green, mark the points of inflection of deconvolved signal and the respective signal variations of PZ which prompted it.



Comparing the results of Figure 66 with those obtained in Figure 64, we can conclude that the variations in the piezoelectric signal that correspond to the interference of waves reflected and which correspond to changes in the original pressure signal.

### ***5.7 - Conclusions***

Developed and characterized the probes proved to be able to reconstruct the wave of pressure detected at the entrance to the sensor, and thus access to the carotid pressure wave of human. Sensors developed are low cost, simple, and easy to operate and that in early access to hemodynamic parameters, by the pressure wave.

The Deconvolution has proven to be a robust method for obtaining the original pressure waveform and by the convolution can understand that variations in the detected signal correspond to changes of the piezoelectric signal original pressure.

## Chapter 6

**Double probe**

---

This chapter is devoted to the process of characterization of the double probe and to its temporal resolution determination. Focus to the algorithms developed for determination of the pulse transit time, to obtain the velocity of wave pulse and prove the temporal resolution for this measurement.

**6.1 – Pulse Wave Velocity Determination – The Double Probe**

The stiffening of the aorta and large elastic arteries is a biophysical manifestation of vascular aging with important prognostic implications. It is elevated in conditions such as renal failure, diabetes, and hypertension, and in each of these conditions, it is predictive of subsequent cardiovascular events. It is recommended as one of the best methods for measuring stiffness and is the measure used in most large clinical studies.<sup>[46] [47]</sup> The measurement of PWV is generally accepted as the most simple, non-invasive, robust, and reproducible method to determine arterial stiffness.

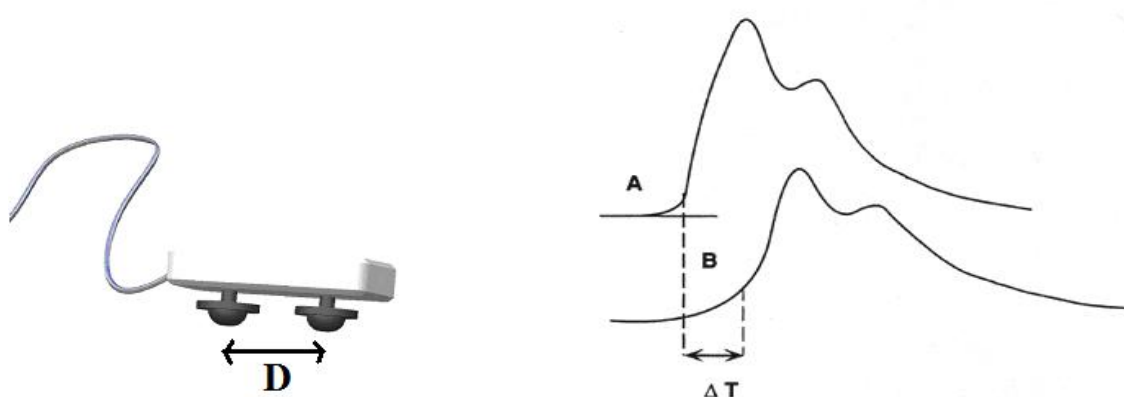
Many different pulse waves have been used to assess pulse wave velocity, such as pressure waves, distension waves or flow waves. The most often used signal is pressure wave, although this choice may not be the best as it implies the application of a pressure transducer on the artery of interest, and inadequate application may result in distorted waves. Multiple methods to measure local PWV have been explored, including wave intensity analysis<sup>[43]</sup>, the flow/area method<sup>[44]</sup>, the gradient method<sup>[45]</sup>, waveform decomposition of the central aortic pressure pulse<sup>[49]</sup>, and measured using the foot-to-foot method from various waveforms. The transit time is usually measured between two different sites. These are usually obtained, transcutaneously at the right common carotid artery and the right femoral artery and the time delay measured between the arrival of a predefined part of the pulse wave, such as the foot, at these 2 points is obtained either by simultaneous measurement (as in the Complior device), or recorded sequentially using a single probe and the carotid-femoral PTT determined with reference to the R wave of the ECG signal (as in the SphygmoCor device). The distance travelled by the pulse wave is measured over the body surface and PWV is then calculated as distance/time (m/s). However, distance should be measured precisely because small inaccuracies may influence the absolute value of PWV. The shorter the distance between two recordings sites, the greater the absolute error in determining the transit time. Some limitations should be underlined. The femoral pressure waveform may be difficult to record accurately in patients with metabolic syndrome, obesity, diabetes, and peripheral artery disease, and it tends to become more tortuous with age, potentially leading to an underestimation of PWV.

The method of determining PTT from waveform decomposition of central aortic pressure use a single pulse measurement. Aortic pressure was estimated from a transformed radial pulse and decomposed into forward and backward waves using a

triangular flow wave. Pulse transit time was determined from cross-correlation of reflect wave, forward, and backward waves. <sup>[49]</sup>

The studies developed by Westerhof et al <sup>[51]</sup> concluded that when the time of return of the reflected wave, is used to calculate PWV, inaccurate data are obtained. With aging PWV increases but transit time hardly decreases, suggesting that the reflection site moves toward the periphery. So, hypothesized that the forward and reflected waves in the distal aorta are not in phase, leading to an undefined reflection site.

The main advantage of Double Probe is be able to determine the pulse wave velocity, based on the basic expression of velocity calculation. The distance between the two sensors is fixed and known, 2cm, the pulse detected present an undoing time between the signal received by the piezoelectric A and the piezoelectric B (figure 67).



$$PWV = D / \Delta T$$

Figure 67 - Methodology of calculation of the PWV.

This probe will allow a local characterization of the circulatory system and probably more rigorous measurement of PWV.

The double probe, by its mechanical configuration is a sensor easy to operate, and can be placed on a leash, in such a way that it doesn't required the presence of an operator to collect data on carotid. There are two reasons that carotid PWV is the preferred measurement. The first is anatomic, the vessels whose organs are particular targets of hypertension all are connected to the carotid. The second reason is that the carotid stiffness is more predictive of CVD deaths compared with PWV measured in the brachial or femoral. The change in PWV in the carotid from aging and various comorbidities is greater than the change in PWV in muscular artery circuits such as the brachial or the femorotibial. The robustness of PWV measures in the carotid makes it the most informative vessel for cardiovascular outcomes prediction.

The first step to take was the characterization of the double probe sensors. It was necessary to do the determination of the impulse responses (IR) of each sensor, the study of reproducibility of these, and notice if there was crosstalk between the sensors.

## 6.2 - Study of the sensors

In Chapter 5, we saw how the IR was obtained for the two sensors that make up the double probe; however more studies were done to prove that the probe had temporal resolution, in order to measure the pulse wave velocity. We began by examining the reproducibility of the obtained IR and made a study of the crosstalk between PZ sensors. After these results it will be necessary to develop algorithms capable of proving the temporal resolution.

For each piezoelectric sensor of the double probe it was calculated the IR, since there are small variations in piezoelectric crystal that could originate differences in impulse responses.

### 6.2.1 – Study of Reproducibility

For the results obtained in chapter 5, it was studied the reproducibility of the values so the tests were repeated again at different times. It was found that there is a great reproducibility in the results as shown by the coincidence of the IR.

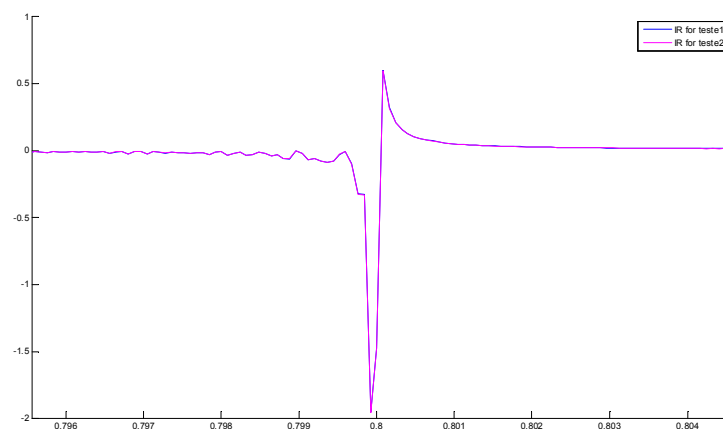


Figure 68– IR for piezoelectric sensor 1 for different testes.

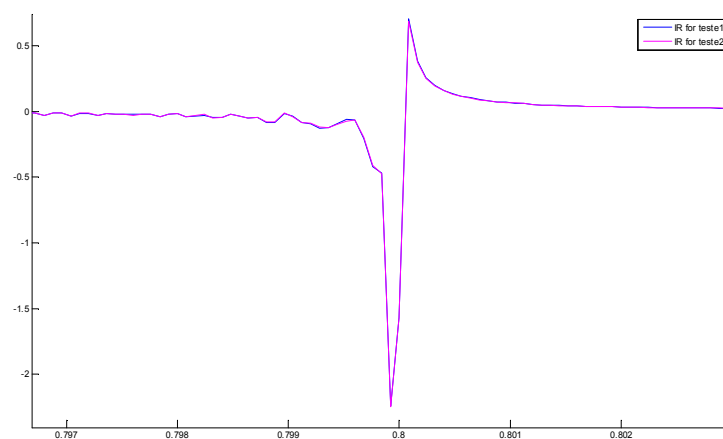
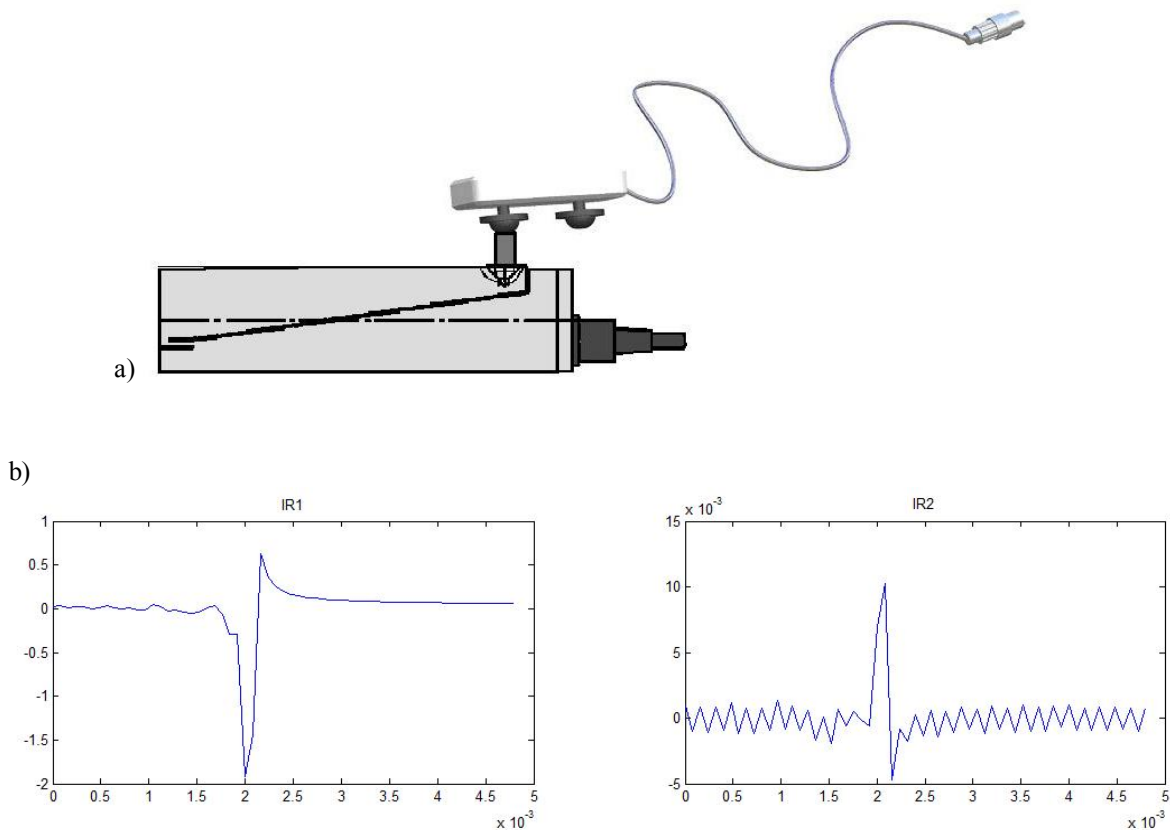


Figure 69 – IR for piezoelectric sensor 2 for different testes.

### 6.2.2 - Study of the crosstalk

As already mentioned our double probe consists of two piezoelectric sensors, which are on the same PCB, so it was crucial see if there was crosstalk between sensors. The term crosstalk refers to any phenomenon by which a signal transmitted on one circuit or channel of a transmission system creates an undesired effect in another circuit or channel. In order to verify the existence or absence of crosstalk it was followed the next methodology:

1. Acting on only one of the sensors and the other was free, it and were acquired for both the impulse responses. The interface used for these tests was a species of clay bonded, between the actuator and the sensor under study. Both are fixed in structures with large mass of inertia to avoid oscillations.



**Figure 70** – IR for two sensors, actuating only on one piezoelectric (a).  
b) The IR for sensor 1 and IR for sensor 2.

By analysis of the obtained IR it can be verify that the sensor that is being actuated shows the typical form of the impulse response for a piezoelectric sensor, while the sensor which is free provides an IR inverse of much less amplitude. The particularities of the impulse response given by the sensor that was free, without suffering the action of the actuator were studied further ahead.

2. Putting one of the sensors on the tube it was recorded both signals that each was to detect (figure 71a). In this case, the signal generated was a triangular wave with duration of 1s and the sensor was placed in the tube at the position 194cm.

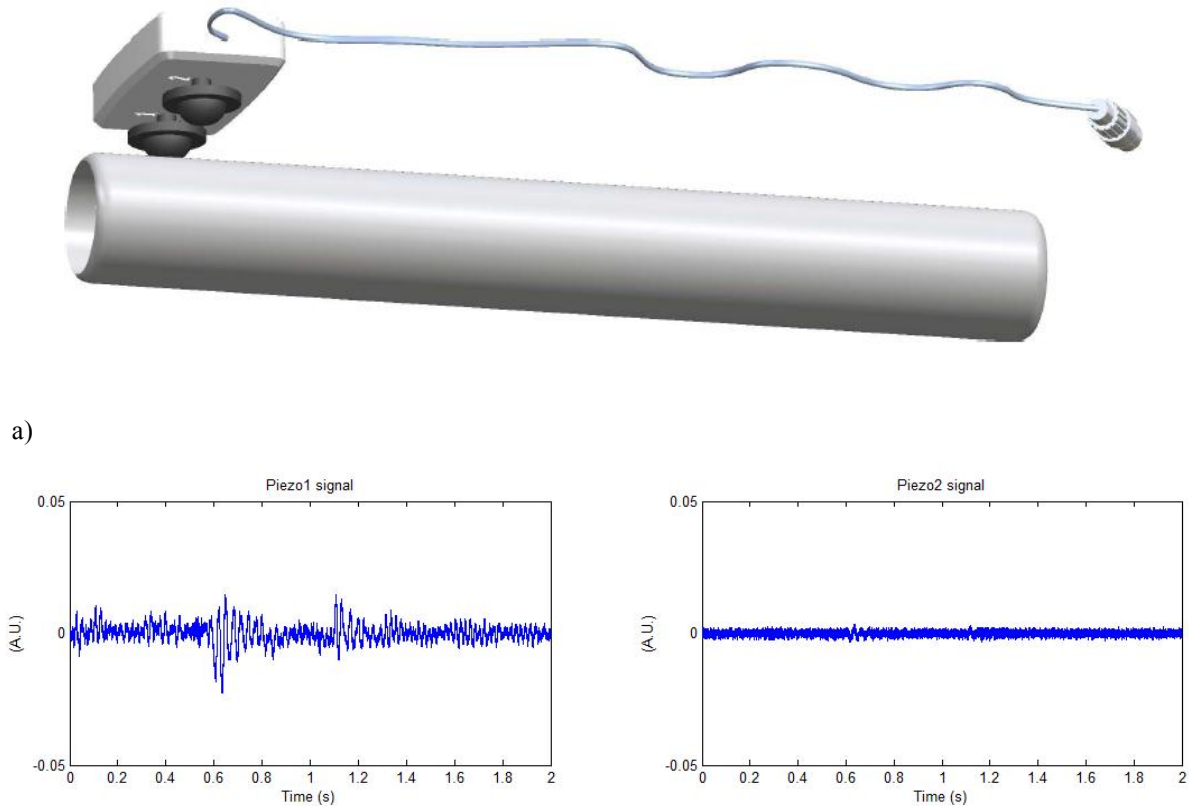


**Figure 71** – Acquisition signals in the tube, only one sensor of double probe.

- a) Schematic of the experience.
- b) Signal detected by the two sensors.

The signal that was captured by the piezoelectric sensor in the tube is greater in amplitude than the signal detected by the piezoelectric which was suspended in the air.

3. With the IR of the sensor and the captured signal in the tube, by deconvolution it is possible to get the original signal, the signal at the input of sensor.

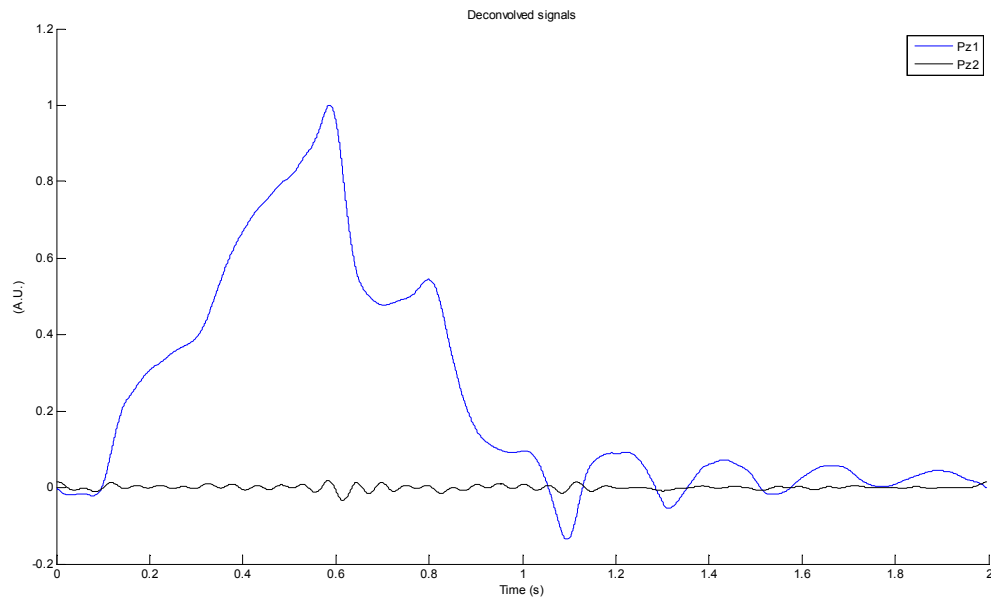


**Figure 72** – Waveform result of deconvolution for the sensor 1 and sensor 2.

It was obtained by the deconvolution of the signal of two sensors, obtained: the triangular 1s duration waveform with all reflections for sensor 1, and almost no signal for sensor 2.

Consequently, can conclude that the signal detected by one sensor does not interfere considerably in the signal that is captured by another sensor, i.e., there is no crosstalk between the sensors.

The same study was done to the other sensor, actuated only on the sensor 2 and used the IR obtained from each sensor. Tube was placed only in the sensor 2 with the other suspended in the air and was the deconvolution for the signals obtained. The results were exactly the same as those previously seen for the sensor 1. Corroborating there it isn't crosstalk between sensors.

### 6.2.3 - Study of the mass of inertia

The previous studies showed that for the free sensor the impulse response has lower amplitude and inverse shape. This response could be caused by the fact that sensors are on the same PCB, and inserted within the same box, above, these structures are responsible for transmitting the applied force. The piezoelectric, are associated with a screw that hold the mushroom interface, by exercising a force on one of the sensors during a sweep, resistance of mass to a change in its state of motion. Opposition to this motion generates an impulse response such as that observed in Figure 70.

To prove that, was associated extra mass of the sensor put two very heavy metal, increased the inertia mass, of which was obtained for IR. A sensor is subjected to action of the actuator that generates sweep the sensor with extra mass is free, and the two signals are acquired. The IR obtained for the sensor that has changed is more amplitude and the same shape, which proves that the small IR which determinate for the sensor free was originated to its inertia mass.

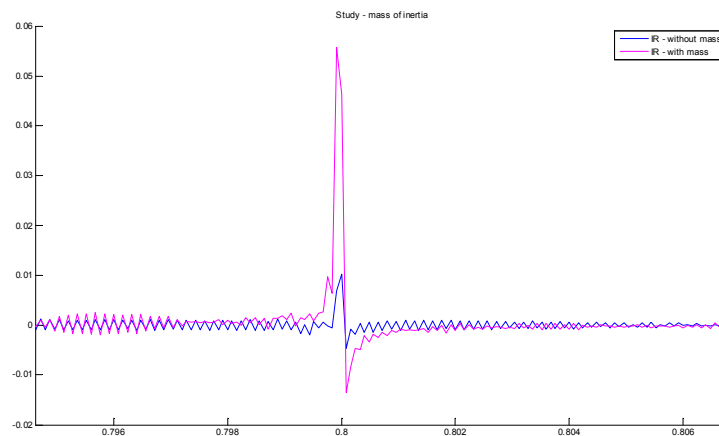


**Figure 73** – IR for sensor 2, with normal mass and extra mass.

After the studies for the characterization of the sensors, can ultimately advance the study of wave propagation and reflection in the model bench.



### 6.3 - Signals Deconvolution and Reflections Time Determination

Deconvolution is the algorithm used to find the original wave at the input of the sensor, with the obtained IR.

For each of the sensors it generated waves on the bench model and calculated the waves detected by the probe.

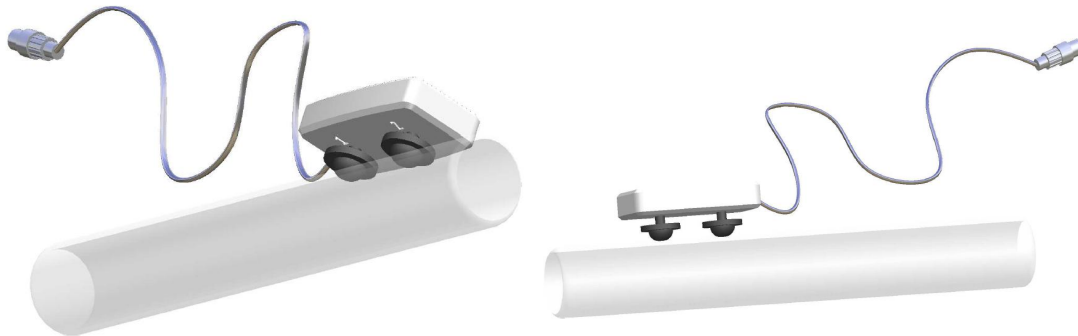


**Figure 74** – Schematic of release the double probe in the silicone tube at different angles.

The knowledge of the pulse wave velocity within the tube by the algorithm that uses the pressure sensors signals, it can be calculated the temporal location of the reflections on the deconvolved wave.

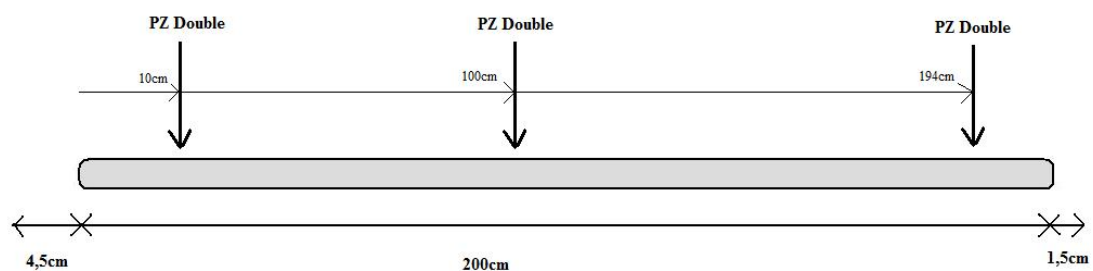


**Figure 75** – Schematic representative of the tube and the positions where the signals were acquired.

The places of reflection, which were studied previously, they are 4.5 cm before the tube and 1.5 cm from the end of the tube, within the parts of the extremities, where the gauges are placed.

To calculate the timings of several reflections, which occur in the tube, we made acquisitions with double probe in three different positions: in the tube at the beginning, 10 cm, the middle, 100cm, and at the end of the tube, 194cm. Triangular waves were generated with different pulse widths.

We placed the double probe in position 10cm, and generated a triangular wave of 1.5 s of pulse width. The signals received by piezoelectric sensors were deconvolved and subsequently it was marked on them the time points that corresponded to reflections.

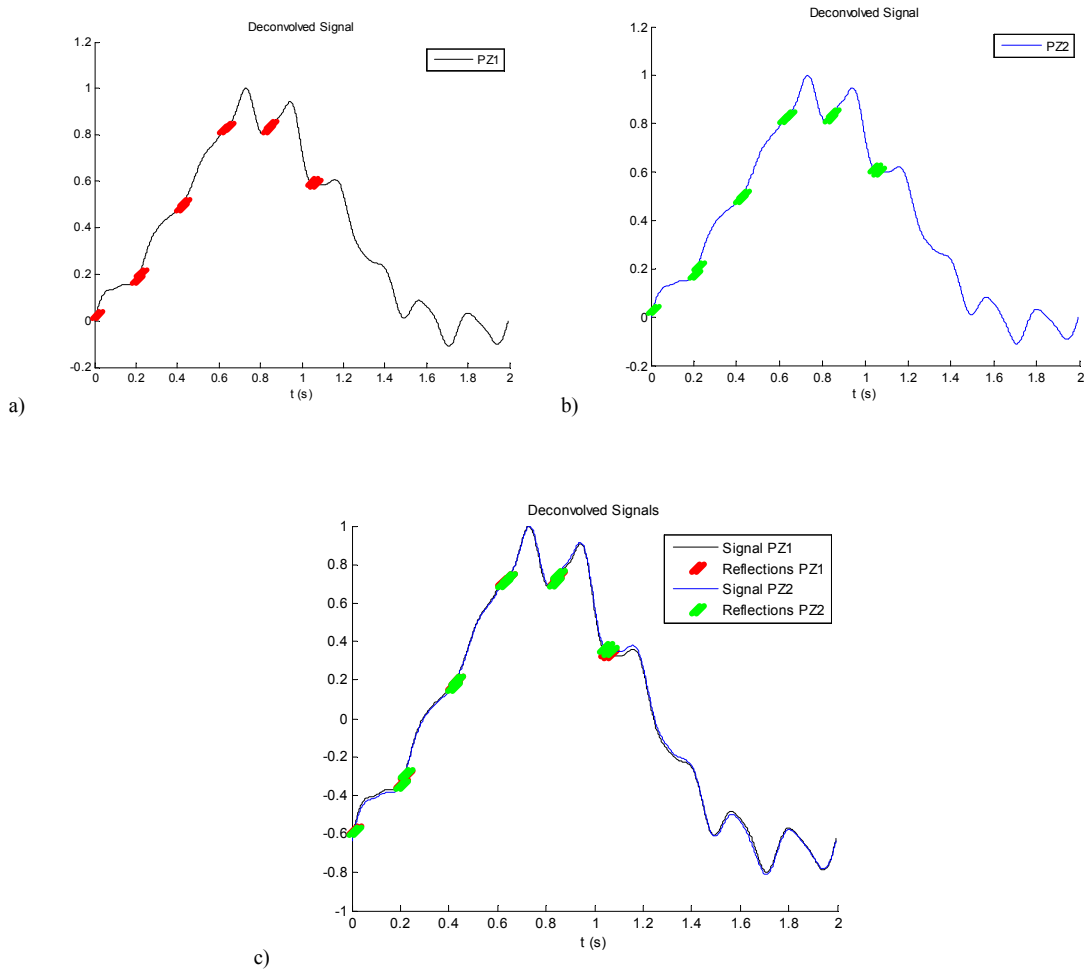


**Figure 76** – Deconvolved signal and reflections timings for position 10cm. Marked on them the time points that correspond to reflections

- a) Signal for PZ sensor 1.
- b) Signal for PZ sensor 2.
- c) Signal Pz1 and Signal PZ2 overlay.

We placed the double probe in position 100cm of tube, and generated a triangular wave of a pulse width of 500ms. The signals received by piezoelectric sensors were deconvolved and marked on them are time points that correspond to reflections.

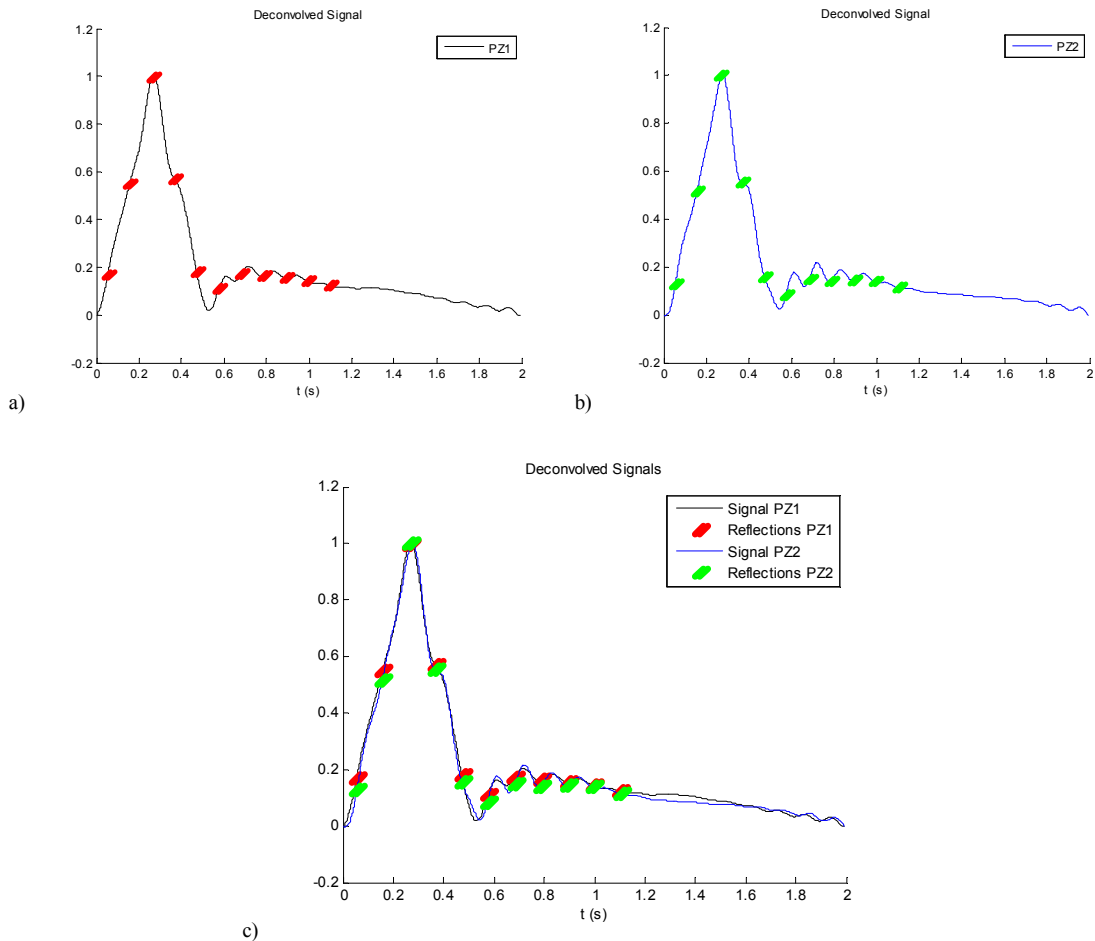


**Figure 77** – Deconvolved signal and reflections timings for position 100cm. Marked on them the time points that correspond to reflections

- a) Signal for PZ sensor 1.
- b) Signal for PZ sensor 2.
- c) Signal Pz1 and Signal PZ2 overlay.

In this test the double probe was placed in 194cm, and generated a triangular wave of a pulse width of 1s. The signals received by piezoelectric sensors were deconvolved and marked on them are time points that correspond to reflections.

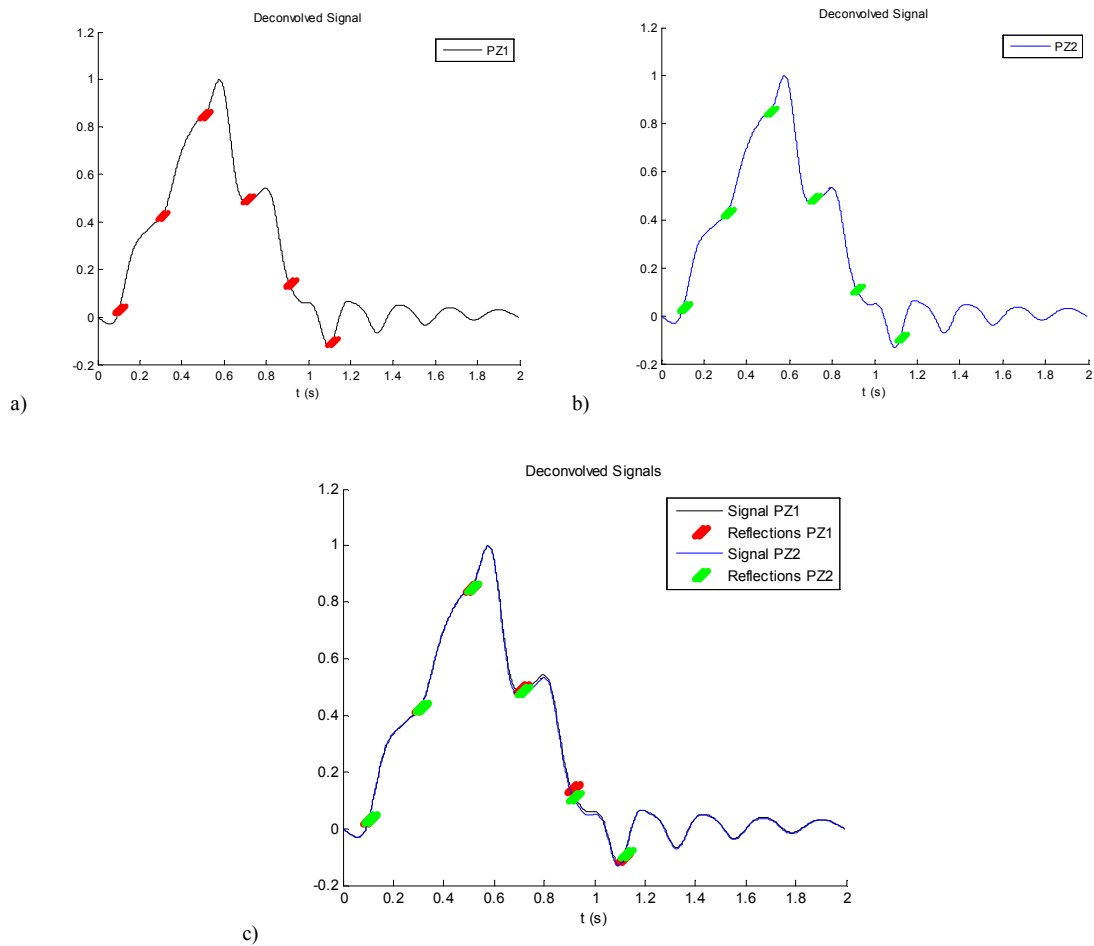


**Figure 78** – Deconvolved signal and reflections timings for position 194cm. Marked on them the time points that correspond to reflections  
 a) Signal for PZ sensor 1.  
 b) Signal for PZ sensor 2.  
 c) Signal Pz1 and Signal PZ2 overlay.

Once again the deconvolution proved to be a robust algorithm to obtain the original signal at the input of the piezoelectric sensor. It saw possible to find a triangular pressure wave that propagates in the tube, and determine the points of inflection which result from reflected waves.

Forms of the wave detected by two sensors can show that the sensor does not interfere with the amount of pressure wave that propagates along the tube, since the second sensor detects a wave whose shape is very similar.

## 6.4 – Temporal Resolution

The great potential of the double probe is the possibility of having temporal resolution to discriminate two points where the time delay between them is 1ms. Since the velocities within the tube of the model are in the order of 20m / s, and the two piezoelectric sensors are to 2cm apart, the time difference between signals detected will be 1ms. All studies were done at a sample rate 12.5 KSpss, so this time difference corresponds to 12.5 samples of difference between the waves of pressure detected.

To achieve this difference it was implemented several algorithms. We began by testing those that are based on finding a key point of the wave and calculate the time difference between the corresponding points of the two sensors.

### *Algorithm for identification of the foot of the wave*

A remarkable point is the reference part of the curve, for which the time delay is determination is usually the foot. The three algorithms that are used to identified the foot are intersecting tangents, maximum upstroke of the first derivative and zero crossing of the second derivative and 10% of the pulse pressure (Figure 79).<sup>[42]</sup>

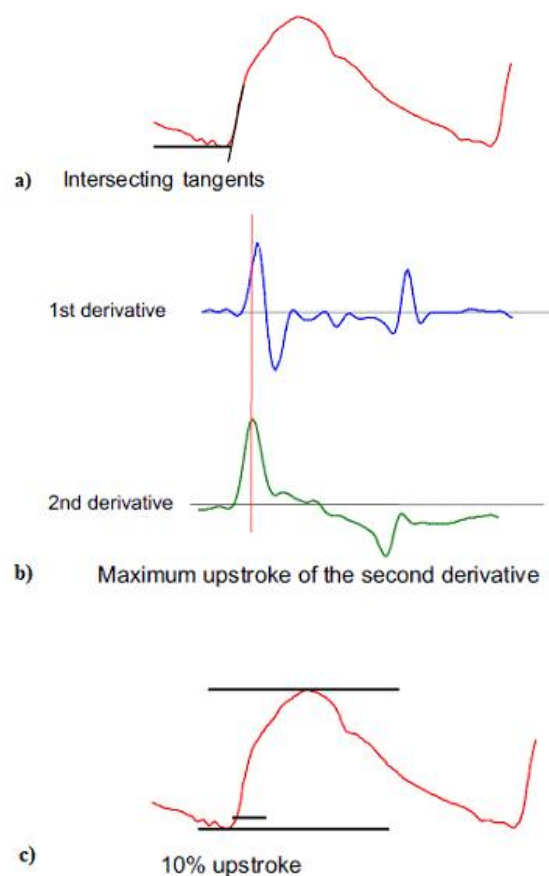


**Figure 79** - Different algorithms used to identify specific part of the pulse signal.

- a) Intersecting tangents.
  - b) Maximum upstroke of the second derivative.
  - c) Percentage of the full amplitude of the cycle.
- Adapted from [42].

After the implementation of the algorithms to detect the foot of wave pressure, it was found that the unfiltered signals did not allow us to find this point, and after filtration it was impossible to detect the time difference between the two signals. Indeed, the foot-to-foot methodology is usually used, as it avoids the confounding influence of wave reflection.

We tried, then to use the algorithms developed for the determination of PTT via the pressure sensors. However, the results obtained were not consistent; the values were of different orders. The algorithm of cross correlation has the limitation of not working for signals of a very large pulse width. The signals received by sensors PZ have despite having a low relationship signal - noise ratio (SNR), such as undo, we seek is of the order of millisecond, this information may be being hidden by the noise, so that all results could be mortgaged for that. To address this limitation we decided that instead of studying only one signal it should be necessary examine a range of signals, so that we could exclude the effect of noise. It were done new tests on the bench system that consisted the generation of a burst of Gaussian signals with a number of points from each Gaussian by the actuator generated.

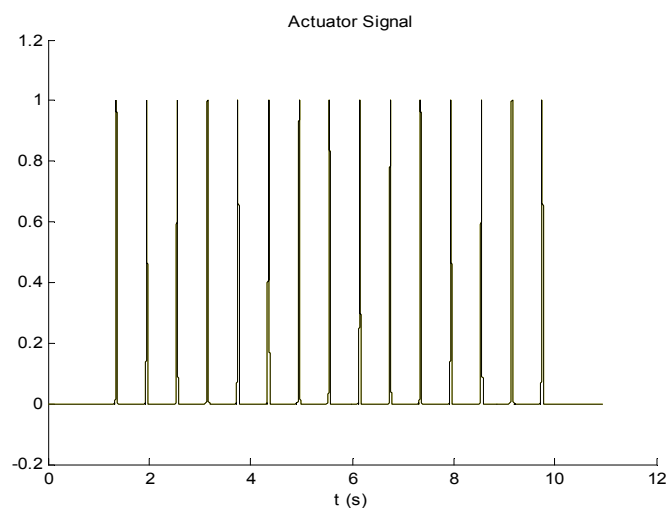


**Figure 80** – Signal of actuator. Burst of 15 gaussian pulse for 600ms width.

The response of PZ sensors was recorded and analyzed pulse by pulse, with the algorithm of cross correlation. The signals were acquired without the trigger with a series of points without interest before and after the signal.

Thus, the algorithm begins by determining the first point by means of a threshold, in this case of 0.0001 (figure 81a). For the signal of the actuator it is necessary to found and calculated the maximum difference between to consecutive signals, which corresponds to the period of the signal (figure 81b).

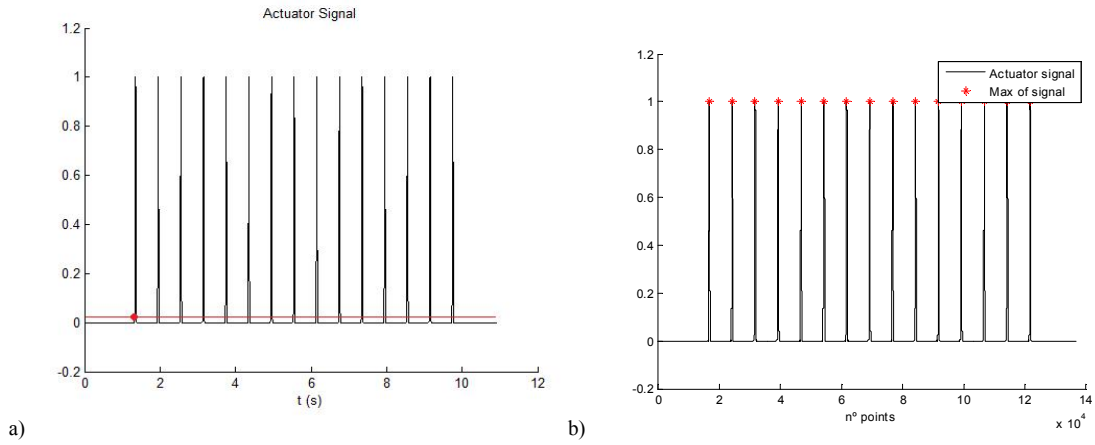


**Figure 81** – Actuator signal.  
 a) Local of first point to exceed the threshold.  
 b) Maximum of the signal.

The first and last pulse generated are excluded from the analysis.

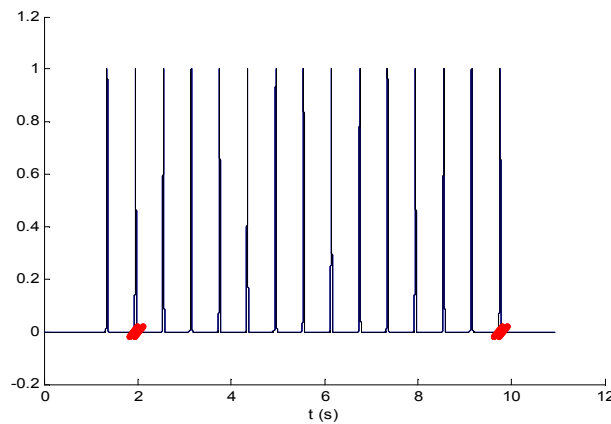


**Figure 82** – Signal of the actuator with the points that mark the limits of analysis of the pulses.

Since the cross-correlation measures the degree of similarity between two signals, the signal from the actuator was convolved twice with each of the IR sensor PZ, yielding a very similar to the piezoelectric signals.

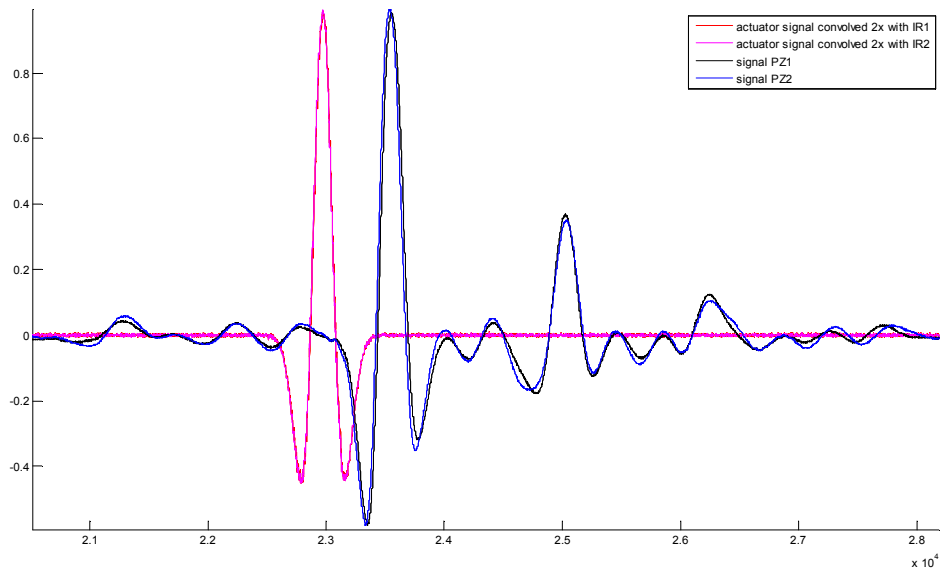


Figure 83 – The actuator signal convolved and the response of the PZ sensors.

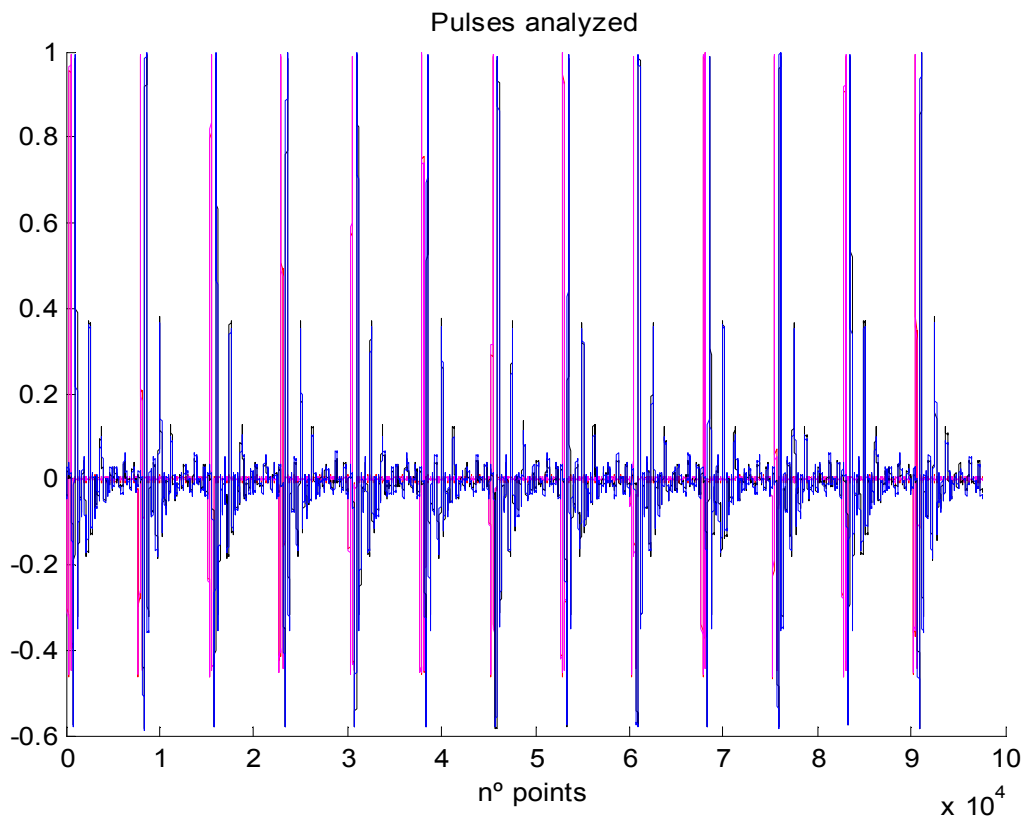
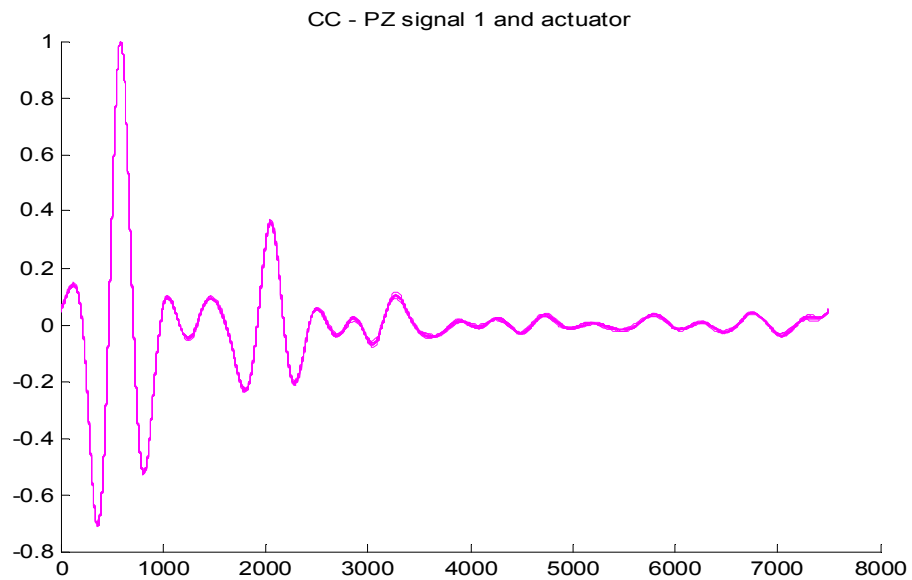


Figure 84 – Signals for the 13 analyzed pulses.

After segmentation of each period, it is made the cross correlation between the signals and the sign of the PZ actuator. The overlap of the correlation for each segment is represented in the graphs below.





**Figure 85** – Overlap of the results for each segment for cross-correlation for PZ signal 1 and the signal from the deconvolved PZ actuator.

It can be seen that there is great consistency of the results for each target. For each segment it is calculated minimum and maximum value of correlation.

For the PZ signal 2 it was followed the same procedure, and the results are available on the following chart.

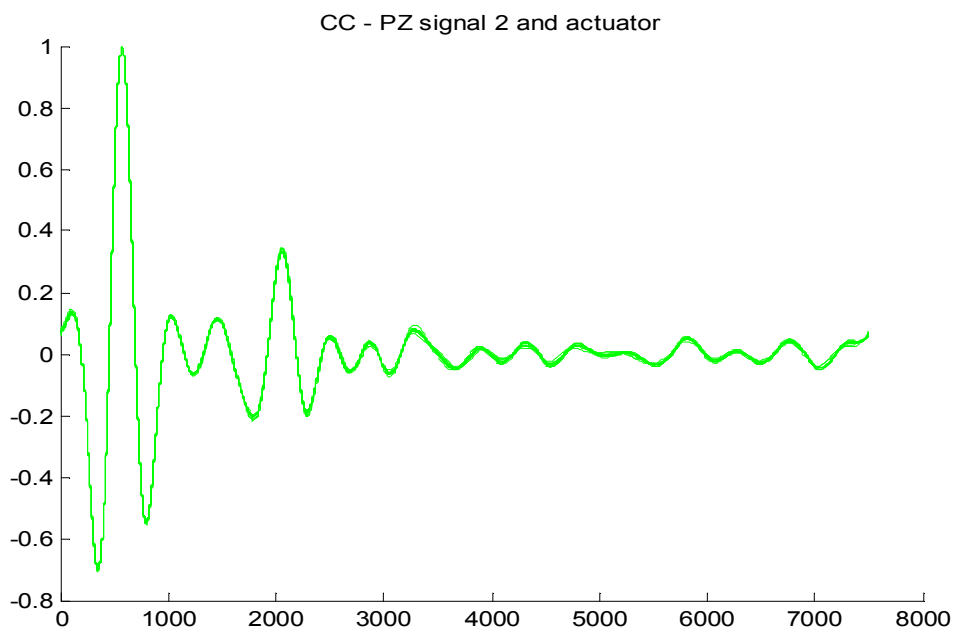


**Figure 86** – Overlap of results for each segment for cross-correlation for PZ signal2 and the signal from the PZ actuator deconvolved.

Again, there is a great consistency in the results of each cycle, as can be seen by the overlap of signals. For each cycle is calculated by the maximum and minimum value of the correlation, and it is determined the difference between each of the maximum correlation of PZ 1 and the maximum of the correlation of PZ 2 and the same is done for the values of the minimum, the average differences for the minimum and the maximum, the gives the PTT value.

This analysis was made for signals of various pulse widths, and with a variable number of pulses. The following table summarizes the results:

**Table X – Results of PWV obtained by cross correlation for signals of PZ double for different pulse widths.**

Pulse Gauss (ms)	N° of pulses	PTT				PWV (m/s)	
		By max		By min		By max	By min
		N° of points	(s)	N° of points	(s)		
300	15	12.0769	9.6612e-04	12.9231	0.00103384	20.7006	19.3452
400	15	12	9.6001e-04	12.3846	9.6001e-04	20.8333	20.5098
500	10	14.1250	0.00113000	13.5000	0.001080	17.6991	18.5185
600	15	13.7692	0.00110153	13.4615	0.00107692	18.1564	18.5714
700	10	14.3750	0.00115000	12.3750	9.9000e-04	17.3913	20.2020
800	10	16.1250	0.00129000	14.8750	0.00119000	15.5039	16.8067

The results show that our probe can discriminate two points removed from 1ms, i.e. the double probe gives a temporal resolution sufficient to allow the calculation of velocity around the 20m / s. The algorithm used has many limitations and the values are somewhat accurate.

Other attempts to better the results were implemented. One was to examine only a portion of the signal, the upstroke, wave free zone and therefore not reflected as interference. However, this analysis did not bring better results.

*Chapter 7*

## **Conclusions and Future Work**

---

Once the project's academic component has been achieved, it is now necessary to evaluate and discuss the work that has been done, the results obtained and the future developments.

### ***7.1 – Conclusions***

The built test bench reproduce quite well the conditions of an artery, allowing the characterization of our sensors and studies on the wave phenomena and enabling the comprehension of the propagation and reflection of pressure waves. The two pressure sensors placed at the ends of the tube allowed us to have a method of determination of PWV which serves as a comparison to the values determined by piezoelectric sensors. The algorithm of cross correlation was shown to be the best method for the determination of PWV, but only valid for small values of pulse width.

The developed piezo sensors allow the assessment of the pressure wave of human carotid as well as the wave of pressure generated by our test bench. The Deconvolution algorithm proved to be a robust for this type of sensors.

The technique of obtaining the impulse response of a sensor using the sweep signal generated by the actuator was very reliable and relatively simple to implement experimentally.

It was proved, that there is no crosstalk between the two piezoelectric sensors of the probe double, i.e., the signals received by sensors do not interfere each other. Conventional methods of calculating the PTT through a remarkable point, usually the foot of the wave, were not successful. The algorithm implemented to calculate the transit time was the cross-correlation and it has shown that the double probe has temporal resolution to discriminate differences in the temporal order of millisecond.

## **7.2 – Future Work**

### Acquisition Unit

Circuit signal conditioning of acquisition box needed to be revised. The PCB must be redesigned in order to simplify the arrangement of wires and connections.

### Test Bench

In the bench test, the control system of the DC level of pressure in the tube by syringe, does not allow small changes. Since the piston needs too much friction, it is only possible to make big changes. It is important that a structure be built to allow more functional changes in the gradual control of pressure.

### Double Probe and algorithms

The double probe is experimentally difficult, were acquired many data series, however, would need a large database, with burst of pulses so that they could draw conclusions more consistent.

The calculation of PTT by the phase spectrum needs to be explored, since the spectrum of phase contains the wanted temporal information we want.

In what concerns to the carotid signals taken in the human carotid, we have the problem of baseline for all sensors, which need to be solved, for example, creating a hybrid probe, with accelerometers.

To show the values obtained by the algorithms for calculating the pulse wave velocity, it was interesting to do tests with a double probe and a simple probe, where the application of the algorithm was developed to give the same values of PWV, using the two signals of the double probe, or between a double probe and other probe for different distances between the two probes.

Finally and with a different fluid within the tube, e.g. a mixture of glycerine and water, it was interesting to do all the tests and verify that the algorithm developed gives values of velocity consistent with the values determinate by the pressure sensors and study the variation in velocity with the density of the fluid in the tube.

## References

---

- [1] – Hatchett, Richard *et al* – *Enfermagem Cardíaca: Um guia polivalente*, 1th ed., Lisboa, Lusociencia, 2002
- [2] – O’ Rourke, Robert A. *et al*– *O coração: Manual de cardiologia*, 11th ed., Lisboa, McGraw-Hill de Portugal, 2006
- [3] – Topol, Eric J. *et al* – *Tratado de cardiologia*, Vol.1, 2th ed., Rio de Janeiro, Guanabara Koogan, 2005
- [4] – Porto, Celmo C. – *Doenças do coração: Prevenção e Tratamento*, 2th ed., Rio de Janeiro, Guanabara Koogan, 2005
- [5] – Pereira, José M. *et al* – *Cardiologia Preventiva*, Lisboa, Revista Portuguesa de Clínica e Terapêutica, 1976
- [6] – Pierre Boutouyrie, Marie Briet, Ce’dric Collin, Sebastian Vermeersch, Bruno Pannier– *Assessment of pulse wave velocity*, Elsevier 2009
- [7] – JP Murgo, N Westerhof, JP Giolma and SA Altobelli – *Aortic input impedance in normal man: relationship to pressure wave forms*. Circulation. 1980;
- [8] – Patrick Segers, Ahmad Qasem, Tine De Backer, Stephane Carlier, Pascal Verdonck, Albert Avolio. - *Peripheral “Oscillatory” Compliance Is Associated With Aortic Augmentation Index*, Hypertension 2001.
- [9] – Koh, Tat W. *et al* – *Analysis of Wave Reflections in the Arterial System using Wave Intensity: a novel method for predicting the timing and amplitude of reflected waves* – Imperial College of Science, London (UK), *Heart and Vessels*, December 1998
- [10] – Suzanne Dyer, Marc Bevan, Jolie Hutchinson – *Peripheral arterial tonometry with ascending aortic waveform analysis using the SphygmoCor system*, 2006
- [11] – Stephanie S. DeLoach, and Raymond R. Townsend – *Vascular Stiffness: Its Measurement and Significance for Epidemiologic and Outcome Studies*, Clin J Am Soc Nephrol, 2008
- [12] – S.C. Millasseau, R.P. Kelly, J.M. Ritter – *Determination of age-related increases in large artery stiffness by digital pulse contour analysis*, Clinical Science, 2002
- [13] – Gary E. McVeigh – *Pulse Waveform Analysis and Arterial Wall Properties*, Hypertension 2003

- [14] – Borges E. S. – *Assesment of Hemodynamic Parameters*, 2008
- [15] - James Karki, *Signal Conditioning Piezoelectric Sensors*, Texas Instruments, 2000
- [16] - Sandrine C. Millasseau, Andrew D. Stewart, Sundip J. Patel, Simon R. Redwood, Philip J. Chowienczyk, “*Evaluation of Carotid–Femoral Pulse Wave Velocity Influence of Timing Algorithm and Heart Rate*”, *Hypertension* 2005
- [17] - Marek W. Rajzer, Wiktoria Wojciechowska, Marek Klocek, Ilona Palka, Małgorzata Brzozowska-Kiszka and Kalina Kawecka-Jaszcz, “*Comparison of aortic pulse wave velocity measured by three techniques: Complior, SphygmoCor and Arteriograph*”, 2001
- [18] - Stephanie S. DeLoach and Raymond R. Townsend, “*Vascular Stiffness: Its Measurement and Significance for Epidemiologic and Outcome Studies*”, *Clin J Am Soc Nephrol* 3: 184–192, 2008.
- [19] - Laurent, S. et al, “*Expert consensus document on arterial stiffness: methodological issues and clinical applications*”, *European Heart Journal*
- [20] - [http://www.rush.edu/rumc/images/ei\\_0019.gif](http://www.rush.edu/rumc/images/ei_0019.gif)
- [21] - [http://applications.spectrumhealth.org/media/coe\\_heart/images/GS\\_Anatomy%00of%20Hearts%20Electrical%20System\\_lg.jpg](http://applications.spectrumhealth.org/media/coe_heart/images/GS_Anatomy%00of%20Hearts%20Electrical%20System_lg.jpg)
- [22] - <http://www.nicksnowden.net/images/artery-vein%20diagram.jpg>
- [23] - Neto, Jorge E. “Great arteries contribution in orthostasis cardiovascular adaptation”, *Arquivos Brasileiros de Cardiologia*, 2006.
- [24] - <http://z.about.com/f/p/440/graphics/images/en/18020.jpg>
- [25] - Safar, M. *et al* – *Aortic Pulse Wave Velocity: an Independent Marker of Cardiovascular Risk*, 2002
- [26] - [http://www.som.uq.edu.au/research/cig/images/waveform\\_1.jpg](http://www.som.uq.edu.au/research/cig/images/waveform_1.jpg)
- [27] - [http://www.complior.com/UK/COMPLIOR\\_PC\\_pt.gif](http://www.complior.com/UK/COMPLIOR_PC_pt.gif)
- [28] - [http://www.ispub.com/ispub/ijbe/volume\\_3\\_number\\_1\\_8/modeling\\_the\\_human\\_cardiovascular\\_system\\_and\\_peristaltic\\_motion\\_of\\_descending\\_arteries\\_using\\_the\\_lumped\\_method/modeling-fig6.jpg](http://www.ispub.com/ispub/ijbe/volume_3_number_1_8/modeling_the_human_cardiovascular_system_and_peristaltic_motion_of_descending_arteries_using_the_lumped_method/modeling-fig6.jpg)
- [29] - <http://www.clinsci.org/cs/103/0371/cs1030371f03.gif>
- [30] - Nichols, W.W. and O'Rourke, M.F. – *McDonald's Blood Flow in Arteries: Theoretical Experimental and Clinical Principles* – 5th ed., London, 2005

- [31] - <http://soundlab.cs.princeton.edu/learning/tutorials/sensors/node7.html>
- [32] - James Karki, *Signal Conditioning Piezoelectric Sensors*, Texas Instruments, September 2000
- [33] - PulScope: Manual, Set 2008
- [34] - H.C. Pereira, J.M. Cardoso, V.G. Almeida, T. Pereira, E. Borges, E. Figueiras, L.R. Ferreira, C. Correia, “*Programmable test bench for hemodynamic studies*”, University of Coimbra, 2009
- [35] - Alan J. Bank, Daniel R. Kaiser, “*Smooth Muscle Relaxation: Effects on Arterial Compliance, Distensibility, Elastic Modulus, and Pulse Wave Velocity*”, Hypertension 1998
- [36] - J.M. Boese, M.Bock, M.L.Bahner, J.Alhers’, L.R. Schad, “*In vivo Validation of Aortic Compliance Estimation by MR Pulse Wave Velocity Measurement*”, Universitit Heidelberg, Germany
- [37] - Lorenzo Picinali, “*Techniques for the estration of the impulse response of a linear and time-variante system*”, De Montfort University Leicester, UK
- [38] - Ó Tolvan, “*Sirp - Loudspeaker analyzer*”, Version 1.0 User’s Guide, 2008
- [39] - Edward J. Ciaccio and Gary M. Drzewiecki “*Tonometric Arterial Pulse Sensor With Noise Cancellation*”, IEE, 2008
- [40] - Lorenzo Picinali, “*Techniques for the estration of the impulse response of a linear and time-variante system*”, De Montfort University Leicester, UK.
- [41] - Ó Tolvan, “*Sirp - Loudspeaker analyzer*”, Version 1.0 User’s Guide, 2008.
- [42] - Pierre Boutouyriea, Marie Briet, Ce’dric Collin, Sebastian Vermeersch, Bruno Pannier, “*Assessment of pulse wave velocity*”, France, 2008.
- [43] - Laurent S, Cockcroft JR, Van Bortel L, Boutouyrie P, Giannattasio C, Hayoz D, et al. “*Abridged version of the expert consensus document on arterial stiffness*” Artery Res 1-3-2007.
- [44] - Rabben SI, Stergiopulos N, Hellevik LR, Smiseth OA, Slordahl S, Urheim S, et al. “*An ultrasound-based method for determining pulse wave velocity in superficial arteries*” J Biomech 2004.
- [45] - Brands PJ, Willigers JM, Ledoux LA, Reneman RS, Hoeks AP. “*A noninvasive method to estimate pulse wave velocity in arteries locally by means of ultrasound*”. Ultrasound Med Biol 1998.

- [46] - Laurent S, Katsahian S, Fassot C, Tropeano AI, Gautier I, Laloux B, Boutouyrie P. “*Aortic stiffness is an independent predictor of fatal stroke in essential hypertension*” Stroke. 2003.
- [47] - Blacher J, Guerin AP, Pannier B, Marchais SJ, Safar ME. “*Impact of aortic stiffness on survival in end-stage renal disease*” Circulation. 1999.
- [48] - Asmar R, Benetos A, Topouchian J, Laurent P, Pannier B, Brisac AM, Target R, Levy BI. “*Assessment of arterial distensibility by automatic pulse wave velocity measurement: validation and clinical application studies*”. Hypertension 1995.
- [49] - Ahmed Qasem, Alberto Avolio, “*Determination of Aortic Pulse Wave Velocity From Waveform Decomposition of the Central Aortic Pressure Pulse*”, Hypertension 2008.
- [50] - Stephanie S. DeLoach and Raymond R. Townsend, “*Vascular Stiffness: Its Measurement and Significance for Epidemiologic and Outcome Studies*”, Clin J Am Soc Nephrol 3: 184–192, 2008.
- [51] - Berend E. Westerhof, Jeroen P. van den Wijngaard, Joseph P. Murgu and Nicolaas, “*Location of a Reflection Site Is Elusive. Consequences for the Calculation of Aortic Pulse Wave Velocity*”, Hypertension, 2008.



# Appendix – Electronic Circuits Schematics

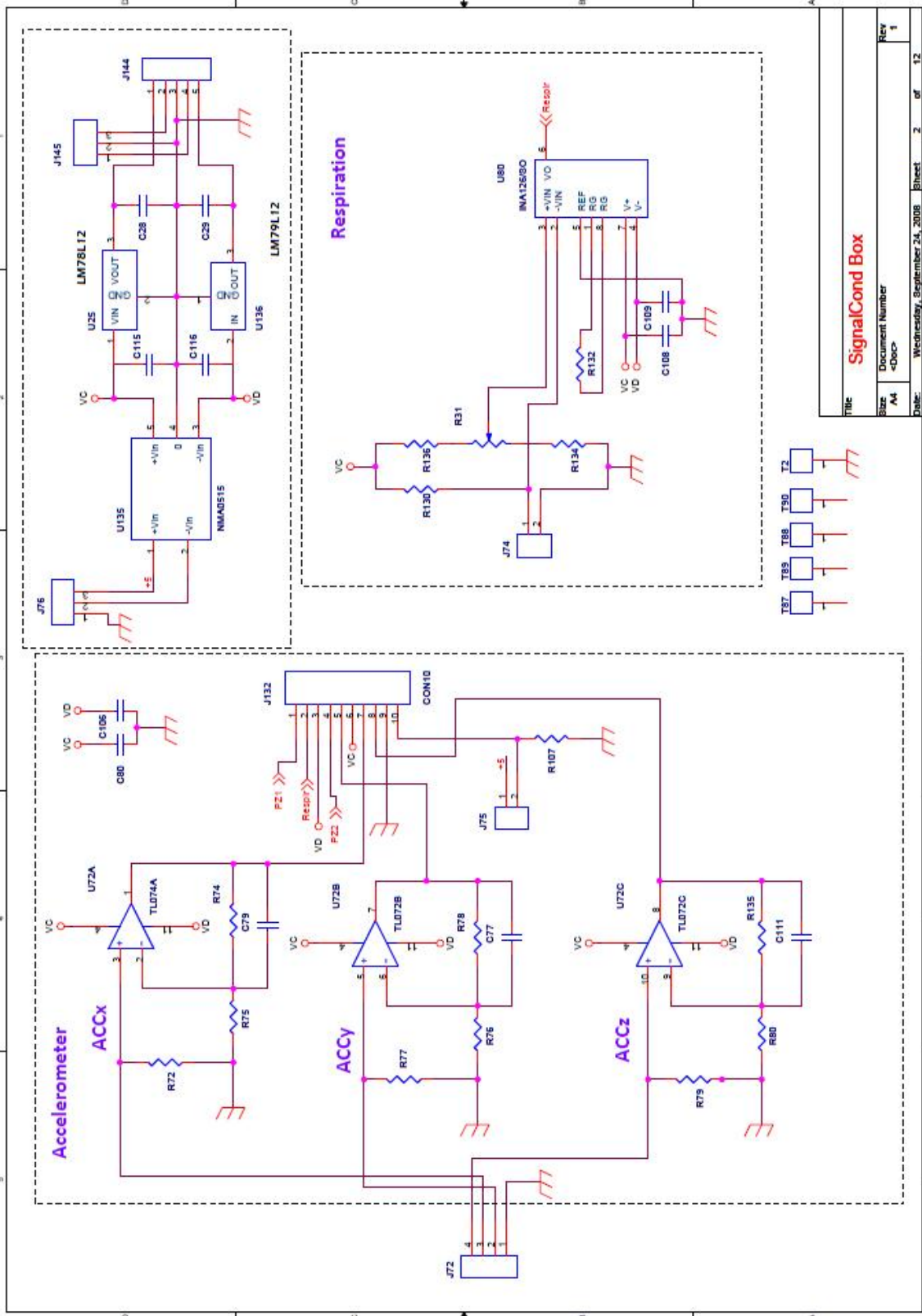
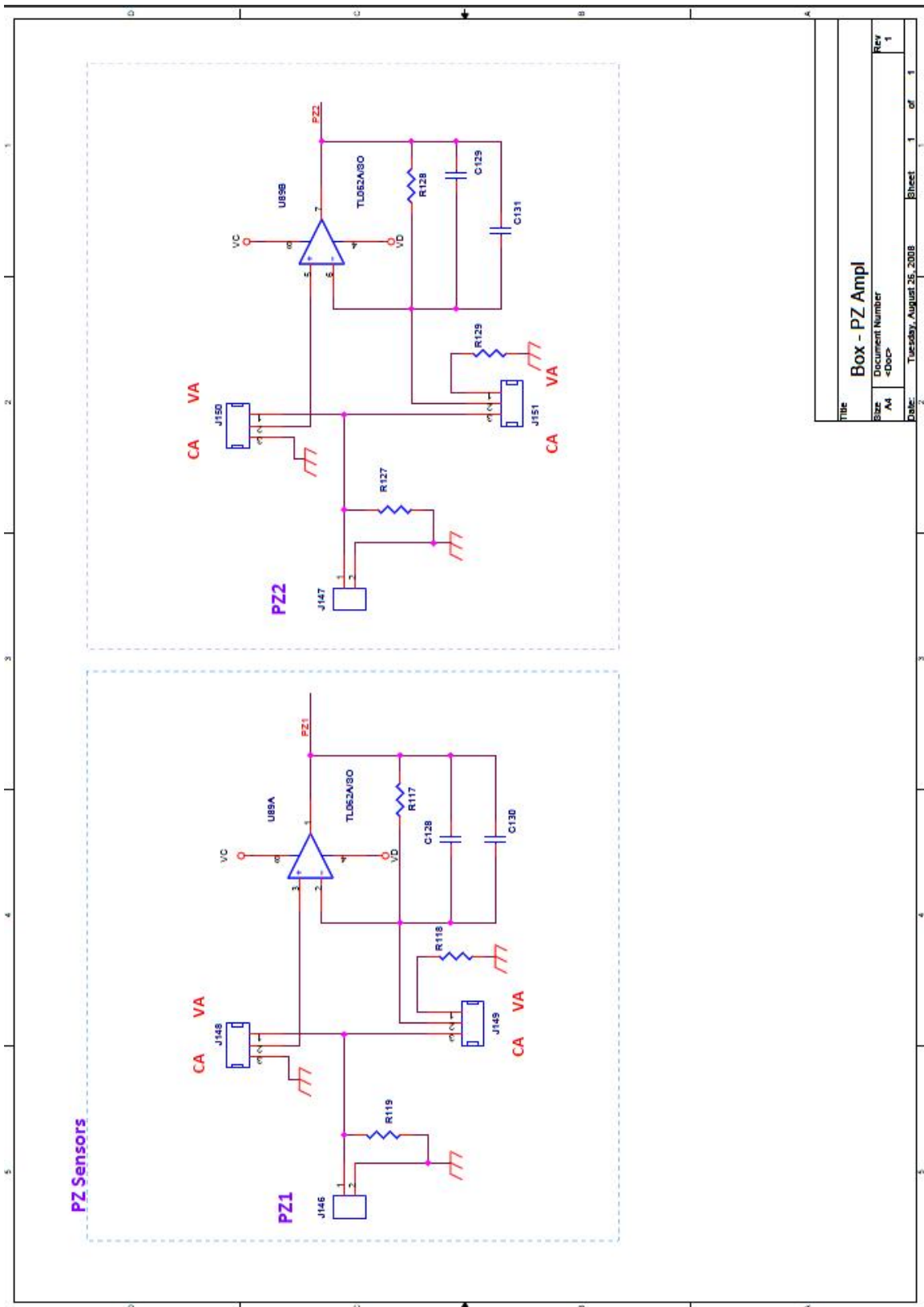
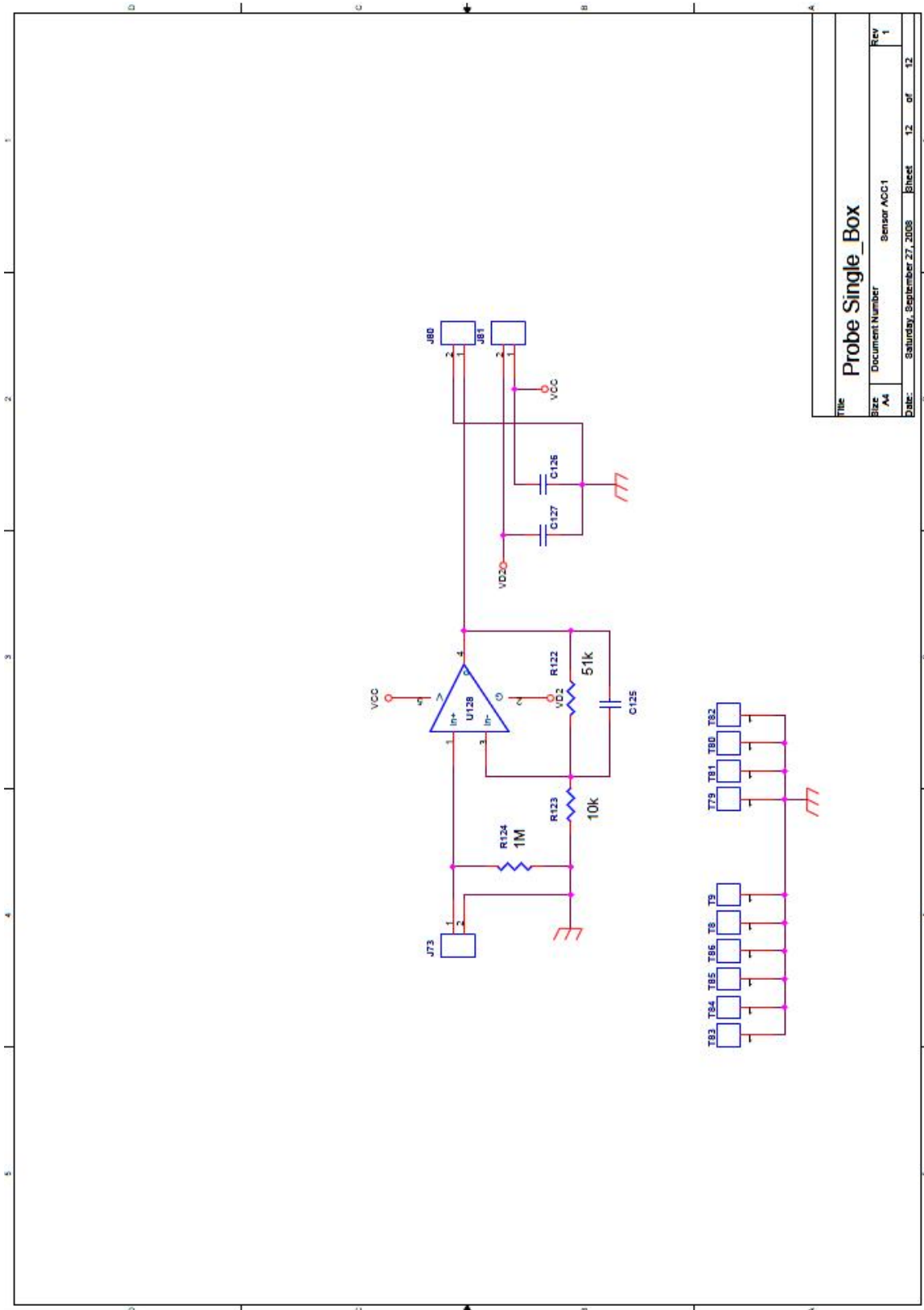


Figure 87 – Signal conditioning box: Electronic Circuit Schematic 1.



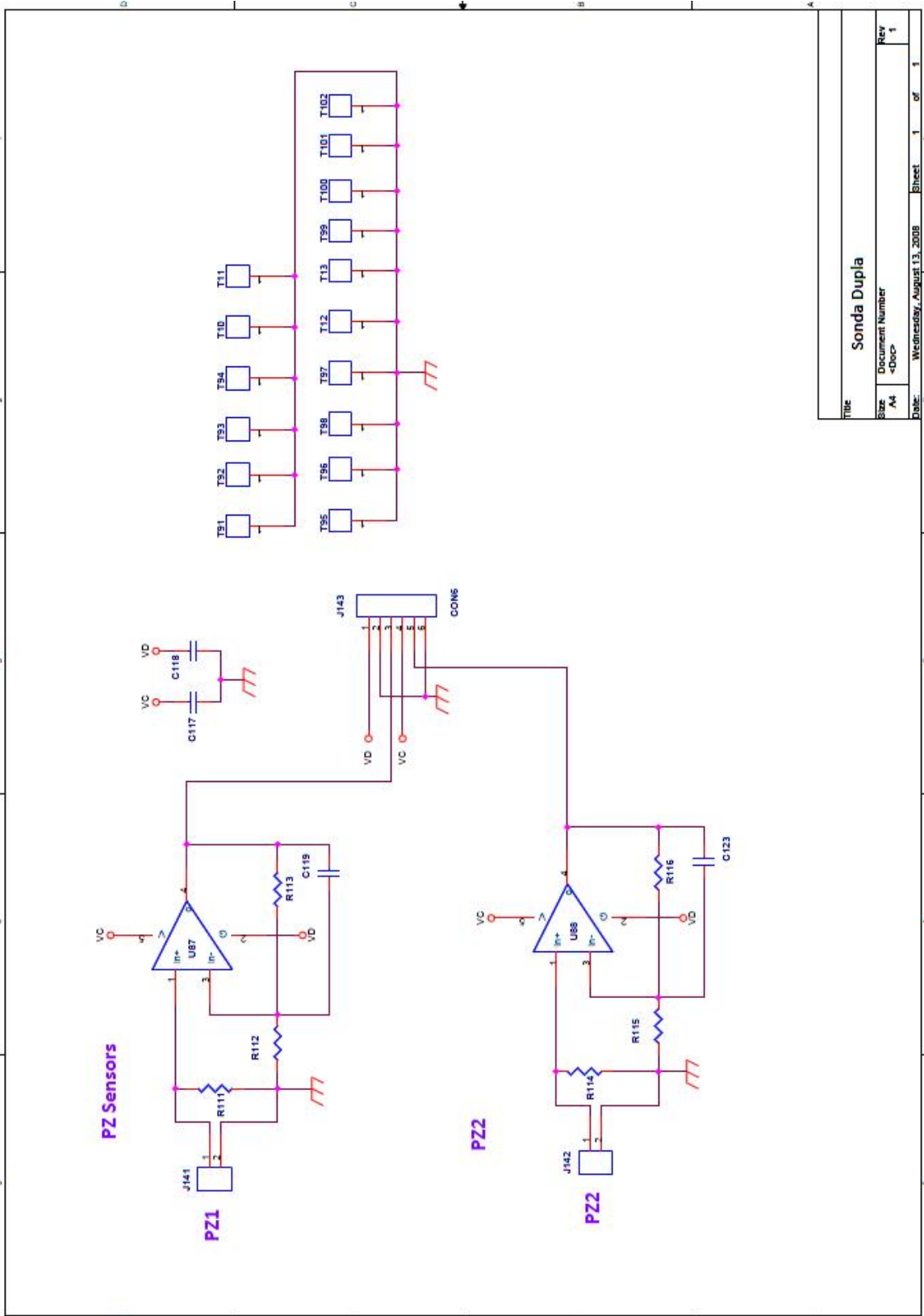
Title	Box - PZ Ampl
Size	Document Number
Rev	A4
Date	<Doc>
Sheet	Tuesday, August 26, 2008
Page	1 of 1

Figure 88 – Signal conditioning box: Electronic Circuit Schematic 2.



File		Probe Single_Box
Size	Document Number	Sensor ACC1
A4		
Date:	Saturday, September 27, 2008	Sheet 12 of 12
		Rev 1

Figure 89 – Simple Probe: Electronic Circuit Schematic.



Title		Sonda Dupla	
Size	A4	Document Number	<Doc>
Date:	Wednesday, August 13, 2008	Sheet	1 of 1
Rev	1		

Figure 90 – Double Probe: Electronic Circuit Schematic.

